Department of Electrical and Computer Engineering

Partial Discharge Modeling and Associated Transients along Medium Voltage Distribution Cables

Zenon A. Achillides

Dissertation

Submitted in Partial Fulfillment of the

Requirements for the Degree of

Doctor of Philosophy

at the University of Cyprus

February 2013

APPROVAL PAGE

Doctor of Philosophy Dissertation

Partial Discharge Modeling and Associated Transients along Medium Voltage Distribution Cables

Presented by

Zenon Achillides

Committee Chair	Dr. Stavros Iezekiel
Research Supervisor	Dr. George.E. Georghiou
Research Supervisor	Dr. Elias Kyriakides
Committee Member	Dr. Charalambos A. Charalambous
Committee Member	Dr. Andreas Kyprianou
Committee Member	Dr. Michael Danikas

University of Cyprus

February 2013

ABSTRACT

Ensuring a reliable electric service to industrial, commercial and residential customers is becoming an important parameter for every electricity company due to the increased demand from the customers for less downtime, high productivity and reduced maintenance cost of machinery caused by unscheduled frequent interruptions due to underground power cable failures. The presence of partial discharges (PD) is one of the most prominent indicators of defects and ongoing degradation processes of electrical insulation. As a high percentage of failures are associated with PD, the need for the classification, extraction and evaluation of PD signals is essential. For the above reasons, an electrical model of a breakdown void, modelled, as part of the power system is more than a necessity.

The capacitive network representation of the void (model) has long been used for the study of the transients generated by a breakdown void. As an alternative to the capacitive representation of the void (model) the induced charge concept has been introduced by researchers at the Technical University of Denmark, expressing strong criticism against the capacitance modeling of void.

This thesis discusses and argues this criticism and exploits the potential and weaknesses of the classical capacitive representation of voids from a theoretical point of view and proposes three new models: a) an improved version of the classical capacitive model b) a model based on the induced charge concept for streamer inception c) an advanced capacitive model of the void based on streamer concepts. Furthermore in this thesis the geometrical and physical parameters governing the classical capacitive model of void (improved version) and the other two proposed models are calculated by utilizing classical electromagnetic theory, concepts of streamer breakdown mechanism and gas discharge physics. The three models are utilized to replicate the transients (PD signals) and propagate them along the core of a typical medium voltage cable from a breakdown void under real time power network conditions. The outcome of the three models is compared to experimental data obtained from the international literature.

ΠΕΡΙΛΗΨΗ

Η εξασφάλιση αξιόπιστης παροχής ηλεκτρικής ενέργειας σε βιομηχανικούς, εμπορικούς και οικιακούς καταναλωτές είναι μια σημαντική παράμετρος για κάθε εταιρεία ηλεκτρικής ενέργειας, λόγω της συνεχώς αυξανόμενης αξίωσης από τους πελάτες για μεγαλύτερη αξιοπιστία και υψηλή παραγωγικότητα. Επίσης, οι μη προγραμματισμένες διακοπές της παροχής ηλεκτρικής ενέργειας οδηγεί σε αυξημένο κόστος συντήρησης των μηχανημάτων. Τέτοιες διακοπές μπορεί να οφείλονται σε αποτυχία της μόνωσης των καλώδιων μέσης τάσης. Η παρουσία των μερικών εκκενώσεων (partial discharges, PD) είναι ένας από τους σημαντικότερους δείκτες της συνεχούς υποβάθμισης της ηλεκτρικής μονώσεως. Καθώς ένα υψηλό ποσοστό των αποτυχιών συνδέονται με την παρουσία μερικών εκκενώσεων, η ανάγκη για την ταξινόμηση και αξιολόγηση των σημάτων PD είναι απαραίτητη. Για τους παραπάνω λόγους, ένα ηλεκτρικό μοντέλο του εν λόγω φαινομένου ως μέρος του ηλεκτρικού συστήματος είναι απαραίτητο.

Η χωρητική αναπαράσταση ενός κενού εντός της μόνωσης (μοντέλο) έχει χρησιμοποιηθεί από καιρό για τη μελέτη των μεταβατικών φαινομένων που δημιουργούνται από μία μερική βλάβη του κενού εντός της μόνωσης. Ως εναλλακτική λύση για την χωρητική αναπαράσταση του κενού (μοντέλο) εντός της μόνωσης, η έννοια της επαγώμενου φορτίου έχει εισαχθεί από ερευνητές του Τεχνολογικού Πανεπιστήμιου της Δανίας εκφράζοντας την έντονη κριτική κατά της χωρητικής μοντελοποίησης του κενού εντός της μόνωσης..

Αυτή η διατριβή συζητά και αντικρούει αυτή την κριτική και εκμεταλλεύεται τις δυνατότητες και τις αδυναμίες της κλασικής χωρητικής μοντελοποίησης του κενού εντός της μόνωσης από θεωρητική άποψη. Προτείνονται τρία νέα μοντέλα: α) μια βελτιωμένη έκδοση του κλασικού χωρητικού μοντέλου, β) ένα χωρητικό μοντέλο που βασίζεται στην επαγωγή του φορτίου και γ) ένα προηγμένο χωρητικό μοντέλο του κενού εντός της μόνωσης που βασίζεται σε έννοιες streamer. Επιπλέον, στην παρούσα διατριβή, οι γεωμετρικές και φυσικές παράμετροι που διέπουν το κλασσικό χωρητικό μοντέλο του κενού εντός της μόνωσης (σε βελτιωμένη έκδοση), όπως επίσης και τα άλλα δύο προτεινόμενα μοντέλα, υπολογίζονται με τη χρήση της κλασσικής ηλεκτρομαγνητικής θεωρίας, με έννοιες του μηχανισμού streamer και της φυσικής που διέπει την ηλεκτρική εκκένωση αερίων. Τα τρία μοντέλα χρησιμοποιούνται για να αναπαράγουν μεταβατικά σήματα (PD σήματα) και να εξετάσουν την διάδοση τους κατά μήκος του πυρήνα ενός τυπικού καλωδίου μέσης τάσης σε πραγματικές συνθήκες δικτύου ηλεκτρικής ισχύος. Τα

αποτέλεσμα των τριών μοντέλων συγκρίνονται με πειραματικά διαθέσιμα δεδομένα που λήφθηκαν από τη διεθνή βιβλιογραφία.

ACKNOWLEDGEMENTS

Being a part time PhD student, with a full time job, family and kids is not an easy task at all. For this reason, first of all I would like to thank my family who believed in me and supported me in this long way.

Also I would like to express my deepest gratitude to my supervisors, Dr. Elias Kyriakides and Dr. George. E. Georghiou for directing the course of this study and for their patience in reading and correcting previous drafts of this work. Throughout my work they provided encouragement, sound advice, good teaching, good company, and lots of good ideas. Without their guidance, inspiration, and support this work would not have been completed.

I am indebted to the rest of the members of my dissertation committee who made invaluable comments for the improvement of this work: Dr. Stavros Iezekiel, Dr. Charalambos A. Charalambous, Dr A. Kyprianou and Dr Michail G. Danikas. This dissertation is more accurate and more clearly expressed because of their input.

Finally, I would like to dedicate this dissertation to my father, even though he is not among us any more. I believe that wherever he is, he is going to be very proud…

LIST OF PUBLICATIONS

Refereed Archival Journal Publications

1. Z. Achillides, G. E. Georghiou, and E. Kyriakides, "Partial discharges and associated transients: the induced charge concept versus capacitive modeling," *IEEE Transactions on Dielectrics and Electrical Insulation*, vol. 15, no. 6, pp. 1507-1516, Dec. 2008.
2. Z. Achillides, E. Kyriakides, and G. E. Georghiou, "Partial discharge modeling: An improved capacitive model and associated transients along medium voltage distribution cables," *IEEE Transactions on Dielectrics and Electrical Insulation*, pp. 1-11 (submitted May 2012, accepted for publication Oct. 2012 with minor corrections.)

Refereed Archival Journal Publications (submitted)

1. Z. Achillides, G. E. Georghiou and E. Kyriakides, "An advanced capacitive model of void," *IEEE Transactions on Dielectrics and Electrical Insulation*, pp. 1-10 (submitted Jan. 2013).

Refereed International Conference Proceedings

1. Z. Achillides, G. Georgiou, and E. Kyriakides, "A theoretical analysis of the capacitive modeling and the induced charge concept in partial discharges," *XVII International Conference on Gas Discharges and their Applications* (*GD2008*), Cardiff, Wales, pp. 1-4, Sep. 2008.
2. Z. Achillides, E. Kyriakides, and G. Georgiou, "Partial discharges and induced transients along medium voltage distribution cables," *International Workshop on Deregulated Electricity Market Issues in South-Eastern Europe* (*DEMSEE08*), Nicosia, Cyprus, paper no. 139, pp. 1-6, Sep. 2008.
3. Z. Achillides, E. Kyriakides, G. E. Georgiou, and A. Kyprianou, "A comparison of matched filter and wavelet transforms for the detection of partial discharges in high voltage cables," *5th Mediterranean IEE Conference and Exhibition on Power Generation, Transmission, and Distribution* (*MedPower '06*), Eilat, Israel, pp. 1-6, Nov. 2006.

TABLE OF CONTENTS

LIST OF SYMBOLS

C	Approximate effective ionization coefficient ($Pa^{\beta-1}m^{\beta-1}V^{-\beta}$)
C_1	Capacitance of the upper part of insulation (F)
C_2	Capacitance of the lower part of insulation (F)
C_v	Capacitance of the void (F)
C_{dipole}	Increase of system capacitance caused by charge separation (F)
$C_{induced}$	Capacitance due to the induced charge (F)
$\boldsymbol{D}$	Electric flux density (C/m^2)
$\boldsymbol{E}$	Electric field strength (V/m)
$\boldsymbol{E_l}$	Limiting field for ionization (kV/mm)
$\boldsymbol{E_i}$	Inception field for discharge (kV/mm)
e	electron charge (C)
ε_o	Permitivity of free space (F/m)
ε_r	Relative permitivity
I	Current (A)
$\boldsymbol{J}$	Current density (A/m^2)
K_{cr}	Coefficient of critical electron number in avalanche
m	Electron mass (kg)
$\boldsymbol{P}$	Polarization (C/m^2)
p	Pressure (Pa)
Q	Charge (C)
Q_b	Bound charge (C)
Q_{bi}	Bound induced charge (C)
Q_f	Free charge (C)
q_i	Induced charge (C)
Q_{min}	Minimum physical charge within the void for streamer inception (C)
R_a	Position of upper side of void (m)
R_b	Radius of the insulation (m)
R_c	Radius of the core of the cable (m)
R_{diss}	Resistance of ionized path for the improved capacitive model (Ω)
R_s	Radius of sheath of the cable (m)
$R_{streamer}$	Resistance of ionized path for the advanced capacitive model (Ω)
R_v	Radius of void (m)

R_V	Resistance of space charge free void (Ω)
R_x	Location of the void (m)
R_1	Resistance of upper part of insulation (Ω)
R_2	Resistance of lower part of insulation (Ω)
Za	Length of the cylidrical void (m)
β	Approximate effective ionization coefficient
B	Characteristic of the gas (constant)
γ	Ratio of streamer channel field to critical field
ΔV_c	Change in the voltage on the core of the cable due to PD activity (V)
$\boldsymbol{\eta}$	Normal unit vector
λ_o	Dimensionless scalar function of the void location
σ	Conductivity of streamer (S/m)
Φ_{max}	Offset angle (radians)

LIST OF FIGURES

LIST OF TABLES

CHAPTER 1

INTRODUCTION

1.1 Motivation

COMPOSITE insulation materials used as insulating media in power cables contain small gaseous voids caused by the manufacturing process and/or by mechanical stress. Voids have deleterious effects on the electrical performance of solid insulation, as they are the source of discharges, which in turn cause deterioration, and eventually breakdown of the insulation.

The dipole charge distribution and discharge activity caused by a Partial Discharge (PD) induces charges on the conductor of the cable, which partially bridge the insulation. To effectively analyze the PD signal an electrical model of the breakdown void is required. This model must be capable of representing the physical phenomenon and accommodating the transients related with the PD activity.

The main motivation of this work is to understand the physical process regarding the partial discharge mechanism and to improve the performance of the existing partial discharge models, in order to replicate and estimate the transients generated, travel and attenuated by partial discharge activity along the core of medium voltage distribution cables. The simulation results generated by breakdown voids of radii of 0.5, 1 and 1.5 mm, located in the middle of the insulation of an XLPE medium voltage cable, will be compared to laboratory data obtained from the international literature,

1.2 Literature Review

This section describes briefly the main scholarly articles considered in this work and which are directly related to the scope of this research. The references below are discussed in detail in the relevant chapters of the thesis.

For sufficient representation of PD activity a model of a breakdown void capable of representing the physical phenomenon and accommodating the transients related to the PD activity [1] as faithfully as possible is more than a necessity. For this particular reason, Gemant and Philippoff in 1932 developed the simplest electrical representation of a defect (void) within the insulation, known as the capacitive model [2]. The void is represented by a capacitor and discharges are simulated as discharges of this capacitor. As a further improvement of this model, Whitehead replaced the spark gap with an

electronically controlled device [3]. For even better accuracy, Paolleti and Golubev have included in the model the shunt conductance of the healthy part of the insulating material and void [4].

As an alternative to the capacitive model of void (which is based on the change of the capacitance of the system during breakdown conditions), Crichton, Karlsson and Pedersen introduced the induced charge concept [5] and criticized the capacitance model. The criticism was based on the absence of any change in capacitance during the discharge process, the absence of a Laplacian field where the void is created and the absence of an equipotential surface at the wall of the void [1], [5, 6].

There are two methods to calculate the induced charge on the conductive part(s) of a system (due to the presence of space charges): the direct and the indirect methods. The direct method is a theoretical one and is based on the Maxwellian and or quasi-molecular description [1]. The indirect method is an experimental method and calculates the induced charges on the electrodes, by taking measurements on the system under consideration before and after the discharge occurs [1, 7].

The induced charge concept has been criticized in [8] by Danikas, based on measurements presented in [9], but this criticism was opposed in the discussion of this paper [8] by McAllister by concluding (based on [6]) that the capacitance invoked in the model does not exist in reality. Further, the induced charge concept (as presented in [5]) has been modelled in PSpice in [10].

Since the introduction of the induced charge concept in the mid 90's there has been an on ongoing dispute regarding the validity of each model. For this reason, laboratory measurements were carried out by Danikas to validate the two models [11]. The outcome of this work, as discussed in [11] and supported by [12], concluded that the induced charge model is more apropriate to estimate the magnitude of discharge, at least for initial conditions, It further concluded that intitially the streamer type of discharges are prevalent.

As a step forward to the above research work the two models were merged together, leading to a new proposed model as presented and discussed in [13]. The new proposed model is a part of this thesis.

1.3 Contribution

Since 1932 and until the mid 90's the capacitive model of void was utilized in order to replicate partial discharge signals. During the mid 90's scientists and engineers from the technical University of Denmark proposed a new model (based on the induced charge concept) and criticized the classical capacitive model relating the capacitance of a gaseous void as a trivialization of electric field theory and lack of knowledge. As a consequence of this criticism, the capacitive model of void was almost since then abandoned and models based on the induced charge concept have emerged.

In this work the potential and weakness of the capacitive model are discussed, the criticism on the capacitive model is argued and the correlation between the induced charge concept and the change in capacitance (capacitive model) is proved. The following are the main contributions of this work:

(a) The physics relating bound charges within dielectrics and free charges on the conductor's surface is discussed and proved.

(b) The transients related to change in capacitance is proved.

(c) The induced charge concept and change in capacitance are correlated.

(d) The Poissonian field in relation to bound and free charges is correlated with the truthfulness of the capacitive model of the void.

(e) The physics and transients relating the transformation of an insulating material into a conductive one under the influence of an external electric field are discussed and proved.

(f) An analytical method is proposed for calculating all elements (*R*-*L*-*C*-*G*) of the capacitive model of void for cylindrical void(s) within the insulation of medium voltage cables by utilizing classical electromagnetic equations in integral form.

(g) Gas discharge physics (streamer concept) is utilized in order to calculate the conductivity of a breakdown void.

(h) By utilizing (a) to (g) three new capacitive models are proposed: i) a capacitive model of void based on the induced charge concept, ii) the improved capacitive model of void, iii) the advanced capacitive model of void based on streamer concepts.

(i) Modeled the three proposed models in MATLAB/Simulink

(j) Modeled the high frequency components of medium voltage cable in MATLAB/Simulink for time domain analysis

(k) A code in MATLAB was developed for calculating elements for the three

proposed models as described in (f)-(g) and the high frequency components of the Medium Voltage (MV) cable under investigation.

(l) Examined the transients generated by the three models in MATLAB/Simulink against laboratory measurements.

(m) The correlation between the induced charges and relative permittivity is proved.

The research work described in this dissertation is a contribution to electric power distribution engineering, electromagnetism and cold plasma theory related to partial discharges. Three new capacitive models of void are proposed and discussed in this thesis: a) The improved capacitive model, b) A new capacitive model of the void based on induced charge concept c) An advanced capacitive model of void based on streamer concepts. Further an analytical method is proposed for calculating all the components for the above models for cylindrical voids. Cylindrical voids of different diameters are utilised in the models and the simulated outcomes are compared and discussed against laboratory results obtained from international literature of partial discharges.

1.4 Outline of the thesis

This thesis is organized as follows. In Chapter 2 the potential and weaknesses of the classical capacitive representation of the void are exploited, the induced charge concept is introduced, and the criticism related to the capacitance model is argued. Further, the relationship between the induced charge concept and the change of capacitance is demonstrated and three new capacitive models are proposed and discussed by utilising the relevant physics.

In Chapter 3 an analytical method for calculating all parameters of the three proposed models is demonstrated and proposed based on classical electromagnetism. In Chapter 4 the electrical network of Pafos town is presented and modeled in MATLAB/Simulink. Further, the high frequency dependent components (R-L-C-G) of the medium voltage cable under investigation are calculated and utilized associated with the proposed capacitive model of void.

In Chapter 5 the simulation results of the classical capacitive model and the three proposed models are presented. In Chapter 6 the theoretical performance of the three proposed model is evaluated and the high frequency and low frequency propagation characteristics of the MV cable are compared and discussed. The simulation results of

Chapter 5 are compared against laboratory measurements obtained from the international literature and the MATLAB/Simulink performance is evaluated in terms of the generation and propagation of partial discharge signals.

In Chapter 7 an outline of the scope and the contribution of this thesis is presented and discussed and an overall assession of the performance of the three proposed models is performed. A critical discussion is included, which identifies the preferred model to be used. Relevant future work is also proposed.

CHAPTER 2

VOID MODELING: THE PHYSICS

In this Chapter the three proposed capacitive models of void are introduced, discussed and justified based on the relevant physics. Furthermore the capacitive modeling and change of capacitance is proved in relation to the induced transients and the criticism on the capacitive model of void is discussed and counter argued.

2.1 The Capacitive Model of Void

a. Capacitance

Consider two oppositely charged conductors M_1 and M_2 surrounded by air as shown in Fig. 2.1. Conductor M_1 carries a total positive charge of Q and M_2 carries an equal negative charge. There are no other charges present and the total charge of the system is zero.

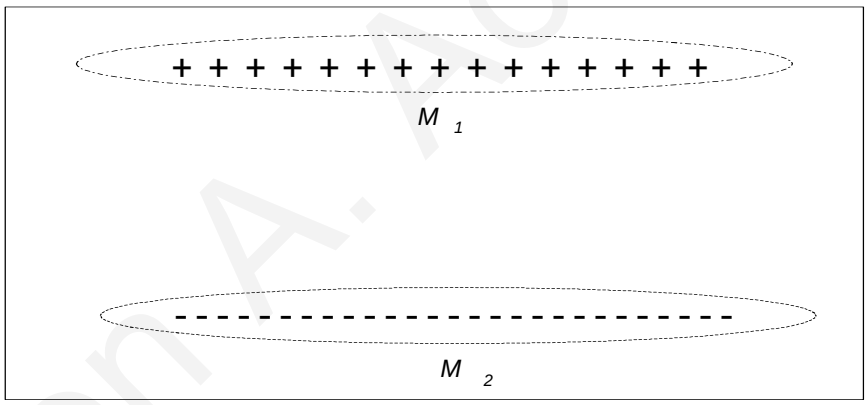

Fig. 2.1. Two oppositely charged conductors

If the potential difference between the two conductors is V, then the capacitance (between the conductors) is defined as the ratio of the magnitudes of the total charge on either conductor to the potential difference between the conductors,

$$C = \frac{Q}{V} = \frac{\iint \vec{D} \bullet \vec{ds}}{-\int \vec{E} \bullet \vec{dl}} \tag{2.1}$$

where $\boldsymbol{D}$ is the electric flux density and $\boldsymbol{E}$ the electric field strength.

Fig. 2.2 shows a parallel plate capacitor with each of its plates having an area S, containing two dielectrics of permittivity ε_1 and ε_2, and thickness d_1 and d_2 respectively.

It can be shown that a double dielectric capacitor is effectively two capacitors in series as depicted in Fig. 2.2 and the total capacitance is given by,

$$C_t = \frac{1}{\frac{1}{C_1} + \frac{1}{C_2}} \tag{2.2}$$

where C_1 and C_2 are the capacitances due to the two different dielectrics.

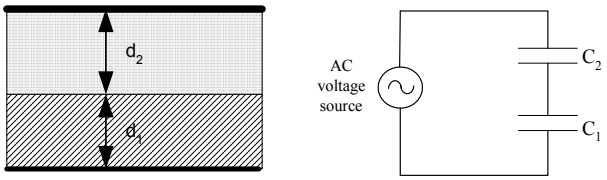

Fig. 2.2. A parallel plate capacitor containing two dielectrics is effectively two capacitors in series

b. The prime electrical model of void

Based on (2.1) and (2.2), Gemant and Philippoff in 1932 [2] developed the simplest electrical representation of any kind of defect within the insulation known as the classical capacitance model as shown in Fig. 2.3. According to this model, the internal cavity (void) can be represented by the capacitance C_c in the equivalent circuit, while C_b is a resultant capacitance of the healthy dielectric in series with the void and C_a is the capacitance of the rest of the insulation. Void breakdown is simulated by turning on the switch parallel to C_c, when the voltage across C_c reaches the breakdown value. The voltage across the switch (prior to breakdown) is given by:

$$V_{switch} = V_{dc} \frac{C_b}{C_b + C_c} \tag{2.3}$$

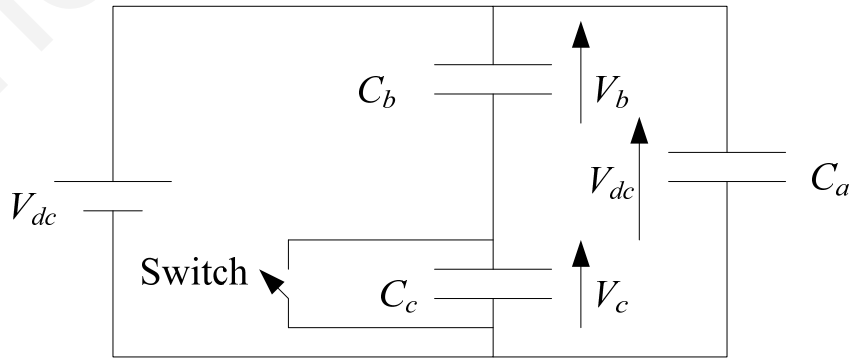

Fig. 2.3. The classical capacitive model of void [2]

For an improved representation of the operation of the breakdown of the void, Whitehead replaced the switch by a thyristor controlled device as shown in Fig. 2.4. In this case, the breakdown voltage can be set at any desired value in accordance to the

breakdown level of the void [3], [15]. Capacitance C_v represents the capacitance of the void, C_{s1} and C_{s2} represent the capacitances of the healthy insulation and C_p the capacitance of the rest of the system.

As a further improvement to the capacitance model, the shunt conductance of the healthy insulation and the void has been included in the model as shown in Fig. 2.5 [4].

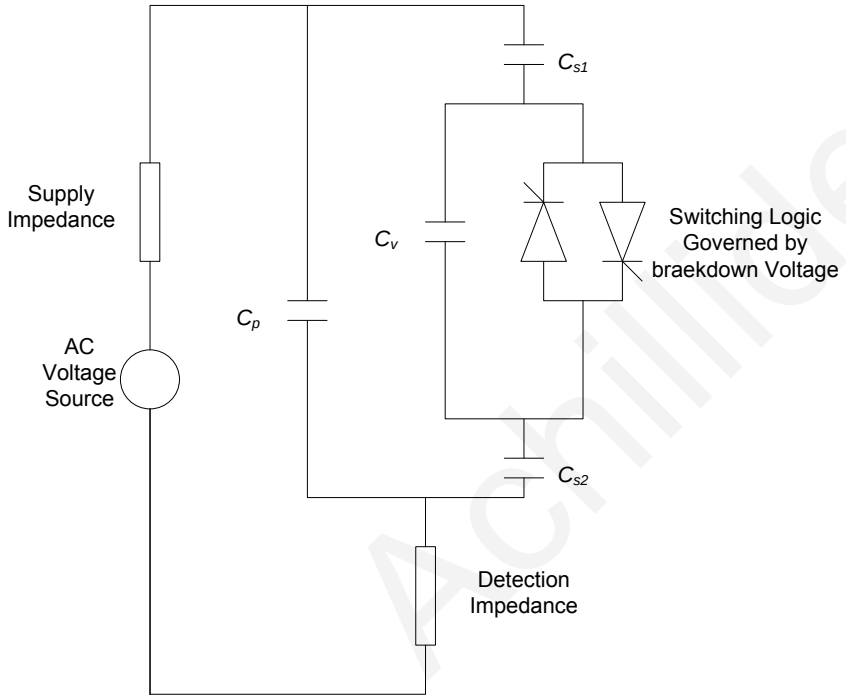

Fig. 2.4. Whitehead's equivalent circuit [2]

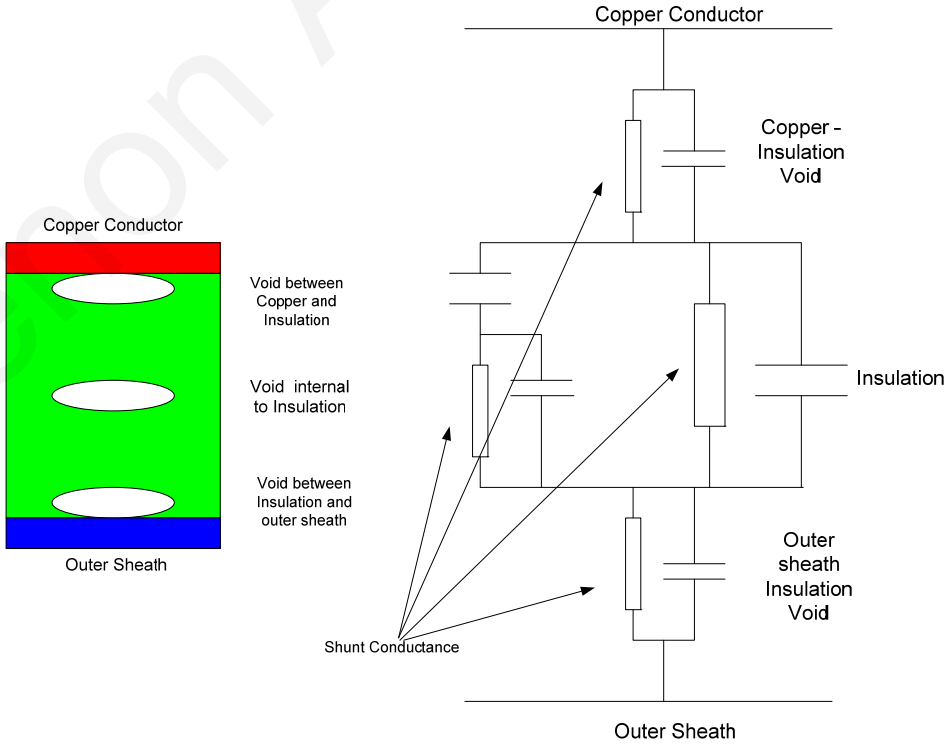

Fig. 2.5. Classical capacitive model with shunt conductance [4]

2.1.1 Void Modeling: Capacitors in Series Reflecting Multiple Dielectric Layers – The Physics Behind

a. The nature of dielectric materials

The characteristic which all dielectric materials have in common whether solid, liquid, or gas, crystalline in nature or not, is their ability to store electrical energy. This storage takes place by means of a shift in the relative position of the internal (bound) positive and negative charges against the normal molecular and atomic forces. These are not free charges and they cannot contribute to conduction. They are called bound charges, in contrast to the free charges that determine conductivity**.** The actual mechanism of charge displacement differs in various dielectric materials. Some molecules termed polar molecules have a permanent displacement at the centers of neutral position between positive and negative charges and each pair of charge acts as a dipole. Normally, these dipoles are oriented randomly in the interior of the material, but under the influence of an applied electric field, a small degree of order is imposed on their chaotic behavior and that is sufficient to establish a polarization field of significant magnitude.

A non-polar molecule (such as H_2, N_2, O_2) does not have this permanent dipole arrangement (Fig. 2.6(a)), but under the influence of an external field the negative and positive charges shift in opposite directions (Fig. 2.6(b)) against their mutual attraction and produce a dipole, which is aligned with the external electric field [14].

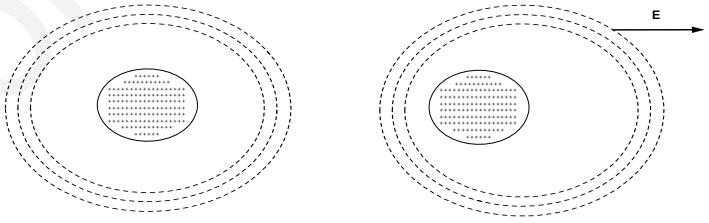

(a) Non-polar molecule.

(b) Non-polar molecule under the influence of an external field.

Fig. 2.6. Atomic/molecular polarization

b. Void modeling: Capacitors in series-theoretical validation

As has been discussed in Section 2.1 and in relation to Fig. 2.2, two metal plates (conductors) separated by a two-layer dielectric can be represented by two capacitors in series. However, this electrical representation (of the two dielectrics) gives the possibility

to extract electrons in that case where a resistor is connected across the lower capacitor as shown in Fig. 2.2. This is in conflict with the nature of dielectric materials as discussed in the previous paragraph. The 'stored' charges between the boundaries of the two dielectric layers are bound charges and are not available as a pool of free charges. To extract them, a third conducting plate is required. If there was a third conducting plate between the interfaces, then we would expect to find charges of opposite sign on this plate and the magnitudes of these charges to be equal. This is because those electric lines will not pass directly from one outer plate to the other but would terminate on one side of the third conducting plate and then would continue on the other side**.** For this particular reason, the capacitance is unchanged provided that the added plate is of small thickness (in order to avoid any change of insulation thickness) [14, 16]. In fact, if there were to be no conducting plate, the capacitance would still be unchanged.

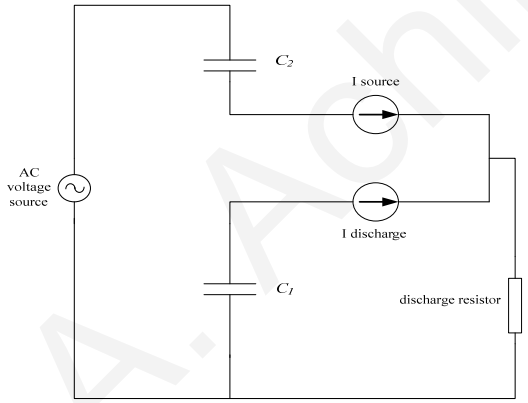

Fig. 2.7. Simplified capacitive model simulating large discharge current**.**

This phenomenon creates a major obstacle for the capacitance model of void (as presented in Figs. 2.3, 2.4 and 2.5). In the above configuration the void is supposed to be created in the middle of the insulation (Fig. 2.5) where no conducting plate exists**.** When breakdown occurs (which is simulated by turning on the thyristor shown in Fig. 2.4), then the fully charged capacitor (C_1) will be discharged rapidly and a very large initial discharge current is expected to flow (Fig. 2.7). This is physically impossible due to the absence of any conducting material within the insulation of the cable. This discharge current flow from the capacitor does not represent by any means the generated signal caused by a PD and consequently it does not represent the flow of space charge (current) within the void under breakdown conditions either.

Despite the weakness of the capacitance model to represent electrically the magnitude and physics behind a PD signal (e.g., space charge – avalanche breakdown and streamer theory), the capacitance model is capable of representing sufficiently the transients

related to a breakdown void (apparent charge/current – local voltage dips) which are the most important and easier to detect signals as far as PD signal detection and evaluation is concerned [1]. The importance of the generated transients is presented in the second part of the equation below,

$$I_{pi} = \frac{dq_i}{dt} - \sum_{j=0}^{N} C_{ij}\left[\frac{d\Delta U_i}{dt} - \frac{d\Delta U_j}{dt}\right] \tag{2.4}$$

where U_i and U_j are the potentials of the i^{th} and j^{th} electrodes of a space charge free system consisting of N electrodes and C_{ij} is the partial capacitance between these electrodes. I_{pi} is the total current of the i^{th} electrode in a space charge system and is the sum of the induced charge (first part of (2.4)) caused by space charge and the charge (second part of (2.4)), which is linked to the partial capacitances and new potentials of the electrodes. The first part of (2.4) is normally of very short duration as is related with the creation of a PD**.** The second term depends strongly on the impedances of the external circuit and will therefore in most cases dominate over the observed transients.

Although in (2.4) the capacitance of the system is assumed to be constant and in fact this equation was meant to be used to support the absence of any change in capacitance [1], in the following discussion it is going to be demonstrated how the capacitance model (which is directly related to changes in capacitance) associated with the external impedance of the circuit reflects with sufficient accuracy (actually produces) the right second part of (2.4).

c. Transients related to change in capacitance

Consider an underground power cable where it is assumed that a void is created at the far end of the cable within the insulation between the core and the outer sheath of the cable as shown in Fig. 2.5 (assuming no conducting plate exists). Based on the discussion in Sections 2.1.2-2.1.3 and by taking into account the impedance of the void-free part of the cable and the rest of the electrical network impedance (the impedance of the external circuit Z and C_s), then the void (and insulation above and below the void) can be modelled as shown in Fig. 2.8(a) (C_1, C_2, C_3). The capacitive representation of the void can be further seen as a simple potential divider as shown in (2.3), and can be modelled as in Fig. 2.8(b). For this case it is important to mention that the relative permittivity of air (within the void) is lower than the relative permittivity of the insulating medium of the cable, and as a result a large percentage of the system's operating voltage is expected to

emerge across the void (C_2 and V_2 of Figs. 2.8(a) and 2.8(b).

During a simulated breakdown of the void (by turning on the switch of Figs. 2.8(a) and 2.8(b) as discussed in Section 2.1.3) (and even for physical breakdown [17]), the voltage across the void was shown to collapse rapidly to almost zero. This produces a sudden flow of a fast transient current in the circuit (due to the voltage difference between the ac voltage source and the opposing voltage across C_1 and C_3), which in turn creates a fast transient voltage signal due to the sudden voltage drop caused by the impedance of the external circuit. Both signals will travel and will be attenuated along the core of the cable.

The classical capacitive model of void as shown in Figs. 2.3, 2.4, and 2.5 associated with the impedance of the external circuit (Z and C_s) as shown in Fig. 2.8(a) reflects adequately the second part of (2.4), and possesses the potential to represent and examine the transients generated from a breakdown void. In the next section the criticism on the capacitive model of the void expressed in the literature is discussed.

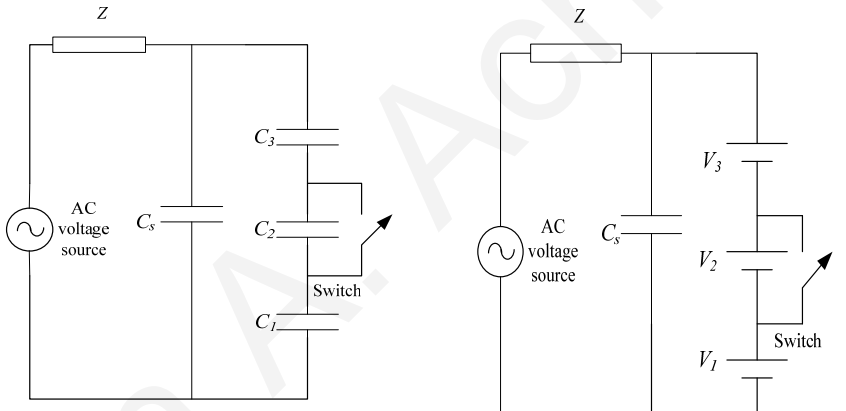

(a) Classical capacitive model of void in conjunction with the impedance of the healthy part of the cable

(b) Classical capacitive model of void as a potential divider

Fig. 2.8. The classical capacitive model of void associated with the external impedance of the circuit

2.1.2 Criticism on the Capacitance Model of a Void

The capacitive model of the void has been criticized based on three major areas [1, 5, 6, 18]:

(a) The induced charge concept suggests the absence of any change in capacitance during the discharge process.

(b) The presence of space charge and eventually the absence of a Laplacian field where the void is created.

(c) The absence of an equipotential surface at the wall of the void.

These major objections are discussed below.

a. The induced charge concept

In [1] and [5] the induced charge concept is introduced and discussed against capacitance modeling. The primary source of these induced charges is the charges, which, as a result of partial discharge activity, are distributed around the wall of the void, forming dipole moments at the dielectric interface. In [5] the induced charge concept (q_i) is presented indirectly, relating the measured transient and the induced charge. This is expressed as the difference between the charge on the electrode when discharges have occurred, and the charge, which would have been on the electrode, with the system being discharge-free. This concept is presented in (2.5), which is based on Green's reciprocity theorem [19]:

$$(U - \Delta U)Q = U(Q + \Delta Q) + q_i \tag{2.5}$$

where Q and U are the charge and voltage potential (of the electrode) prior to the discharge activity. ΔU is the voltage on the electrode, ΔQ is the charge transfer to the electrode from the source, and q_i is the induced charge on the electrode due to the void. All these parameters are the values just after the discharge quenched. Substituting $Q=CU$ (where C is the capacitance of the system) in (2.5), leads to:

$$q_i = C\Delta U + \Delta Q \tag{2.6}$$

In [1] the induced charge concept (q_i) is presented directly by (2.7) below and is based on the superposition theorem, and Green's reciprocity theorem for electrostatics,

$$q_i = -\int_v \lambda_i \rho d\Omega - \int_s \lambda_i \sigma dS \tag{2.7}$$

where ρ is the volume charge density, σ the surface charge density of the void and λ_i is a dimensionless function that depends only on the location of the void [1]. By applying Green's reciprocity theorem on (2.7),

$$q_i = -\int_v \frac{V}{U}\rho d\Omega - \int_s \frac{V}{U}\sigma dS \tag{2.8}$$

where, V represents the scalar potential at $d\Omega$ and dS, when the electrode is at potential U and the system is space charge-free. V can then be calculated by solving Laplace's equation:

$$\nabla^2 V = 0 \tag{2.9}$$

Based on (2.5) and (2.6), it is claimed in [5] "that the capacitance of the system is not affected by the partial discharge and that as a consequence, the transients cannot be related to the change in capacitance."

b. The presence of space charge and the absence of a Laplacian field

The criticism is extended in [1] where it is claimed, "that the presence of space charges (as presented in (2.8)) creates a Poissonian field, which negates a meaningful use of $Q = CV$." Also in [18] it is claimed that "The proper concept of capacitance implies that the field between the electrodes is Laplacian and the field is not Laplacian if space charges are present" [20, 21].

c. The absence of equipotential surface at the wall of the void

The criticism is further extended in [6] where it is claimed that "the void wall is not an equipotential surface and thus to ascribe a capacitance to a void violates the basic definition of capacitance, concluding void capacitance does not exist." As an example, the voltage (Φ_w) at the surface of a spherical void as described in [22] is given below,

$$\Phi_w = \frac{3\varepsilon_r}{2\varepsilon_r + 1} RE_0 \cos\Theta \tag{2.10}$$

where ε_r is the relative permittivity, Θ is the spherical coordinates (Φ,Θ,r) and R is the radius of the sphere and E_0 is the uniform electric field.

2.1.3 Discussion of the Criticism on the Capacitive Model

The criticism on the capacitance model as presented in Section 2.1.2 is counter argued in the following discussion.

a. Change in capacitance during discharge process

The criticism on the classical capacitance model (which is based on the change of the capacitance of the system) as presented in Section 2.2.1 and in [1, 5], is based on the assertion that the PD transients are not related to any change in capacitance of the system. Instead, the PD transients are based on the induced charge concept which is summarized by (2.6) and related to (2.7) and (2.8). The absence of any change in capacitance during the discharge process can be opposed as follows:

First by substituting to (2.6): $\Delta Q = Q_{pi} - Q_x$ we get:

$$Q_{pi} = q_i + Q_x - C\Delta V \tag{2.11}$$

where Q_{pi} , is the total charge and ΔV is the change in voltage just after the PD quenched. Q_x and C are the total charge and capacitance of the system respectively before the PD activity and q_i is the induced charge. By also substituting $Q_x = CU$ to (2.11),

$$Q_{pi} = q_i + C(U - \Delta V) \tag{2.12}$$

where U is the voltage of the system before the PD activity. Finally, by substituting $Q_{pi} = C'(U - \Delta V)$ to (2.12),

$$C' = \frac{q_i}{U - \Delta V} + C \tag{2.13}$$

where C' is the effective (total) capacitance seen by the system just after the discharge has been quenched. Equation (2.13) was deduced from (2.6) (which is also included in [1]) and represents a change in capacitance, (as discussed in Section 2.1.4.3) which opposes the assertions made in [1] and [5]. Further, by taking into account that the charges (σ and ρ) of (2.8) form dipoles [17] and have a negative sign (electrons)–pointing towards the system's positive conductor, then the outcome q_i of (2.8) must be positive (Faraday's experiment) [23]. Also, by further considering that $U - \Delta V$ is positive, then the first part of (2.13) is positive and hence C' is greater than C.

As a result, (2.13) indicates not only a change in capacitance but also an increase in the overall capacitance of the system as predicted by the classical capacitance model. This increase in overall capacitance is also presented in Fig. 2.8 and reflected in (2.2) where the middle capacitance is bypassed (during simulated breakdown) resulting in an overall increase in the effective capacitance seen by the system as indicated in (2.13).

b. The Poissonian field and the absence of capacitance

Criticism on the capacitance model as presented in Section 2.1.2 is based on the fact that the field is not Laplacian if space charge is present as shown in (2.14) and the "proper" concept of capacitance requires the presence of a Laplacian field as shown in (2.9).

$$\nabla^2 V = -\frac{\rho}{\varepsilon} \tag{2.14}$$

In (2.14), ρ is the charge density, ε is the relative permittivity and V is the voltage. In the following discussion it is demonstrated that the above statement is in conflict with the nature of dielectrics associated with the presence of bound charges (as discussed in Section 2.1.4.1), which indicates the presence of a Poissonian field.

Consider Fig. 2.9, which represents a parallel plate capacitor with no dielectric material inserted between the conducting plates (vacuum).

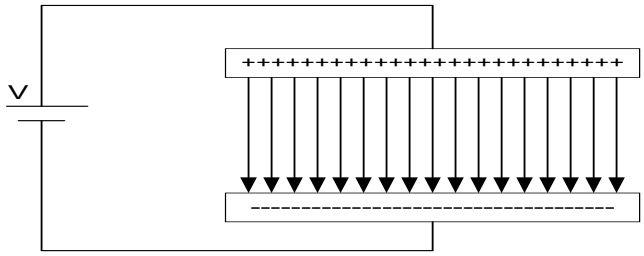

Fig. 2.9. Parallel plate capacitor with no dielectric material

The relationship between charges and voltage is given by:

$$Q_f = \frac{V \varepsilon_o A}{d} \tag{2.15}$$

where Q_f represents the 'free' charges on the conducting surface of the capacitor and V, A and d are the voltage, area and distance between conducting plates respectively.
By substituting $Q_f = CV$ in (2.15),

$$C = \frac{\varepsilon_o A}{d} \tag{2.16}$$

where C is the capacitance of Fig 2.9. In the presence of insulation between the plates, (2.16) becomes,

$$C' = \frac{\varepsilon_o \varepsilon_r A}{d} \tag{2.17}$$

Now we take a closer look at the behaviour of an insulator immersed in an electric field. Consider Figure 2.10a, which represents a parallel plate capacitor with dielectric material inserted between the conducting plates. As explained in Section 2.4.1 the inserted dielectric will store electric energy by means of a shift in the relative neutral position of internal (bound) charges, forming dipole moments p in each molecule (Fig. 2.10(b)). Polarization P is defined as the dipole moment per unit volume (Δv) given by,

$$\vec{P} = \lim_{\Delta V \to 0} \frac{1}{\Delta v} \sum_{i=1}^{n\Delta v} \vec{p}_i \tag{2.18}$$

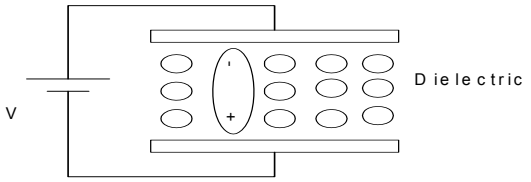

(a) Parallel plate capacitor with dielectric material inserted between the conducting plates.

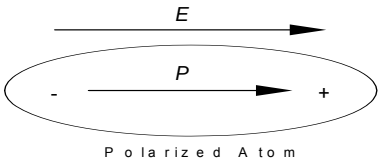

(b) Dipole moment *p* in each molecule.

Fig. 2.10. Insulator immersed in an electric field

In isotropic materials, polarization ***P*** can be directly related to the external electric field as,

$$\vec{P} = \varepsilon_o X_e \vec{E} \tag{2.19}$$

where X_e is the electric susceptibility of the material. Bound charges Q_b, a net surplus or deficit of electrons in the insulation can be related to polarization ***P*** as,

$$Q_b = -\oint_s \vec{P} \bullet \vec{ds} \tag{2.20}$$

Also bound charge Q_b is related to bound charge densities ρ_b, by:

$$Q_b = \oint_v \rho_b dv \tag{2.21}$$

Bound charge density ρ_b can be substituted in Maxwell's equations and obtain,

$$\vec{\nabla} \bullet \vec{\mathrm{E}} = \frac{\rho_f + \rho_b}{\varepsilon_o} \tag{2.22}$$

where ρ_f is the free charge density. Also,

$$\vec{E} = -\nabla \bullet V \tag{2.23}$$

and by substituting (2.23) into (2.22),

$$\nabla^2 V = -\frac{\rho_f + \rho_b}{\varepsilon_o} \tag{2.24}$$

Equation (2.24) relates the Laplacian operator of voltage with the bound (ρ_b) and free (ρ_f) charge density. Based on (2.24) three different cases will be considered.

b1. Capacitor with insulating material and void

Consider Fig. 2.10 and assume a small void within the insulation. By taking into account that there are free charges (σ) available on the wall of the void and within the volume of the void (ρ) then, (2.24) becomes,

$$\nabla^2 V = -\frac{\rho + \sigma + \rho_b}{\varepsilon_o} \tag{2.25}$$

Equation (2.25) indicates a Poissonian field within the insulator and the void, which not only opposes the concept of capacitance as described in Section 2.2.2 but also the presence of ρ and σ indicates an increase in the total capacitance (after PD activity is quenched) of the system as discussed in Section 2.3.1.

b2. Capacitor with insulating material only

In this case, σ and ρ are equal to zero, so (2.25) becomes:

$$\nabla^2 V = -\frac{\rho_b}{\varepsilon_o} \tag{2.26}$$

The presence of an insulator only, indicates the presence of the Poissonian field (due to bound space charges ρ_b) as shown in (2.26) and not a Laplacian field, which in turn naturally opposes the discussion in Section 2.2.2.

Equation (2.20) can be rearranged in the differential form giving:

$$\vec{\nabla} \bullet \vec{P} = -\rho_b \tag{2.27}$$

By adding (2.27) and (2.22),

$$\vec{\nabla} \bullet (\vec{E}\,\varepsilon_o + \vec{P}) = \rho_f + \rho_b - \rho_b \tag{2.28}$$

Substituting (2.19) into (2.28),

$$\vec{\nabla} \bullet (\vec{E}\,\varepsilon_o + X_e \vec{E}\,\varepsilon_0) = \rho_f + \rho_b - \rho_b \tag{2.29}$$

It is also known that,

$$\varepsilon_r = X_e + 1 \tag{2.30}$$

Substituting (2.30) into (2.29),

$$\vec{\nabla} \bullet \vec{E} = \frac{\rho_f + \rho_b - \rho_b}{\varepsilon_o \varepsilon_r} \tag{2.31}$$

and by substituting (2.23) to (2.31),

$$\nabla^2 V = -\frac{\rho_f}{\varepsilon_o \varepsilon_r} \tag{2.32}$$

In this particular case where no free charges exist within the insulator (i.e., $\rho_f = 0$), then (32) becomes,

$$\nabla^2 V = 0 \tag{2.33}$$

Equations (2.26) and (2.33) represent exactly the same situation (a void free capacitor with insulating material between the two plates) with two different outcomes: (2.26) represents a Poissonian field within the insulation whereas (2.33) represents a Laplacian

field within the insulation. This "strange" duality is the outcome that is linked to the assumption that the polarization ***P*** can be related linearly to ***E*** as shown in (2.19) and X_e with ε_r as shown in (2.30), which in turn makes consideration of the polarization, dipole moments and bound charges unnecessary [14] and eventually leads to an apparent absence of a Poissonian field as shown in (2.33). However when anisotropic materials and microscopic phenomena are considered then (2.26) should be used which in turn indicates the presence of a Poissonian field even in the total absence of any free charges (space charges). Based on the discussion in this section, (2.33) can only be seen as a simplification of (2.26) in order to make the solution of electrostatic problems easier.

b3. Capacitor without insulating material (vacuum)

In this particular case, no free or bound charges between the capacitor plates exist (vacuum) so (2.26) equals zero and it is the only true case where the field is Laplacian.

Summarizing this section, and by considering the structure of atoms forming the materials (and based on the discussion in Section 2.1.3) one can conclude that the only true Laplacian field exists in the presence of vacuum, because any kind of material under the influence of an external electric field will be either polarized and ionized or excited according to the nature of the material and the strength of the external electric field.

c. The absence of an equipotential surface

As has been described in Section 2.1.2 and based on [6] "The void wall is not an equipotential surface and thus to ascribe a capacitance to a void violates the basic definition of capacitance, concluding void capacitance does not exist." If we assume that this statement is correct, then the emergence of non-equipotential lines along the surface of a spherical void as described in [6] is caused simply by the specific geometry of the void (spherical void) as will be explained below.

Consider a parallel plate capacitor with a void, which is in the middle of an insulator, filled with air. In this case consider that the void has a perfect rectangular shape, similar to the geometry of the two metallic plates (conductors) enclosing the void as shown in Fig. 2.11.

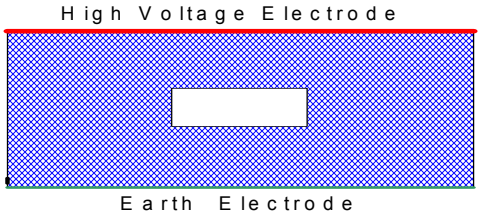

Fig. 2.11. Parallel plate capacitor with a void

At the point of interface between the two dielectrics the tangential component of the electric field E_t is equal to zero giving a zero value of F indicating an equipotential surface [24].

$$\int \vec{E}_t \bullet \vec{dl} = \vec{F} = 0 \tag{2.34}$$

Therefore, the presence of a non-equipotential surface on the walls of the void has nothing to do with the presence or the nature of the void itself within the insulation but only with the geometry of the void and of the conductors enclosing that void. In other words, the cavity (void) within the insulation can be modelled as capacitors in series; therefore, even a spherical void (where there is a non-equipotential surface on the walls of the void) can still be modelled by an infinite number of capacitors connected in parallel and separated by conductances as shown in Fig. 2.12. Each of these capacitors accommodates a small increment of voltage variation indicated by (2.10).

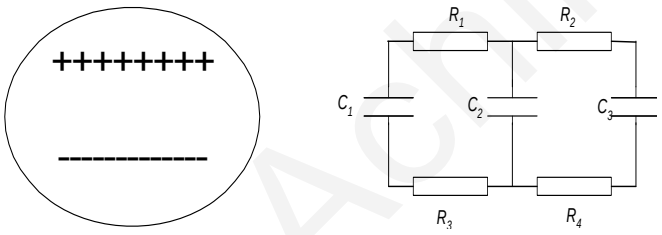

(a) Spherical void (b) Model of spherical void

Fig. 2.12. General model of a spherical void

2.2 The Improved Capacitive Model of Void

For adequate analysis of the transient behaviour of the electrical network under the influence of a breakdown void within the insulation of a medium voltage cable, a model based on passive components (R-L-C) of the electrical network is presented. The core of the proposed model is based on the classical capacitive model improved by the addition of the resistance of the ionized path in the following way.

2.2.1 Improved Capacitive Model – The Physics Behind: Classical Electromagnetics

Consider a parallel plate capacitor filled with an insulating material at both conducting sides and separated by air in its centre as shown in Fig 2.13(a) where $E_{ext,}$ E_{air} and E_{ins} represent the electric field across conducting plates, air and dielectric material respectively. These electric fields are related as follows:

$$\vec{E}_{ext} = 2\vec{E}_{ins} + \vec{E}_{air} \tag{2.35}$$

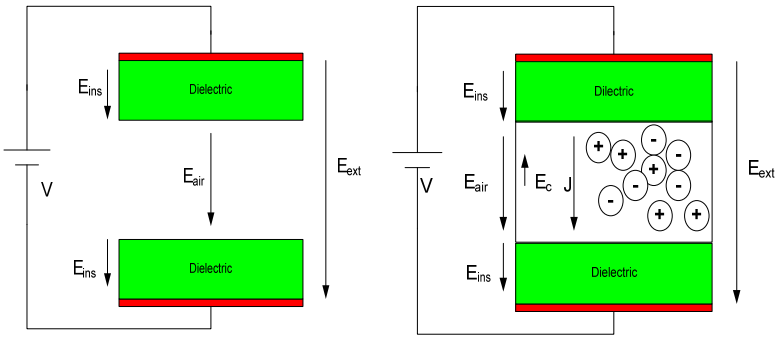

(a) Parallel plate capacitor –air filled

(b) Parallel plate capacitor with conductor – charge evolution phase I

Fig. 2.13. Parallel plate capacitor

Now let's assume that in the capacitor of Fig. 2.13(a) we place a conductor inside the centre of the capacitor occupying the whole volume of the air (Fig. 2.13(b)). At that time the electric field across air ($\boldsymbol{E_{air}}$) will penetrate the conductor and as a result the free electrons in the conductor will move in opposite direction of electric field leaving empty holes in the direction of the $\boldsymbol{E_{air}}$. This motion of the free electrons will produce a current density within the conductor ($\boldsymbol{J_c}$) which is related to $\boldsymbol{E_{air}}$ as follows:

$$\vec{J}_c = \sigma_c \vec{E}_{air} \tag{2.36}$$

where σ_c represents the conductivity of the conductor. At the same time this electron - hole separation will produce an internal electric field within the conductor ($\boldsymbol{E_c}$) which in turn will opposed the $\boldsymbol{E_{air}}$ and eventually reduce the current density $\boldsymbol{J_c}$. The $\boldsymbol{E_c}$ can be entered in (2.35) and (2.36) as follows:

$$\vec{E}_{ext} = 2\vec{E}_{ins} + \vec{E}_{air} - \vec{E}_c \tag{2.37}$$

$$\vec{J}_c = \sigma_c (\vec{E}_{air} - \vec{E}_c) \tag{2.38}$$

Initially $\boldsymbol{J_c}$ is very large but as time passes it will be reduced (Fig. 2.14(a)) and eventually becomes zero (Fig. 2.14(b)). At that time the internal electric field ($\boldsymbol{E_c}$) will be equal to $\boldsymbol{E_{air}}$ (Fig. 2.14(b)) thus (2.37) will become:

$$\vec{E}_{ext} = 2\vec{E}_{ins} \tag{2.39}$$

The result of this process is that $\boldsymbol{E_{ext}}$ will appear across the insulation and the field across the conductor will disappear

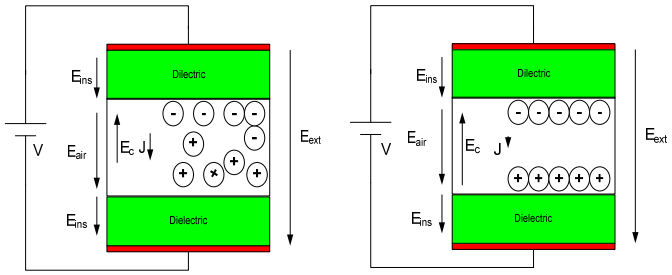

(a) charge evolution phase II (b) charge separation phase III

Fig. 2.14 Parallel plate capacitor with conductor-charge evolution.

The physical model of the insulation – void configuration (Fig. 2.15(a)) is represented by the classical capacitive model as capacitors in series and the PD breakdown is simulated by discharging of the void capacitor (C_{air}) by closing the ideal switch (Fig. 2.15(b)).

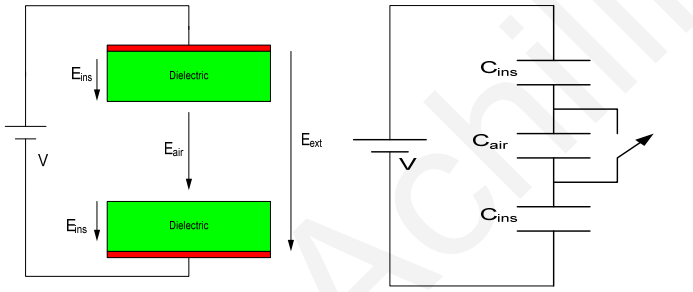

(a) Physical model (b) Electrical representation of physical model

Fig 2.15. Classical capacitive model.

As already discussed in [1] the discharge of this capacitor (C_{air}) by no means represents the physical breakdown mechanism of void, but is directly related to the induced transients generated on the associated conductor (induced transients will be discussed in detail in Chapter 6). Furthermore based on the following discussion it is going to be proved the correlation between the simulated discharge current of the capacitive model of void with the physical breakdown of void for streamer concepts will be established.

The current density relation is given by:

$$I = \iint \vec{J} \bullet dS \,, \tag{2.40}$$

By substituting (2.38) to (2.40) we have:

$$I_c = \iint \sigma_c (\vec{E}_{air} - \vec{E}_c) \bullet dS \,, \tag{2.41}$$

where I_c is the current flowing within the conductor. The electric field within the conductor $\boldsymbol{E_c}$ is related to conductor charge (Q_c) as follows:

$$Q_c = \iint \varepsilon_o \vec{E}_c \bullet ds \tag{2.42}$$

where ε_o is the relative permittivity of vacuum. For simplicity purposes we can assume that $\boldsymbol{E_c}$ and $\boldsymbol{E_{air}}$ are always normal to the conductive plates of the capacitor, so by solving (2.42) with respect to $\boldsymbol{E_c}$ and by substituting to (2.41) we get:

$$I_c = \iint \sigma_c (\vec{E}_{air}) \bullet dS - \frac{\sigma_c}{\varepsilon_o} Q_c \,, \tag{2.43}$$

By further expanding (2.43) we get:

$$I_c = \sigma_c A E_{air} - \frac{\sigma_c}{\varepsilon_o} Q_c \,, \tag{2.44}$$

where A is the area of the conductive plate of the capacitor. The solution of (2.44) is given below:

$$I_c = \sigma_c A E_{air} e^{-\frac{\varepsilon_o}{\sigma_c} t} \,. \tag{2.45}$$

The outcome of the discussion given in this subsection supported by (2.35-2.45) is of great importance in the following manner: One of the main disadvantages of the capacitive model of void is that the electrical representation of two or more dielectrics in series (by connecting capacitors in series) and by further by-passing this capacitor in order to simulate breakdown, gives the possibility to extract electrons from conductive plates of the capacitor as shown in Fig. 2.15(b) and eventually discharge this capacitor in an exponential decay. This is of course is in conflict with the nature of dielectric materials (as discussed in detailed in [13]) and against the nature of void itself where no conductive material exist on the wall of the Void.

As a result of the discussion in Section 2.2.1 and through (2.35)-(2.45) it has been demonstrated that by transforming the air, separating two insulators (Fig. 2.15(a) into a conductive medium (Fig. 2.15(b)) then:

a) The available free electrons within the conductive medium will produce a current density under the influence of the external electric field (2.36).

b) The magnitude of this current is related to dimension and conductivity of the conductive medium (2.44) itself.

c) This current has an exponentially decay form (2.45), similar to the expected discharge current flowing from a capacitor to a resistor.

In other words, the capacitive model of the void is not only capable to represent the transients induced on the system's conductor as discussed in [13] (and extended in

Section 6 of this work) but is also capable of replicating the physical current (I_c) flowing within the insulator after establishing breakdown conditions.

2.2.2 Improved Capacitive Model – The Physics Behind: Gas Discharge Concepts

Electric breakdown can be defined as the transformation process of an insulating material to a conducting one under the influence of an electric field [25]. For gas breakdown (cold plasma) there are two known mechanisms: Townsend's mechanism and the streamer theory of breakdown [26]. A streamer is moderately a weakly ionized thin channel formed from the primary avalanche in sufficiently strong electric field [25].

In the classical capacitive model, simulated breakdown of void is utilized by turning on the ideal switch (i.e., $R_{diss} = 0$, of Fig. 2.15), which eventually this means that a highly conductive channel – an ideal conductor should be established across the void capacitance C_v to simulate breakdown condition as discussed in section 2.2.1 In the streamer type of discharge this is not the case. The gas posseses a certain conductivity that makes the plasma a non-ideal conductor. This non ideal conductor is presented as R_{diss} in Fig. 2.16 of the proposed model and represents the conductivity (σ_c) of (2.45) in relation to discussion of section 2.2.1.The proposed model reflects partially the physical parameters governing the PD mechanism as presented in [17].

2.2.3 Improved Capacitive Model: The Electrical Model

The proposed electrical model is developed in MATLAB/Simulink as shown in Fig. 2.16. This electrical model is responsible for giving 'birth' to the PD simulated signal and is based on the low frequency components R-L-C of the cable/void representation. The reason for this is that the discharge process within the void itself is directly related to the strong external electric field which in this case is the 50 Hz power frequency voltage waveform.

The model represents an electrical equivalent circuit of the pre-, during- full breakdown and post- breakdown mechanism of a void. The upper and lower healthy parts of the insulation are represented by elements C_1, R_1 and C_2, R_2 respectively. The space charge-free void is represented by elements C_{void} and R_{void}. R_{diss} represents the resistance of the ionized path during breakdown conditions. Moreover, in the model of Fig 2.16, a voltage-controlled triggering device is utilized in order to control the ideal switch in the following way: when the voltage across the void reaches the minimum voltage level required to initiate the discharge-inception voltage (V_{on}), then the control circuit will turn on the ideal switch resulting in bypassing the elements C_{void} and R_{void}. When the voltage

across the void reaches a value where breakdown ceases (V_{off}), then the element "Ideal Switch" will be switched off. The values of V_{on} and V_{off} can be set to any desired value based on the theory and/or measurements of the PD. The model is also capable of handling different V_{on} and V_{off} pre-set values for positive and negative voltages across the void.

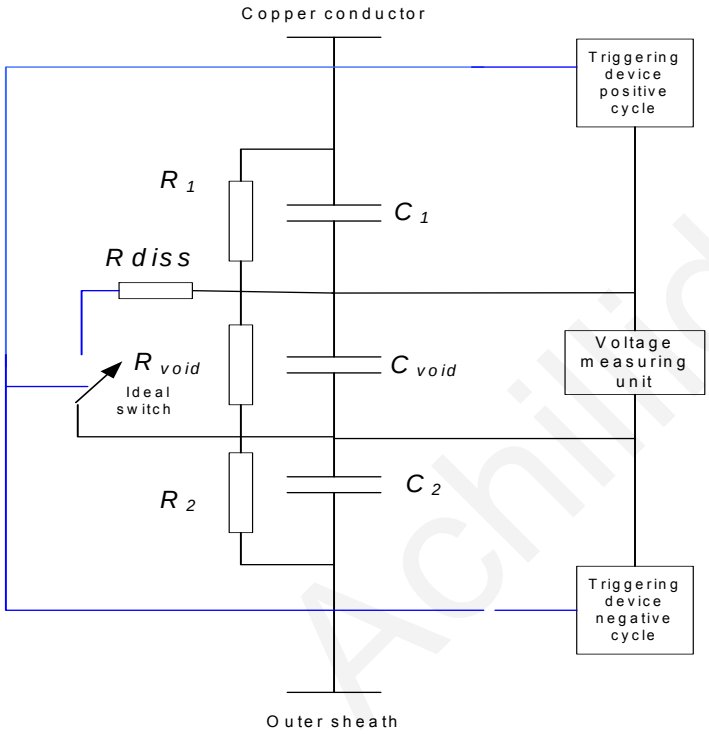

Fig. 2.16. Improved capacitive model

2.3 Bound Charges, Induced Charges and Change in Capacitance: A Model Based On the Induced Charge Concept

In this section it is demonstrated that bound charges (within insulating materials) which have the ability to induce free charges [13] on the conducting surface of the capacitor are responsible and are related to the increase of the total capacitance of the capacitor. Further, a new capacitive representation of the void based on the induced charge concept is presented.

2.3.1 Induced Charges in Relation with the Change in Capacitance

Consider Fig. 2.9, and equations (2.15) and (2.16), which represent the free charges on conducting plates and the capacitance of the capacitor respectively. Now consider Fig. 2.10(a) where bound charges Q_b (within the insulation) are capable of inducing free charges Q_{bi} on the conducting plates of the capacitor [13]. Equation (2.20) then becomes,

$$Q_{bi} = \oint_s \vec{P} \bullet \vec{ds} \tag{2.46}$$

By substituting (2.19) into (2.46),

$$Q_{bi} = \oint_s \varepsilon_o X_e \vec{E} \bullet \vec{ds} \tag{2.47}$$

By taking into account that C is the capacitance in the absence of any insulating material and assuming that C' is the capacitance of the capacitor with the insulation immersed between the plates then,

$$C' = \frac{Q_{f+}Q_{bi}}{V} \tag{2.48}$$

Expanding (2.48),

$$C' = C + \frac{Q_{bi}}{V} \tag{2.49}$$

Assuming no fringing and symmetrical geometry of the capacitor, (2.47) becomes,

$$Q_{bi} = \varepsilon_o X_e EA \tag{2.50}$$

Substituting (2.23) into (2.50),

$$Q_{bi} = \frac{\varepsilon_o X_e VA}{d} \tag{2.51}$$

and by substituting (2.51) and (2.16) into (2.49),

$$C' = \frac{\varepsilon_o A}{d} + \frac{\varepsilon_o X_e VA}{Vd} \tag{2.52}$$

Further simplification yields,

$$C' = \frac{\varepsilon_o (X_e + 1)A}{d} \tag{2.53}$$

Substituting (2.30) into (2.53),

$$C' = \frac{\varepsilon_o \varepsilon_r A}{d} \tag{2.54}$$

Equation (2.54) gives exactly the same result as the classical (2.17), which represents the value of the capacitance (based on $\boldsymbol{D} = \varepsilon_r \boldsymbol{E}$) of a parallel plate capacitor with an insulating material between the plates. Through (2.46)-(2.54) it has been proved that bound charges, which are able to induce free charges, contribute to the increase of the capacitance of the capacitor, which in turn indicates a change in capacitance as has been discussed in this work. Also according to [1, 5, 6, 18], if the space charges within the

void (forming dipole moments) make the capacitive representation of the void inappropriate, then following the same logic (as it has been proved through (2.18)-(2.33) and (2.46)-(2.54)), a normal capacitor with insulation (polarized under the influence of external electric field) between its plates would not have been a "proper" one due to the presence of bound charges.

2.3.2 A Capacitive Model of Void Based on the Induced Charge Concept

In this section, the direct relationship between the induced charge concept and the change in capacitance is going to be discussed. A capacitive model of the void based on the induced charge concept is proposed.

In (2.48) apart from Q_f and Q_{bi}, q_i is included to obtain,

$$C'' = \frac{Q + Q_{bi} + q_i}{U} \tag{2.55}$$

where C'' is the total capacitance, U is the system voltage, Q_f represents the free charges on the conducting surface of the capacitor, and Q_{bi} and q_i are the induced charges on the conducting surface of the capacitor due to bound charges and space charges in the insulation and within the void respectively. By further simplification of (2.55),

$$C'' = C + \frac{Q_{bi}}{U} + \frac{q_i}{U} \tag{2.56}$$

where C is the capacitance of an insulation free and void free capacitor and the other two parts constitute the increase of the capacitance due to the insulation and space charges. Equation (2.56) can be further expanded by substituting (2.46) into (2.56) giving,

$$C'' = C + \frac{\int_s \vec{P} \bullet \vec{ds}}{U} + \frac{q_i}{U} \tag{2.57}$$

Also q_i can be represented as follows (which applies to streamer discharges) [5]:

$$q_i = K\Omega\varepsilon(\vec{E_i} - \vec{E_l})\vec{\nabla}\lambda_o \tag{2.58}$$

where K and Ω are constants relating to the shape and nature of the void, $\boldsymbol{E_i}$ and $\boldsymbol{E_l}$ are the inception field strength and limiting value (beyond which ionization growth is not possible [5]) respectively, and λ_o is a dimensionless function dependent only on the location of the void. In our particular case, we have taken as reference the positive plate of the capacitor. Also, by taking into account that the surface charges within the void form dipoles in alignment with the external field [5, 17], then the outcome of (2.58) must be positive. By substituting (2.58) into (2.57),

$$C'' = C + \frac{\int_s \vec{P} \bullet \vec{ds}}{U} + \frac{K\Omega\varepsilon(\vec{E}_i - \vec{E}_l)\vec{\nabla}\lambda_o}{U} \tag{2.59}$$

Assuming that the insulation of the capacitor is an isotropic material and by utilizing (2.19), (2.46)-(2.52) (also equating $V = U$), then (2.59) can be further simplified as,

$$C'' = C' + \frac{K\Omega\varepsilon(\vec{E}_i - \vec{E}_l)\vec{\nabla}\lambda_o}{U} \tag{2.60}$$

The first part of (2.60) (C') represents a capacitor with insulating material between the plates (the outcome of (2.54)) and eventually a change in capacitance due to the presence of bound charges. The second part of (2.60) represents a change in capacitance caused by the breakdown void based on the induced charge concept. Equation (2.49) represents a capacitive model of the void based on the induced charge concept and can be used as an alternative to the classical model as shown in Fig. 2.8 and the model presented in [10]. The proposed capacitive model of a void based on the induced charge concept was implemented in MATLAB and is presented in Fig. 2.17.

The void is located between the insulation at the far end of a power cable. Fig. 2.17 represents a tiny cross section of the cable, wide enough just to accommodate the physical dimensions of the void. The upper and lower healthy parts of the insulation are represented by elements C_1 and C_2 and a space charge free void is represented by element C_{void}. The element $C_{induced}$ reflects the second part of (2.60). This value of $C_{induced}$ can be set to a constant value for simplicity. For even better results, a time varying $C_{induced}$ can be included in the model, based on the time varying elements of the second part of (2.60), and by taking into consideration the impedance of the external circuit (as reflected in (2.13)). By utilizing (2.13) into (2.60),

$$C'' = C' + \frac{K\Omega\varepsilon(\vec{E}_i - \vec{E}_l)\vec{\nabla}\lambda_o}{U - \Delta V} \tag{2.61}$$

where ΔV is the change in voltage just after the PD quenched.

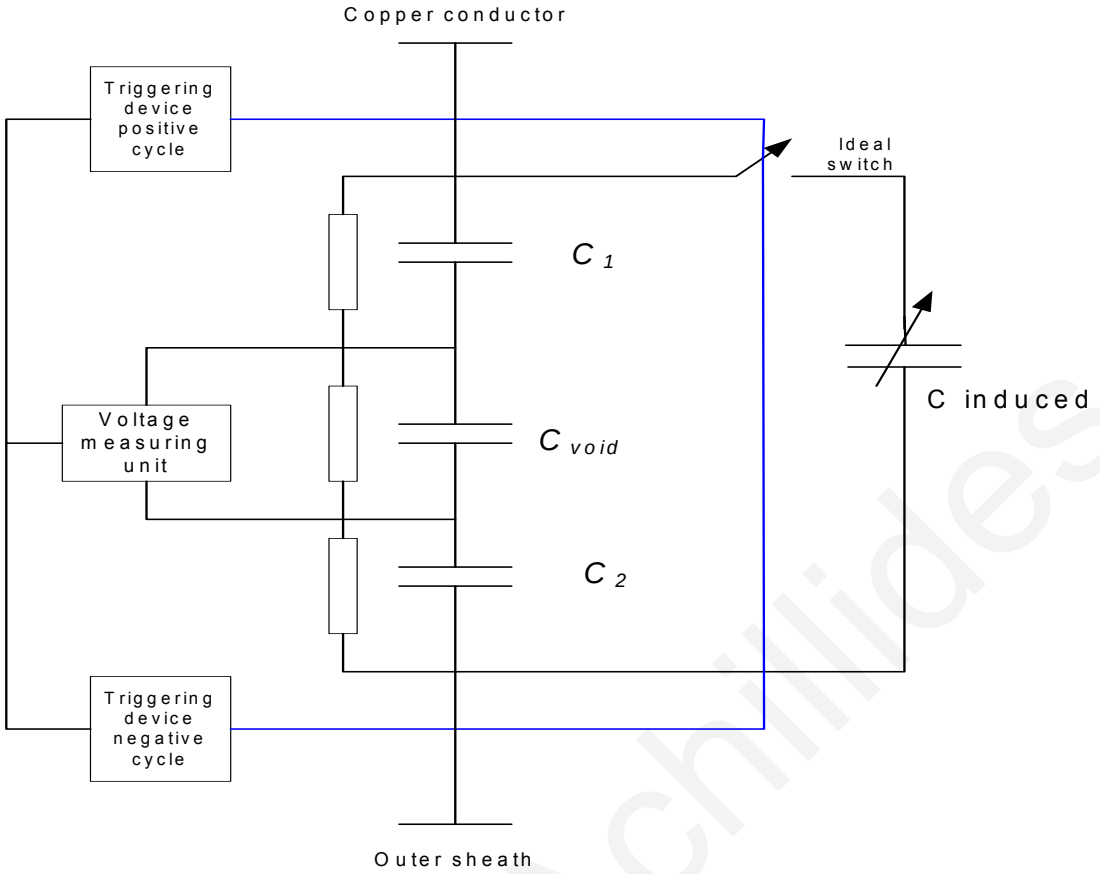

Fig. 2.17. Proposed electrical model: Capacitive model of void based on the induced charge concept

Moreover, in the model of Fig. 2.17 a voltage-controlled triggering device is utilized in order to control the ideal switch in the following way: when the voltage across the void reaches the minimum voltage level (V_{on}) required to initiate the discharge, then the control circuit will turn on the ideal switch resulting in connecting the element $C_{induced}$ in parallel with the rest of the circuit. When the voltage across the void reaches a value where breakdown ceases (V_{off}) then the element "Ideal Switch" will be switched off. The values of V_{on} and V_{off} can be set to any desired value based on the theory and/or measurements of PD. The model is also capable of handling different preset values for positive and negative voltages (V_{on} and V_{off}) across the void.

2.4 The Advanced Capacitive Model of Void

In the following discussion an improved capacitive model of void is proposed reflecting some of the physical processes regarding the PD mechanism.

2.4.1 A Brief History of Breakdown Mechanisms

The breakdown mechanism in low pressure gases was well formulated by Townsend at the beginning of the 20th century. The two dominant factors that control the onset of spark are coefficients α and γ, where the α coefficient represents the number of new ions per centimeter produced by an electron when moving in the direction of applied field and the γ coefficient (as originally presented by Townsend) relates to the secondary electrons released per positive ion bombardment of the cathode.

As a consequence of many experimental observations on spark development, a new theory of spark was proposed in early 1940's which involves the ionization process being dependent on the gas only including ionization by electron collisions according to Townsend's α mechanism, photoionization, and space – charge field effects caused by avalanches and streamers. The streamer theory is based on the gas mechanism only without the introduction of secondary cathode effects (γ coefficient), in accordance with experimental observations which show the decreasing influence of the cathode material of the sparking voltage as the gap length and gas pressure are increased. [26, 27].

2.4.2. The Proposed Model – The Physics Behind

The proposed model is based on lumped capacitors (as the classical capacitive model of void) enhanced by two more factors: a) the deployment of charges for anode directed streamers and b) the conductivity of streamer channel.

a. ***The deployment of charges***

Streamer is created from an avalanche if the internal field produced by the space charge reaches a value of the order of the external field [25]. If this criterion is fulfilled then the avalanche transforms into streamer before electrons at the tip of the streamer crossing the gap.

As the avalanche propagates towards the anode, the fast traveling electrons are separated from the slow speed positive ions. By taking into consideration that the number of electrons and positive ions generated by avalanche/streamer formation are almost equal (extraction of electrons from wall insulation is unlike) then this electron-positive ion separation will result to dipole moment formation within the void itself as shown in Fig. 2.18(a), where $\boldsymbol{E_o}$ represents the external field, $\boldsymbol{E_{sc}}$ the internal field due to present of space charge, $\boldsymbol{P_{sc}}$ the dipole moment due to the presence of the space charge and $\boldsymbol{DE}$ the difference between the external field and space charge field.

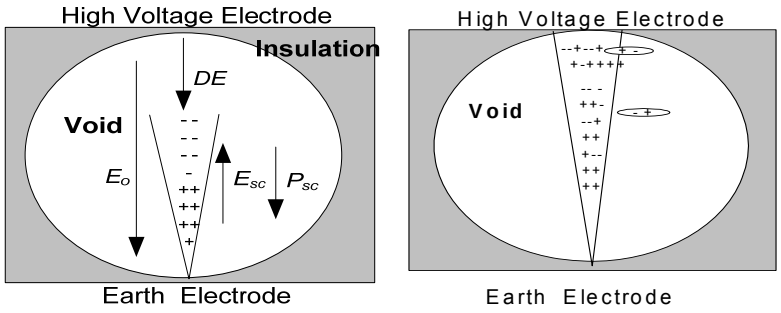

(a) Dipole moment formation (b) Neutralization of charges

Fig. 2.18. Avalanche propagation towards the anode

b. The neutralization of charges

This avalanche will grow until the negatively charged tip of the streamer reaches the upper side of the insulation. If by that time (or just prior) electrons and the positive ions densities of the avalanche fulfill the well known criterion for streamer inception [17] then the auxiliary avalanches created in the vicinity of the primary avalanche (due to photoionization) will be attracted towards the primary avalanche. In this particular situation it is worth mentioning that due to the presence of the insulation the electrons will not be absorbed by the anode electrode. The primary and secondary avalanches will be mixed together forming a quasineutral plasma [25] as shown in Fig. 2.18. This plasma mixture has two major characteristics:

i The dipole moment formations will cease to exist and eventually the internal field will be reduced to almost zero ($\boldsymbol{E_{sc}}$).

ii The plasma mixture behaves like a conductor (a semiconductor). This will lead to reduction of the external field ($\boldsymbol{E_o}$) across the void, and eventually the ionization grow will stop and the PD will seize.

b. The impact of charge deployment

As has already been discussed, the charge separation, as the primary avalanche grows, forms dipole moments within the voidit self.

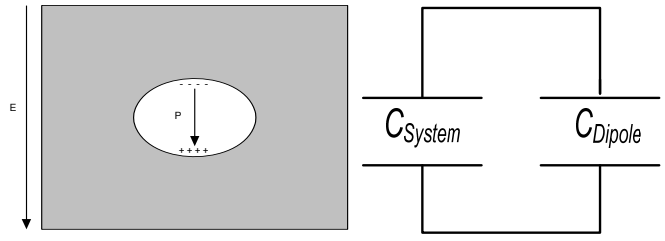

(a) Dipole moment formation (b) Model

Fig. 2.19. Dipole moment formation resulting in increase in capacitance of the system

These dipole moments are capable of inducing charges on adjacent conductors and eventually contributing to an increase in the overall capacitance of the system under consideration as discussed in [13]. This charge separation is modeled as presented in Fig.2.19.

c. The impact of neutralization of charges

From a theoretical point of view, a streamer can be defined as a "weakly ionized thin channel formed from primary avalanche in a sufficiently strong electric field" [25]. In [2-4] and [28-30] simulated breakdown of PDs are utilized by turning on the ideal switch (Fig. 2.8), which this means that a highly conductive channel, an ideal conductor should be established across the diameter of the void as shown in Fig. 2.20.

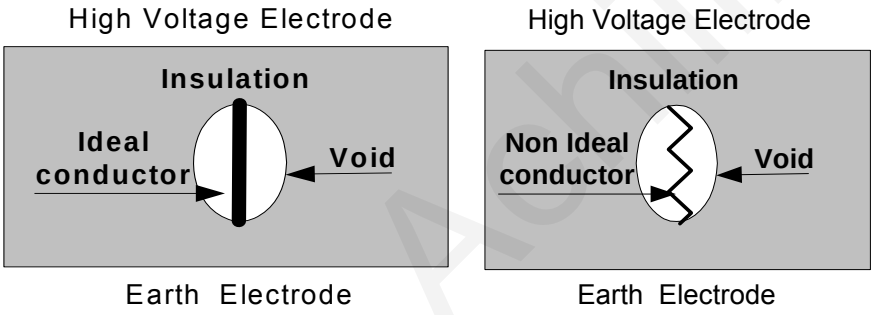

(a) Ideal conductor (b) Non ideal conductor

Fig. 2.20. Conductive channel across void

In the streamer type of discharge this is not the case. The gas possesses a certain conductivity that makes the plasma a non-ideal conductor as this is presented in Fig. 2.20(b).

2.4.3 The Proposed Model – The Components

The core of the proposed model is based on lumped capacitors and reflects partially the physical parameters governing the PD mechanism for streamer inception as presented in [17]. The proposed electrical model is modeled in MATLAB/Simulink as shown in Fig. 2.21.

The model represents an approximate electrical equivalent circuit of a pre-, during-full breakdown and post- breakdown mechanism of a void. The upper and lower healthy parts of the insulation are represented by elements C_1, R_1 and C_2, R_2. The space charge free void is represented by elements C_{void} and R_3. R_{stream} represents the conductivity of the weakly ionized thin channel (streamer) and C_{dipole} represents the increase of system capacitance [13] caused by charge separation (forming dipole moments) within the void

as described in 2.4.2. Moreover, in the model of Fig. 2.21 a voltage-controlled triggering device associated with a time delayed triggering device are utilized in order to control the ideal switches in the following two stages simulating the breakdown mechanism: Stage (I) when the voltage across the void reaches the minimum voltage level required to initiate the discharge (V_{on}), then the control circuit will turn on the ideal switch i, connecting the element C_{dipole} across elements C_{void}, and R_3. After a time of the order of nanoseconds (ns) ideal switch ii will close and eventually C_{dipole} and C_{void} will be discharged through the resistor R_{stream}. The discharge of the capacitors C_{void} and C_{dipole} (through resistor R_{stream}), from a physical point of view, represents the collapse of the external field ($\boldsymbol{E_o}$) due to the establishment of a semi-conductive path across the void. This phenomenon will generate a fast transient current in the circuit due to a voltage difference between the ac voltage source and the opposing voltage across capacitors C_1 and C_2 as discussed in [13]. This transient current is predominant and represents the measured transient in the circuit.

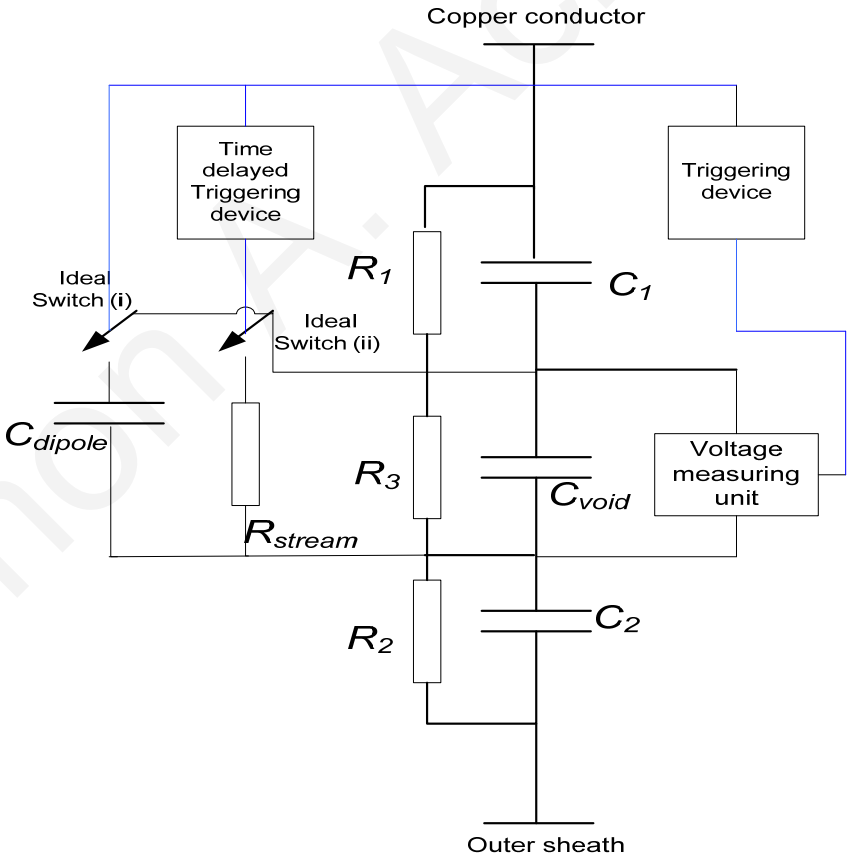

Fig. 2.21. Proposed electrical model: The advanced capacitive model of void

At the same time the capacitors C_{dipole} and C_{void} will be discharged through resistor R_{stream}. This discharge current represents the physical PD charge, which is expected to flow within the PD itself during breakdown conditions.

Furthermore when the voltage across the void reaches a value where breakdown ceases (V_{off}), then the elements "Ideal Switch i&ii will be switched off. The values of V_{on} and V_{off} and the time delay value can be set to any desired value based on the theory and/or measurements of the PD. The model is also capable of handling different V_{on} and V_{off} pre-set values for positive and negative voltages across the void and also different time delay values.

2.5 Discussion – Conclusions

Many authors in the literature oppose the capacitive model of a void. Their main point is based on the assumption that "due to the presence of the space charges within the void the field is no longer Laplacian and hence the proper concept of capacitance cannot be valid, concluding that the recorded transients cannot be related to a change in the capacitance." In [6], the capacitive representation of the void is translated as a lack of knowledge and trivialization of electric field theory.

In this chapter, the potential and weaknesses of the classical capacitance representation of the void have been exploited, the induced charge concept has been introduced, and the criticism related to the capacitance model has been argued. Also the relationship between the induced charge concept and the change of capacitance has been demonstrated. Furthermore, three new models have been proposed: a) The improved capacitive model, b) A capacitive model of a void based on the induced charge concept, and c) The advanced capacitive model of a void. Based on the discussion and the equations presented in this work, the main conclusions can be summarized below.

(i) The classical capacitive model (associated to the spark gap or thyristor) cannot represent by any means the physics behind (and magnitude) of the discharge current, but it is capable of representing the transients related to the discharge based on the change in capacitance.

(ii) The presence of bound charges within the insulation (between the conducting plates of the capacitor) indicates the presence of a Poissonian field, which in turn does not oppose the proper concept of capacitance.

(iii) The true case of Laplacian field occurs only in the presence of vacuum. For all the other cases, any kind of material under the influence of an external electric

field will be either polarized and ionized or excited according to the nature of the material and the strength of the external electric field.

(iv) Bound charges behave like free charges and apart from their contribution to conductivity they can induce free charges on any conducting surface and eventually contribute to an increase in the capacitance.

(v) The absence of equipotential surfaces along the void walls is just a geometrical phenomenon and has nothing to do with the presence or nature of the void within the insulation itself. This specific geometry can be modelled by an infinite number of capacitors connected in parallel and separated by resistances (representing the insulating surface material of the wall of the void), each one accommodating a small increment of voltage variation.

(vi) Three new capacitive models have been proposed.

Based on the discussion given in this chapter and by utilising the relevant physics, mathematics and basic electric theory, it can be concluded that the capacitance representation of the void is a valid and powerful tool assisting engineers to analyze the transients related to a breakdown void located within the insulating material of cables

CHAPTER 3

CALCULATION OF THE COMPONENTS OF THE THREE PROPOSED MODELS: THE MATHEMATICS BEHIND

3.1 Introduction

One of the scopes of this work is the calculation of the components for the three proposed models under investigation with sufficient accuracy. This in turn will give a clear indication regarding the influence of these componets to the generated transients and a better understanding of the PD prosess..In order to achieve this scope, an analytical method is proposed in this section based on the classical electromagnetic theory (electostatics).

The three models are: a) the improved capacitive model of void [30], b) the capacitive model of void based on the induced charge concept [13] and c) the advanced capacitive model of void as presented in Figs. 3.1, 3.2 and 3.3 respectively.

The exact calculation of the components as presented in Figs. 3.1, 3.2 and 3.3 is an extremely complicated process even for numerical methods. For this reason, the superposition theorem has been utilized as follows: First the components C_1, R_1,C_2, R_2, R_{void} and C_{void} have been calculated by assuming a space charge free void and second the components of R_{stream} and C_{dipole} have been calculated by considering the space charge within the void it self.

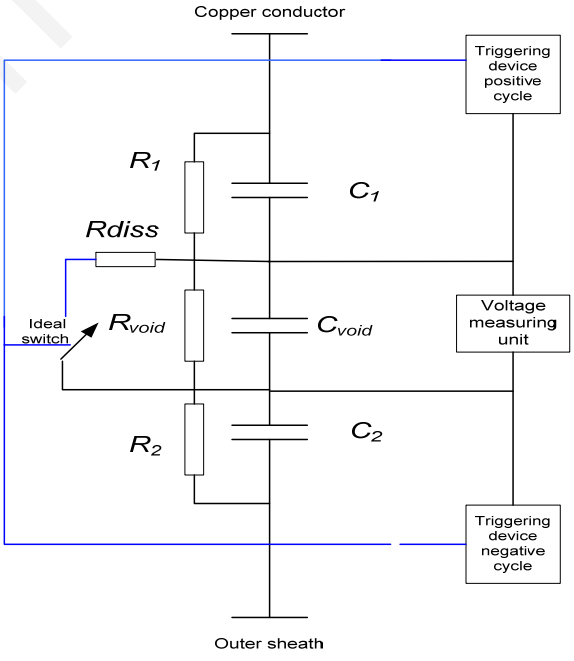

Fig. 3.1. The improved capacitive model of void

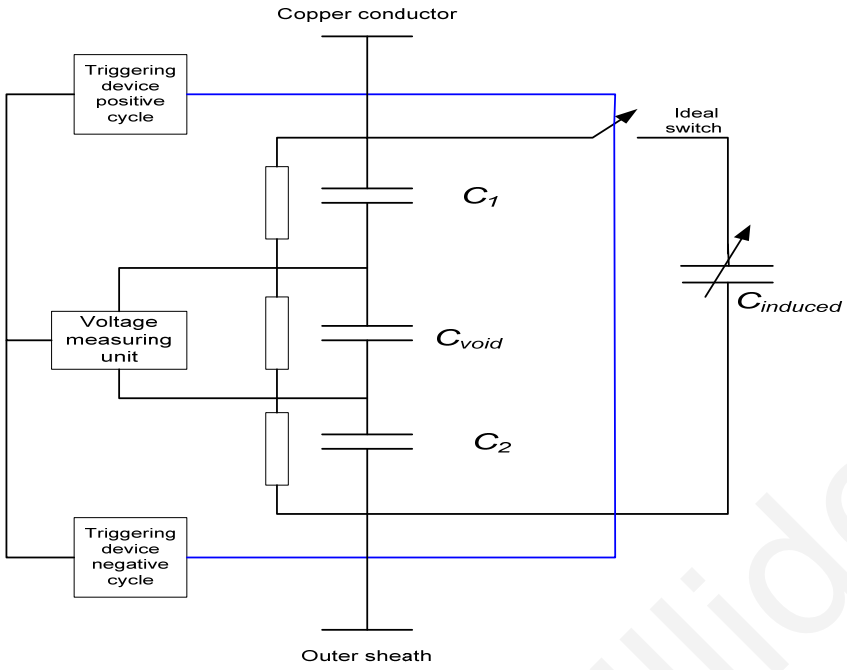

Fig. 3.2. A capacitive model of void based on the induced charge concept

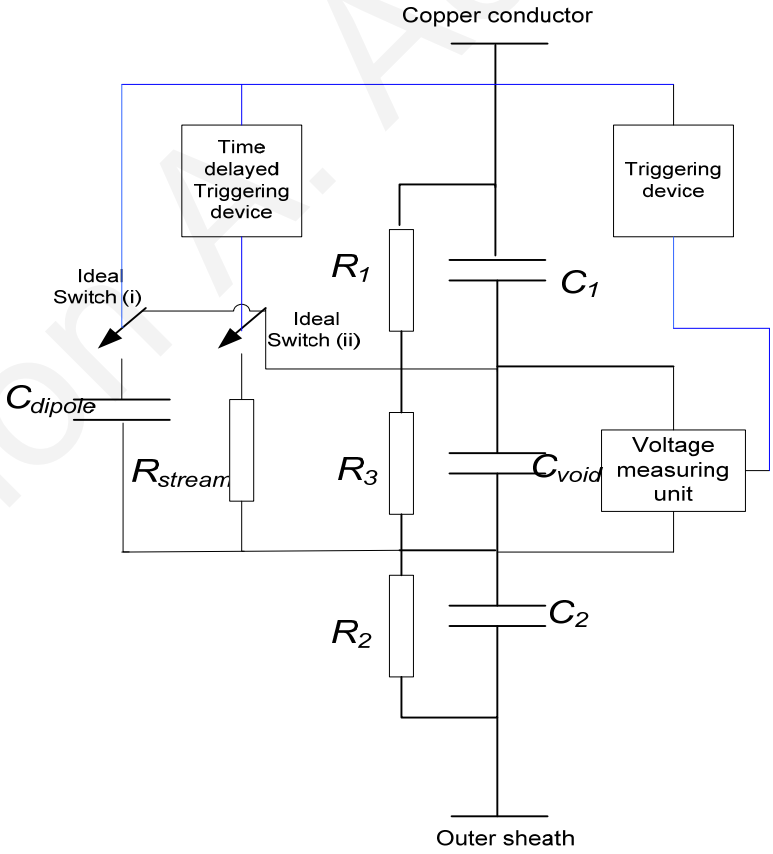

Fig.3.3. The advanced capacitive model of void

3.2 Calculation of Components

Two assumptions are made in order to minimize the effort in the calculations, but keeping also the adequate accuracy.

(a) The void is a space charge free region.

(b) The dimensions of the void are much smaller than the dimensions of the cable.

A cross section of a typical medium voltage cable is shown in Fig. 3.4 (not to scale). A cylindrical void is supposed to be created between the core and the outer sheath of the cable within the middle of the insulation.

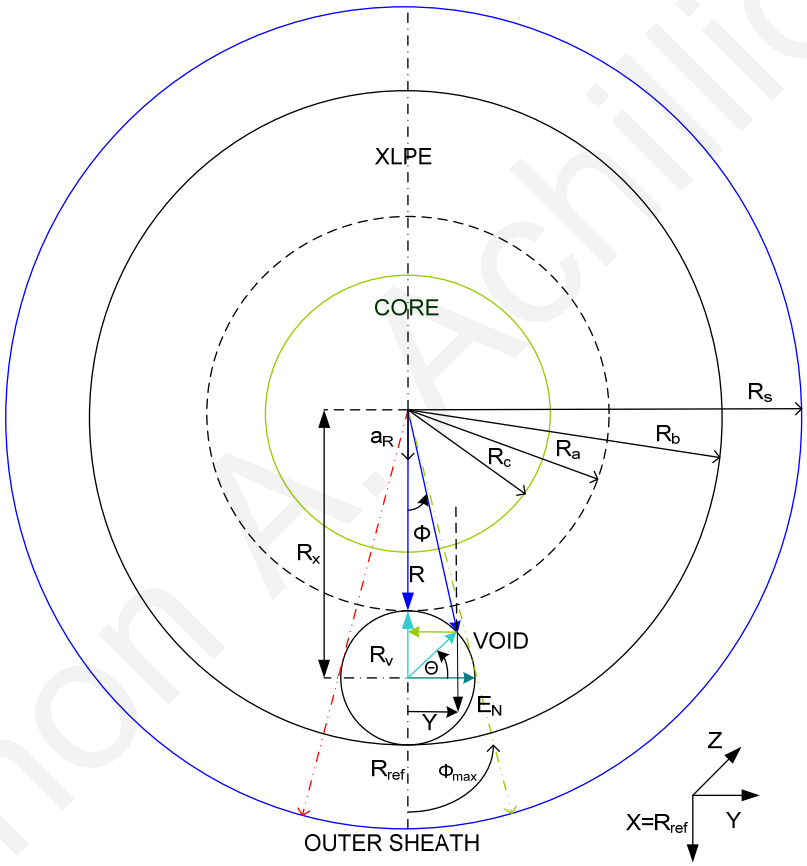

Fig. 3.4. Cross section of a medium voltage cable

The radius of the void is R_v. R_c and R_s represent the radii of the core and outer sheath of the cable respectively. R_x is the distance between the centres of the void and the core. Θ and Φ are the offset angles (from the R_{ref} axis) for the core and the void respectively. The cylindrical void is extended perpendicular to the paper (along the Z direction) with a defined length of Z_a.

3.2.1. Capacitance of Healthy Part of Insulation (C_1 and C_2).

With reference to Fig. 3.4 and by utilizing Gauss' law,

$$Q' = \int_s \overrightarrow{D'} \bullet \overrightarrow{ds} \tag{3.1}$$

where Q' is the amount of surface charge density on the core and $\boldsymbol{D'}$ is the electric flux density emitted by the charge density over the surface defined by dotted lines in Fig. 3.4. By using cylindrical coordinates along the R direction, (3.1) becomes,

$$Q' = 2\int_0^{\Phi_{\max}} \int_0^{Z(\Phi)} \varepsilon_0 \varepsilon_r E' a_R \bullet R dZ d\Phi a_R \,, \tag{3.2}$$

where Z is the length of the cable enclosing the void and a_R is the unit vector along R_{ref}. By taking into consideration that between regions $R_c < R < R_a$ and $R_b < R < R_s$, $\boldsymbol{E'}$ is not a function of Z and Φ and also Z is not a function of Φ, then

$$\vec{E}' = \frac{Q'}{2\varepsilon_0 \varepsilon_r R Z_a \Phi_{\max}} a_R \,, \tag{3.3}$$

and the voltage (V) is related to $\boldsymbol{E'}$ as follows:

$$V = -\int_b^a \overrightarrow{E'} \bullet \overrightarrow{dl} \,, \tag{3.4}$$

By further substitution of (3.3) to (3.4) and by equating $dl = dRa_R$ the voltage along the healthy part of insulation can be found (3.5)

$$V = \frac{Q'}{2\varepsilon_0 \varepsilon_r Z_a \Phi_{\max}} \ln\left(\frac{R_a}{R_c}\right). \tag{3.5}$$

Since $Q = CV$, (3.5) becomes,

$$C = \frac{2\varepsilon_0 \varepsilon_r Z_a \Phi_{\max}}{\ln\left(\frac{R_a}{R_c}\right)} \,, \tag{3.6}$$

Further, Θ can be related directly to the dimensions and location of the void (Fig. 3.2) as follows:

$$Y = R\sin\Phi = R_v \cos\Theta \tag{3.7}$$

$$R_x = R\cos\Phi + R_v \sin\Theta \,. \tag{3.8}$$

Solving (3.7) and (3.8),

$$R = \frac{R_v \cos\Theta}{\sin\Phi} \,. \tag{3.9}$$

$$R\cos\Phi = R_x - R_v \sin\Theta \tag{3.10}$$

.

By substituting (3.9) to (3.10) and solving with respect to Θ we obtain:

$$\Phi = \tan^{-1}\left(\frac{R_v \cos\Theta}{R_x - R_v \sin\Theta}\right). \tag{3.11}$$

Based on Fig. 3.2, Φ_{max} can be found by substitution of $\Theta = 0$ to (3.11)

$$\Phi_{\max} = \tan^{-1}\left(\frac{R_v}{R_x}\right). \tag{3.12}$$

By further substitution of (3.12) into (3.6),

$$C = \frac{2\varepsilon_0 \varepsilon_r Z_a (\tan^{-1}(\frac{R_v}{R_x}))}{\ln(\frac{R_a}{R_c})}. \tag{3.13}$$

Using (3.13) the elements C_1 and C_2 (by adjusting the denominator of (3.13)) in Figs. 3.1, 3.2 and 3.3 can be calculated.

3.2.2. Capacitance of Void (C_{void})

In Fig. 3.4 a cylindrical void is shown, located in the middle of the insulation of the cable. At the point of interface (between void and insulation) the electric flux density (***D***), is a function of R and Φ. This makes the solution of (3.1) a very difficult problem. Nevertheless, due to the small size of the void, ***D*** does not vary significantly along the surface of the void, so it can be regarded as constant, and (3.1) can be expanded as follows:

$$Q' = \int_s \vec{D}' \bullet \vec{ds} = \int_s \vec{D}' \bullet \vec{n} dS, \tag{3.14}$$

where n is the unit normal vector at the point of interface surface. Based on [29] ***n*** can be defined as follows,

$$\vec{n} = \frac{\nabla f}{|\nabla f|} \tag{3.15}$$

where f is a function representing the surface under consideration (void) in the three dimensional form of $f(x,y,z) = 0$ [31]. By substitution of (3.15) into (3.14) we get:

$$Q' = \iint \vec{D}' \bullet \frac{\nabla f}{|\nabla f|} dS, \tag{3.16}$$

With reference to Fig. 3.2 the equation of the void (surface under consideration) can be represented in the form $f(x,y,z) = 0$ at $0 < Z < Za$ as follows:

$$f(x,y,z) = (X - R_x)^2 + (Y)^2 - R_v{}^2 = 0, \tag{3.17}$$

The gradient and gradient magnitudes of (3.17) are given by:

$$\nabla f(x,y,z) = -[2(X - R_x)\overrightarrow{a_x} + 2(Y)\overrightarrow{a_y}], \tag{3.18}$$

$$\left|\nabla f(x,y,z)\right| = 2R_v, \tag{3.19}$$

where $\boldsymbol{a_x}$ and $\boldsymbol{a_y}$ are the unit vectors along the X and Y directions respectively (the negative sign indicates an inward pointing normal unit vector along the surface of the void). By substituting (3.18) and (3.19) to (3.16) we get:

$$Q' = \iint \vec{D}' \bullet \frac{-[2(X - R_x)\overrightarrow{a_x} + 2Y\overrightarrow{a_y}]}{2R_v} dS, \tag{3.20}$$

Before further processing (3.20), symmetry considerations make sense to switch from rectangular ($\boldsymbol{a_x}$, $\boldsymbol{a_y}$) to cylindrical coordinates ($\boldsymbol{a_R}$, $\boldsymbol{a_\Phi}$). This transformation is presented in [14] and transforms (3.20) in to cylindrical coordinates as follows:

$$Q' = \iint \vec{D}' \bullet \frac{-[A_R\overrightarrow{a_R} + A_\Phi\overrightarrow{a_\Phi}]}{2R_v} dS, \tag{3.21}$$

where A_R and A_Θ are given in (3.22) and (3.23) respectively

$$A_R = 2(X - R_x)\cos\Phi + 2Y\sin\Phi, \tag{3.22}$$

$$A_\Phi = -2(X - R_x)\sin\Phi + 2Y\cos\Phi, \tag{3.23}$$

With reference to Fig. 3.2, further substitution of $(X - R_x) = -R_v \sin\Theta$ and $Y = R_v \cos\Theta$ to (3.22) and (3.23) yields,

$$A_R = -2R_v \sin\Theta\cos\Phi + 2R_v \cos\Theta\sin\Phi, \tag{3.24}$$

$$A_\Phi = 2R_v \sin\Theta\sin\Phi + 2R_v \cos\Theta\cos\Phi, \tag{3.25}$$

Further simplification of (3.24) and (3.25) leads to

$$A_R = 2R_v \sin(\Phi - \Theta), \tag{3.26}$$

$$A_\Phi = 2R_v \cos(\Theta + \Phi), \tag{3.27}$$

By substitution of (3.26) and (3.27) to (3.21) we obtain:

$$Q' = \iint \vec{D}' \bullet -[\sin(\Phi - \Theta)a_R + \cos(\Theta + \Phi)a_\Phi]dS, \tag{3.28}$$

The solution of (3.28) is a very difficult problem. Nevertheless, due to the small size of the void, $\boldsymbol{D}$ does not vary significantly along the surface of the void, so it can be regarded as constant and by further considering symmetry, then only $\boldsymbol{a_R}$ component of $\boldsymbol{D}$ is present [31], giving eventually the following simplification of (3.28):

$$Q' = D' \iint -[\sin(\Phi - \Theta)]dS, \tag{3.29}$$

Re-expanding (3.29) we get:

$$Q' = D' \iint -[-\sin\Theta\cos\Phi + \sin\Phi\cos\Theta)]dS\,, \tag{3.30}$$

By solving (3.8) and (3.9) with respect to sinΘ and cosΘ respectively and by substitution to (3.30) we get

$$Q' = D' \iint -[-(\frac{R_x - R\cos\Phi}{R_v})\cos\Phi + \sin\Phi(\frac{R\sin\Phi}{R_v})]dS\,, \tag{3.31}$$

Further simplification of (3.31) leads to

$$Q' = \frac{D'}{R_v} \iint -[(-R_x\cos\Phi + R\cos^2\Phi + R\sin^2\Phi]dS\,, \tag{3.32}$$

By substitution of $dS = RdZd\Phi$ to (3.32) we get

$$Q' = 2\frac{D'}{R_v}\int_0^{\Phi_{max}}\int_0^{z_a} -[(-R_x\cos\Phi + R)]RdZd\Phi\,, \tag{3.33}$$

And the solution of (3.33) is given by:

$$Q' = 2\frac{D'Z_aR}{R_v}[R_x\sin\Phi_{max} - R\Phi_{max}] \tag{3.34}$$

where Φ_{max} is given by (3.12). By substitution of $\boldsymbol{D} = \boldsymbol{E}\varepsilon_o\varepsilon_r$ and by equating $R = R_a$ to (3.34) then by solving (3.34) with respect to $\boldsymbol{E}$ we obtain:

$$\vec{E}' = R_v\frac{Q'}{2\varepsilon_0\varepsilon_r Z_a R_a[R_x\sin\Phi_{max} - R_a\Phi_{max}]}a_R, \tag{3.35}$$

For simplification purposes the value in the brackets of (3.35) is set equal to K giving finally the value of $\boldsymbol{E}$ equal to:

$$\vec{E}' = R_v\frac{Q'}{2\varepsilon_0\varepsilon_r Z_a R_a K}a_R, \tag{3.36}$$

The outcome of (3.35 and 3.36) represents the value of $\boldsymbol{E}$ along the surface of the void - a generally constant value (for small void), related to the dimension and location of the void itself. The electric flux lines emitted from the core of the cable will reach the surface of the void at an incident angle. With reference to Fig. 3.2 at the point of interface, by utilizing (2.36) and by assuming that void is filled with air ($\varepsilon_{air} = 1$), then the normal component of $\boldsymbol{E}$ (along R_{ref}), $\boldsymbol{E_N}$ and eventually the electric field strength within the void itself (along the *Ref* direction) is given by:

$$\vec{E}_N' = R_v\frac{Q}{2\varepsilon_0\varepsilon_r Z_a R_a K}\cos\Phi a_{R\,ref}. \tag{3.37}$$

By further assuming that the volume of the void is a charge free region ($\nabla\bullet D = 0$) and by substitution of (3.37) to, $\vec{E} = \nabla V$ we obtain:

$$V(\Phi) = -\int_{a}^{b} R_v \frac{Q'}{2\varepsilon_0 \varepsilon_r Z_a R_a K} \cos\Phi dR_{ref}\,, \tag{3.38}$$

where $V(\Phi)$ represents the variation of voltage along the surface of the void as a function of (Φ) and dR_{ref} defines the line integration along the direction of R_{ref} within the void itself. With reference to Fig.3.2, by substitution of $dR_{ref} = R_v cos\Theta d\Theta$ to (3.38) then we get:

$$V(\Phi) = -\int_{a}^{b} R_v{}^2 \frac{Q'}{2\varepsilon_0 \varepsilon_r Z_a R_a K} \cos\Phi \cos\Theta d\Theta\,. \tag{3.39}$$

By further substitution of (3.11) to (3.39) we obtain

$$V = \int_{0}^{\frac{\pi}{2}} R_v{}^2 \frac{Q'}{\varepsilon_0 \varepsilon_r Z_a R_a K} \cos[\tan^{-1}(\frac{R_v \cos\Theta}{R_x - R_v \sin\Theta})]\cos\Theta d\Theta\,. \tag{3.40}$$

where V represents the summation of voltage along the surface of the void. By substituting $Q = CV$ into (3.40) we obtain the total capacitance of the void (C_{void}):

$$C_{void} = \frac{\varepsilon_0 \varepsilon_r Z_a R_a K}{R_v{}^2 \int_{0}^{\frac{\pi}{2}} \cos(\tan^{-1}(\frac{R_v \cos\Theta}{R_x - R_v \sin\Theta}))\cos\Theta d\Theta}\,. \tag{3.41}$$

Using (3.41), the element C_{void} in Figs. 3.1 and 3.2 can be calculated.

3.2.3 Conductance of the Healthy Part of the Insulation

The insulation resistance (conductance) of any non-symmetrical material can be calculated using,

$$R = \frac{V}{I} = \frac{-\int \vec{E} \bullet dl}{\iint \sigma \vec{E} \bullet d\vec{s}}\,, \tag{3.42}$$

where σ is the electrical conductivity of the material (XLPE) and $\boldsymbol{E}$ is the electric field strength. By substituting (3.3) to the denominator of (3.42) and by letting $ds = RdZd\Phi a_R$,

$$I = 2\int_{0}^{\Phi_{max}} \int_{0}^{Z_a} \sigma \frac{Q'}{2\varepsilon_0 \varepsilon_r R Z_a \Phi_{max}} RdZd\Phi\,. \tag{3.43}$$

Following the same logic as in Section 3.2.1 the outcome of (3.43) is,

$$I = \sigma \frac{Q'}{\varepsilon_0 \varepsilon_r}\,, \tag{3.44}$$

and by substituting (3.44) and (3.5) to (3.42) we get:

$$R = \frac{V}{I} = \frac{\ln(\frac{R_a}{R_c})}{2\sigma Z_a \Phi_{\max}}. \tag{3.45}$$

Further substitution of (3.12) to (3.45) gives:

$$R = \frac{V}{I} = \frac{\ln(\frac{R_a}{R_c})}{2\sigma Z_a \tan^{-1}(\frac{R_v}{R_x})} \tag{3.46}$$

From (3.46) the conductance of R_1 and R_2 (by adjusting numerator of (3.46)) of Figs. 3.1, 3.2 and 3.3 can be calculated.

3.2.4 Conductance of Void (R_v)

Following the same logic as presented in Section 3.2.3 and by considering Figs. 3.1, 3.2 and 3.3, and then by further substitution of (3.47) to the denominator of (3.42) we obtain:

$$I = \int\int \sigma R_v \frac{Q'}{2\varepsilon_0 \varepsilon_r Z_a R_a K} \cos\Phi a_{R\,ref} \bullet ds \tag{3.47}$$

By letting $ds = dz.dya_{Rref}$, then (3.47) becomes,

$$I = 2\int_0^{a_1} \int_0^{Z(Y)} \sigma R_v \frac{Q'}{2\varepsilon_0 \varepsilon_r Z_a R_a K} \cos\Phi dzdy\,. \tag{3.48}$$

By solving (3.48) firstly with respect to dz (by letting $Z(y) = Z_\alpha$), and then from (3.7), by substitution of $dy = -R_v sin\Theta d\Theta$ and $a_1 = \pi/2$,

$$I = -\int_o^{\frac{\pi}{2}} \sigma {R_v}^2 \frac{Q'}{\varepsilon_0 \varepsilon_r R_a K} \cos\Phi \sin\Theta d\Theta \tag{3.49}$$

By further substitution of (3.11) to (3.49) we have

$$I = -\int_o^{\frac{\pi}{2}} \sigma {R_v}^2 \frac{Q'}{\varepsilon_0 \varepsilon_r R_a K} \cos(\tan^{-1}(\frac{R_v \cos\Theta}{R_x - R_v \sin\Theta})) \sin\Theta d\Theta \tag{3.50}$$

Finally, by substituting (3.50) and (3.40) to (3.42) we get

$$R_{void} = \frac{1}{\sigma Z_a} \frac{\int_0^{\frac{\pi}{2}} \cos(\tan^{-1}(\frac{R_v \cos\Theta}{R_x - R_v \sin\Theta})) \cos\Theta d\Theta}{\int_0^{\frac{\pi}{2}} \cos(\tan^{-1}(\frac{R_v \cos\Theta}{R_x - R_v \sin\Theta})) \sin\Theta d\Theta} \tag{3.51}$$

3.2.5 Resistance of the Ionised Path

Electric breakdown can be defined as the transformation process of an insulating material to a conducting one under the influence of an electric field [25]. For gas breakdown there are two known mechanisms: Townsend's mechanism and the streamer theory of breakdown, as discussed in Chapter 2.4.

The evolution of electron densities based on the streamer concept (for a 1 mm gap at atmospheric pressure) is presented in [33] by using continuity equations of electrons and ions coupled to Poisson's equation for electric field.

In this work, by utilizing the simulated predictions of electron densities as calculated in [33], and the mobility coefficient of charged particles as presented in [25], the conductivity (σ_i) of the ionized path is approximately predicted. By replacing σ with σ_i in (3.51), the resistance of the ionised path (R_{diss}) can be calculated.

3.3 Calculation of Components of the Induced Charge Capacitive Model

The value of $C_{induced}$ is calculated by utilizing the second part of (2.49) as presented below:

$$C_{induced} = \frac{K\Omega\varepsilon(\vec{E_i} - \vec{E_l})\vec{\nabla}\lambda_o}{U} \tag{3.52}$$

where k= 3 for cylindrical voids [14], $\Omega = \pi(R_v)^2 Z_a$ (void volume), $U = 11e^3\sqrt{3}$ which is the system voltage and $\nabla \lambda_o = \frac{1}{R_x}$.

The value where ionization starts and stops (E_i - E_l) is in kV/mm and for streamer inception is given below:

$$E_i - E_l = \frac{BE_l}{\sqrt{2R_v p}}, \tag{3.53}$$

where $B = 0.86\sqrt{mm.bar}$, E_l/p = 2.42 kV/mmbar [18], where p is the pressure in bar and is taken as 1bar. By further substitution of (3.53) to (3.52) we obtain:

$$C_{induced} = \frac{3\Pi(R_v)^2 Z_\alpha \varepsilon_o \varepsilon_r B\vec{E_l}}{U\sqrt{2R_v p}R_x} \tag{3.54}$$

Furthermore, a dimensional check is performed in order to verify the truthfulness of (3.54) as follows:

$$C_{induced} = \frac{(mm)^2 mm \frac{F}{m} \sqrt{mmbar} \frac{kV}{mm}}{V\sqrt{mmbar}\, mm} = F \tag{3.55}$$

3.4 Calculation of Components of the Advanced Capacitive Model of Void

For the calculation of components C_{dipole} and $R_{stream,}$ the following two assumptions are taken into consideration:

(a) Space charges are equally distributed along the surface of void.

(b) The whole volume of the void is taking part in the discharge possess.

3.4.1 Calculation of $R_{streamer}$

The value of $R_{streamer}$ is calculated in the following way: a) based on the discussion given in Section 7 of [17] and b) based on the calculations as given in [33]

According to [17] the minimal charge is given below:

$$Q_{\min} = \frac{\pi\varepsilon_o}{4}(2\varepsilon_r + 1)(E/p)_{cr} p l^{\beta}[1 - \gamma + \frac{B}{(pl)^{\beta}}] \tag{3.56}$$

Furthermore, B is given by:

$$B = \frac{(K_{cr})^{\frac{1}{\beta}}}{(E/p)_{cr}(C)^{\frac{1}{\beta}}} \tag{3.57}$$

By further substitution of (3.57) to (3.56) we get

$$Q_{\min} = \frac{\pi\varepsilon_o}{4}(2\varepsilon_r + 1)(E/p)_{cr} p l^2[1 - \gamma + \frac{(K_{cr})^{\frac{1}{\beta}}}{(E/p)_{cr}(C)^{\frac{1}{\beta}}(pl)^{\frac{1}{\beta}}}] \tag{3.58}$$

where $Q_{\min}$ is the minimal physical charge within the void for streamer inception, ($\boldsymbol{E/p}$) is the pressure reduced critical field in which the ionization and attachment coefficient are equal, p is the pressure, l is the diameter of the void, and C, K_{cr}, γ and β are parameters related to the gas (within the void) properties. As before, a dimensional check is performed to verify the truthfulness of (3.58) as follows:

$$Q_{\min} = \frac{F}{m}\frac{V}{m(Pa)}(Pa)m^2\left[\frac{1}{\frac{V}{(Pa)m}((Pa)^{(\beta-1)}m^{(\beta-1)}V^{-\beta})^{\frac{1}{\beta}}((Pa)m)^{\frac{1}{\beta}}}\right] \tag{3.59}$$

The conductivity of plasma for streamer inception mechanism is given by equation (3.61) as presented in [25, 27].

$$\sigma = \frac{eq}{mV_m} \tag{3.61}$$

where σ is the conductivity, q is the charge, e is the electron charge, m is the mass of the electron and V_m is the frequency of collision for momentum transfer. By further substitution of (3.58) to (3.61) (by equating $q = Q_s$) we get:

$$\sigma_1 = \frac{e}{mV_m}\frac{\pi\varepsilon_o}{4}(2\varepsilon_r + 1)(E/p)_{cr}pl^2\left[1-\gamma+\frac{(K_{cr})^{\frac{1}{\beta}}}{(E/p)_{cr}(C)^{\frac{1}{\beta}}(pl)^{\frac{1}{\beta}}}\right] \tag{3.62}$$

and then by substituting (3.62) to (3.51) we obtain :

$$R_{streamer\,1} = \frac{1}{\sigma_1 Z_a}\frac{\int_0^{\frac{\pi}{2}}\cos(\tan^{-1}(\frac{R_v\cos\Theta}{R_x - R_v\sin\Theta}))\cos\Theta d\Theta}{\int_0^{\frac{\pi}{2}}\cos(\tan^{-1}(\frac{R_v\cos\Theta}{R_x - R_v\sin\Theta}))\sin\Theta d\Theta} \tag{3.63}$$

Based on [33] the average electron density for 1mm gap for streamer inception is calculated to be 2.0e14 electrons/cm^3. This value is substituted in (3.61) and then (3.61), by substituted in (3.51) we obtain $R_{streamer2}$ as follows:

$$R_{streamer\,2} = \frac{mV}{eqZ_a}\frac{\int_0^{\frac{\pi}{2}}\cos(\tan^{-1}(\frac{R_v\cos\Theta}{R_x - R_v\sin\Theta}))\cos\Theta d\Theta}{\int_0^{\frac{\pi}{2}}\cos(\tan^{-1}(\frac{R_v\cos\Theta}{R_x - R_v\sin\Theta}))\sin\Theta d\Theta} \tag{3.64}$$

3.4.2. Dipole Capacitance (C_{dipole})

The dipole capacitance (C_{dipole}) of a cylindrical void as presented in Fig. 3.3 is calculated in the following way by taking into account two assumptions:

(a) The amount of positive and negative ions generated by the ionization process is equal.

(b) Under the influence of the external electric field ($\boldsymbol{E_{ext}}$) negative ions (electrons) will be accelerated and will occupy symmetrically the upper part of the void whereas, positive ions will occupy symmetrically the lower part of the void.

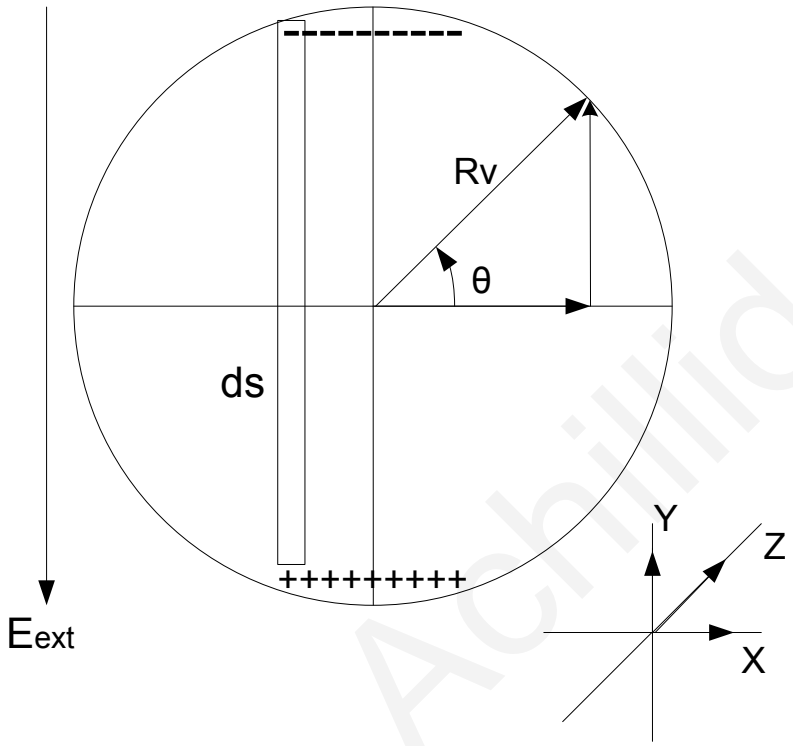

Fig. 3.5. Cylindrical void with space charge

With reference to Fig. 3.5 and by utilizing Gauss law along the *Y* axis, then the electric flux density entering element surface $d\boldsymbol{S}$ is related to the space charge as follows

$$Q_s = \int_s \overrightarrow{D_s} \bullet \overrightarrow{ds} \tag{3.65}$$

where Q_s and $\boldsymbol{D_s}$ represent the enclosed space charge(s) and the electric flux density entering the elementary surface $\boldsymbol{dS}$. By further expanding (3.65) we get:

$$Q_s = \int_s \overrightarrow{D_s} \bullet dxdz\overrightarrow{a_y} \tag{3.66}$$

where $\boldsymbol{\alpha_y}$ represents the unit vector along the Y direction. By further expanding (3.66) we get:

$$Q_s = \int_s D_y \overrightarrow{a_y} \bullet dxdz\overrightarrow{a_y} \tag{3.67}$$

By taking into consideration that $\boldsymbol{D}$ can be regarded as constant along the Y axis, then (3.67) becomes:

$$Q_s = \int_s D_y dxdz \tag{3.68}$$

With reference to Fig. 3.5, then

$$x = R_v \cos\Theta, \qquad dx = -R_v \sin\Theta d\Theta \tag{3.69}$$

By substituting $\boldsymbol{D_y=\varepsilon_o E_y}$ and (3.69) to (3.68), we get

$$Q_s = \int_0^{Z_a}\int_0^{\pi} -\varepsilon_o E_y R_v \sin\Theta d\Theta dz \tag{3.70}$$

where Z_a and R_v represent the length and radius of the cylindrical void. By solving (3.70) we get:

$$\overrightarrow{E_y} = -\frac{Q_s}{2\varepsilon_0 R_v Z_a}\overrightarrow{a_y} \tag{3.71}$$

By substituting (3.71) to (3.4) then the voltage (V) along the Y direction (Fig 3.3) can be calculated as follows:

$$V_y = \int \frac{Q_s}{2\varepsilon_0 R_v Z_a}\overrightarrow{a_y} \bullet dy\overrightarrow{a_y} \tag{3.72}$$

With reference to Fig. 3.5, then

$$y = R_v \sin\Theta, \qquad dy = R_v \cos\Theta d\Theta \tag{3.73}$$

By further substituting (3.73) to (3.72) we get:

$$V_y = \int_{-\pi/2}^{\pi/2} \frac{Q_s}{2\varepsilon_0 R_v Z_a} R_v \cos\Theta d\Theta \tag{3.74}$$

and the solution of (3.74) is given below:

$$V_y = \frac{Q_s}{\varepsilon_o Z_a} \tag{3.75}$$

Since $Q=CV$ then by substituting to (3.75), C_{dipole} can be calculated as follows:

$$C_{dipole} = \varepsilon_o Z_a \tag{3.76}$$

The outcome of (3.76) is worth a comment. It indicates that the capacitance of any cylindrical void resulting from internal space charges only (and by assuming symmetrical distribution of those charges along the surface of void) is independent of the radius of the void and it is just related to the permittivity of vacuum (ε_o) and the length of the cylindrical void!

3.5 Summary of the Final Equations of the Parameters of each Model

Table 3.1. Final Equations of the Improved Capacitive Model

Component	Equation
C_1 & C_2 (F)	$C = \dfrac{2\varepsilon_0 \varepsilon_r Z_a (\tan^{-1}(\frac{R_v}{R_x}))}{\ln(\frac{R_a}{R_c})}$
R_1 & R_2 (Ω)	$R = \dfrac{V}{I} = \dfrac{\ln(\frac{R_a}{R_c})}{2\sigma Z_a \tan^{-1}(\frac{R_v}{R_x})}$
C_{void} (F)	$C_{void} = \dfrac{\varepsilon_0 \varepsilon_r Z_a R_a K}{R_v{}^2 \int_0^{\frac{\pi}{2}} \cos(\tan^{-1}(\frac{R_v \cos\Theta}{R_x - R_v \sin\Theta}))\cos\Theta d\Theta}$
R_{void} (Ω)	$R_{void} = \dfrac{1}{\sigma Z_a} \dfrac{\int_0^{\frac{\pi}{2}} \cos(\tan^{-1}(\frac{R_v \cos\Theta}{R_x - R_v \sin\Theta}))\cos\Theta d\Theta}{\int_0^{\frac{\pi}{2}} \cos(\tan^{-1}(\frac{R_v \cos\Theta}{R_x - R_v \sin\Theta}))\sin\Theta d\Theta}$
R_{diss} (Ω)	$R_{diss} = \dfrac{eq}{mVZ_a} \dfrac{\int_0^{\frac{\pi}{2}} \cos(\tan^{-1}(\frac{R_v \cos\Theta}{R_x - R_v \sin\Theta}))\cos\Theta d\Theta}{\int_0^{\frac{\pi}{2}} \cos(\tan^{-1}(\frac{R_v \cos\Theta}{R_x - R_v \sin\Theta}))\sin\Theta d\Theta}$

Table 3.2. Final Equations of the Induced Charge Capacitive Model

Component	Equation
C_1 & C_2 (F)	$C = \frac{2\varepsilon_0 \varepsilon_r Z_a (\tan^{-1}(\frac{R_v}{R_x}))}{\ln(\frac{R_a}{R_c})}$
R_1 & R_2 (Ω)	$R = \frac{V}{I} = \frac{\ln(\frac{R_a}{R_c})}{2\sigma Z_a \tan^{-1}(\frac{R_v}{R_x})}$
C_{void} (F)	$C_{void} = \frac{\varepsilon_0 \varepsilon_r Z_a R_a K}{R_v{}^2 \int_0^{\frac{\pi}{2}} \cos(\tan^{-1}(\frac{R_v \cos\Theta}{R_x - R_v \sin\Theta})) \cos\Theta d\Theta}$
R_{void} (Ω)	$R_{void} = \frac{1}{\sigma Z_a} \frac{\int_0^{\frac{\pi}{2}} \cos(\tan^{-1}(\frac{R_v \cos\Theta}{R_x - R_v \sin\Theta})) \cos\Theta d\Theta}{\int_0^{\frac{\pi}{2}} \cos(\tan^{-1}(\frac{R_v \cos\Theta}{R_x - R_v \sin\Theta})) \sin\Theta d\Theta}$
$C_{induced}$ (F)	$C_{induced} = \frac{3\Pi (R_v)^2 Z_\alpha \varepsilon_o \varepsilon_r B \vec{E}_l}{U\sqrt{2R_v p R_x}}$

Table 3.3. Final Equations of the Adavanced Capacitive Model

Component	Equation
C_1 & C_2 (F)	$C = \frac{2\varepsilon_0 \varepsilon_r Z_a (\tan^{-1}(\frac{R_v}{R_x}))}{\ln(\frac{R_a}{R_c})}$
R_1 & R_2 (Ω)	$R = \frac{V}{I} = \frac{\ln(\frac{R_a}{R_c})}{2\sigma Z_a \tan^{-1}(\frac{R_v}{R_x})}$
C_{void} (F)	$C_{void} = \frac{\varepsilon_0 \varepsilon_r Z_a R_a K}{R_v^2 \int_0^{\frac{\pi}{2}} \cos(\tan^{-1}(\frac{R_v \cos\Theta}{R_x - R_v \sin\Theta})) \cos\Theta d\Theta}$
R_{void} (Ω)	$R_{void} = \frac{1}{\sigma Z_a} \frac{\int_0^{\frac{\pi}{2}} \cos(\tan^{-1}(\frac{R_v \cos\Theta}{R_x - R_v \sin\Theta})) \cos\Theta d\Theta}{\int_0^{\frac{\pi}{2}} \cos(\tan^{-1}(\frac{R_v \cos\Theta}{R_x - R_v \sin\Theta})) \sin\Theta d\Theta}$
$R_{streamer2}$ (Ω)	$R_{streamer\,2} = \frac{mV}{eqZ_a} \frac{\int_0^{\frac{\pi}{2}} \cos(\tan^{-1}(\frac{R_v \cos\Theta}{R_x - R_v \sin\Theta})) \cos\Theta d\Theta}{\int_0^{\frac{\pi}{2}} \cos(\tan^{-1}(\frac{R_v \cos\Theta}{R_x - R_v \sin\Theta})) \sin\Theta d\Theta}$
σ_1 (S/m)	$\sigma_1 = \frac{e}{mV_m} \frac{\pi\varepsilon_o}{4} (2\varepsilon_r + 1)(E/p)_{cr} p l^2 [1 - \gamma + \frac{(K_{cr})^{\frac{1}{\beta}}}{(E/p)_{cr} (C)^{\frac{1}{\beta}} (pl)^{\frac{1}{\beta}}}]$
$R_{streamer1}$ (Ω)	$R_{streamer\,1} = \frac{1}{\sigma_1 Z_a} \frac{\int_0^{\frac{\pi}{2}} \cos(\tan^{-1}(\frac{R_v \cos\Theta}{R_x - R_v \sin\Theta})) \cos\Theta d\Theta}{\int_0^{\frac{\pi}{2}} \cos(\tan^{-1}(\frac{R_v \cos\Theta}{R_x - R_v \sin\Theta})) \sin\Theta d\Theta}$
C_{dipole} (F)	$C_{dipole} = \varepsilon_o Z_a$

CHAPTER 4

VOID MODELING AND THE ELECTRICAL NETWORK

4.1 The Power Network of Cyprus

The power network of Cyprus is a small isolated grid running at 50 Hz. Before 1955 only the major cities of the island were electrified by local generation companies each one established at the major cities of the island. After 1955 the Electricity Authority of Cyprus (EAC) was established, and the production of electrical energy was centralized. Since the establishment of the Republic of Cyprus in 1960, the generation, transmission and distribution network of the island has been developed rapidly and until 1974 managed to supply with electrical energy all the isolated villages at remote parts of the island.

The industry of the island is based on services and tourism. This makes the electrical load of the island highly seasonable and susceptible to weather conditions. The maximum demand of the island has been recorded on the 31st of July in 2007 reaching the value of 1100 MW.

a. The Generation System of Cyprus

The generation system of Cyprus consists of three oil fired steam power stations located at the coast side of the island. The peak demand of the island is anticipated by means of gas turbines located at Moni power station. During the summer of 2009 the first combined cycle gas turbine unit was commissioned at Vasilikos power station with combined output of 180 MW. Three more similar units are planned to be installed in the near future.

b. The Transmission Network of Cyprus

The Transmission network in Cyprus is a small network consisting only of a few hundreds of kilometres of overhead and underground cables. The transmission system is operated at 132 and 66 kV and interconnects the major cities and big loads with the three power stations of the island. In the last decade the old 66 kV network is under decommissioning and is constantly being upgraded to 132 kV. Due to the sudden growth of the energy demand of the island the transmission voltage it is planed to be upgraded to 220 kV in the near future.

c. The Distribution Network of Cyprus

The distribution Network of Cyprus is operated at 11 kV consisting of underground and overhead lines. Paper insulated oil immersed 11 kV medium cables have been used as the core of the distribution network. During the last fifteen years, EAC has changed insulation technology: from the paper insulated to XLPE cables. This change in insulation technology has been accompanied by cable failures (especially at the transition joints between paper insulated and XLPE cables) with the result of unwanted interruption of electrical energy to the customers. Because of the fact that cable failures were initially related to PD activity, the model of PD activity within the XLPE cables is the main motivation of this work.

4.2 Model of Electrical Network in MATLAB/Simulink

A part of the 11 kV Distribution Network (DN), in the city of Paphos in Cyprus was chosen as the electrical network to be modeled in MATLAB/Simulink as shown in Fig. 4.1. The 11 kV DN is supplied by three power transformers (PT) 15 MVA each, 66/11 kV DYn11. The 6 km 300 mm^2 aluminum 11 kV XLPE cable under investigation is represented by Line and Line1 elements respectively. The cable is loaded at the far end with a 2 MVA load at 0.97 lagging power factor. The load is represented in Fig. 4.1 by the element "Load". The DN is loaded with a 10 MVA load at 0.97 lagging power factor during summer time, and represented by element "Load1" in Fig. 4.1. The 3-phase source represents the Thevenin equivalent circuit of the transmission system and the three power transformers feeding the distribution network. The electrical equivalent circuit of the void(s) as presented in Figs. 3.1 and 3.2 is represented in Fig 4.1 as element "0.5 mm RVoid2" in a sub-circuit configuration and is connected to phase 'A' of the three phase medium voltage cable. The HF model of the cable is represented in Fig. 4.1 as element "HF LINE" in the sub-circuit configuration. The HF model is represented as a single phase distributed line parameter of MATLAB/Simulink's library capable of representing wave propagation phenomena and line-end reflections. The limitation of MATLAB/Simulink's distributed line parameter is its incapability of representing the frequency dependence of R-L-C parameters of the real power lines with sufficient accuracy. For these particular reasons the HF cable R-L-C parameters as presented in [32, 33] have been calculated and utilized in the single phase distributed parameter line in the sub-circuit "HF LINE" configuration.

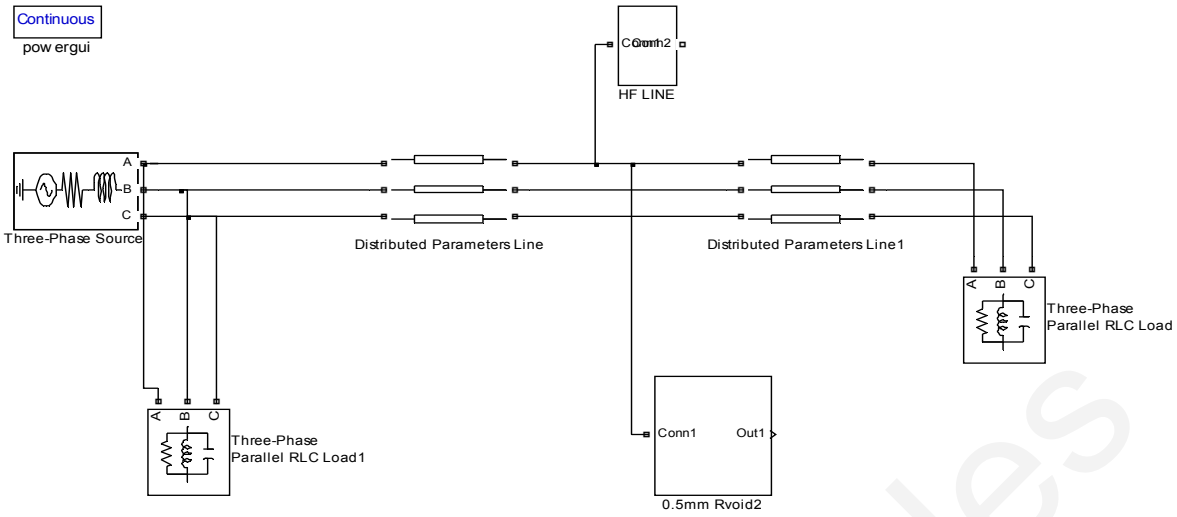

Fig. 4.1. The model of the distribution network and void

All parameters used for the model of Fig. 4.1 were taken from available manufacturer data sheets [34], apart from the '3-phase source', which was calculated using the 'DigSilent' software. The R-L-C, frequency-dependent parameters of the HF model of the cable ("HF LINE" in the sub-circuit configuration of Fig. 4.1) were calculated by utilizing equations of series impedance 'z' and shunt admittance 'y' as discussed in [35] and by utilizing the code of Appendix A. The 50 Hz and HF R-L-C-G elements of the cable under consideration are presented in Table 4.1 below. HF elements were calculated based on 10 MHz frequency.

Table 4.1: R-L-G-C Components of 22 kV 300 mm2 Single Core XLPE Cable

	R/km (Ω)	L/km (H)	G/km (S)	C/km (F)
HF (10 MHz)	24.470	$1.25\text{x}10^{-4}$	$1.611\text{x}10^{-5}$	$1.802\text{x}10^{-5}$
LF (50 Hz)	0.1295	$3.31\text{x}10^{-5}$	_	$5.4\text{x}10^{-7}$

4.3 The Improved Capacitive Model of Void

The electrical model of the improved capacitive model of void is utilised as element void (sub-circuit) in Fig. 4.1 and is presented in detail in Fig. 4.2. The circuits included in element 'void' were calculated in MATLAB (as presented in Appendix A) by utilizing (3.13), (3.41), (3.46) and (3.51) for cylindrical voids for various radii (R_v) and length of Z_a. For all cases the void is supposed to be located in the middle of the distance between the core and the outer sheath of the cable at 3 km away from the origin of the cable. The

value of R_{diss} was calculated by first substituting to (3.61) the values of 'q' as presented in [33] for three different levels of electron densities (average, minimum and maximum) and further substituting (3.61) to (3.51).

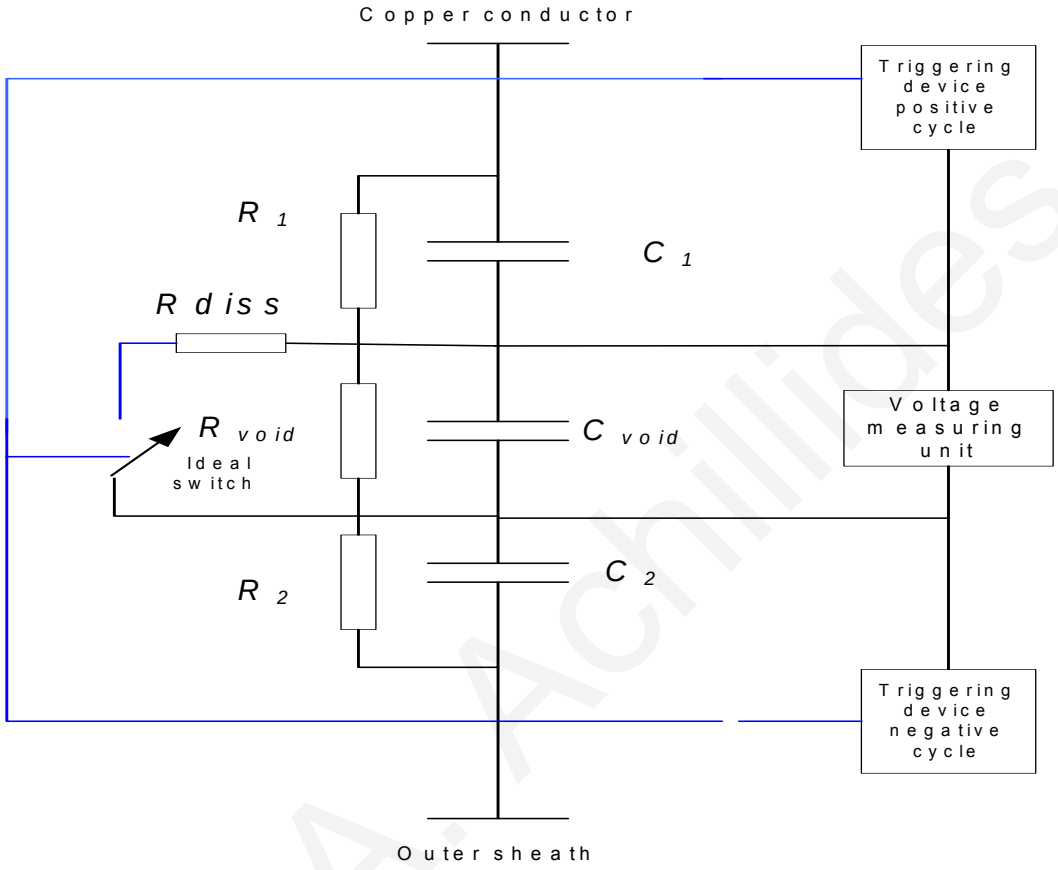

Fig. 4.2. The improved capacitive model of void

In Table 4.2 all elements of Fig. 4.2 are presented for cylindrical void of radius and lengths of 0.5 mm, 1 mm and 1.5 mm respectively.

The minimum voltage level (V_{on}) required to initiate the discharge was taken to be 1.4 kV, 4 kV, 5 kV for 0.5 mm, 1 mm, and 1.5 mm voids diameter and the voltage level across the void where breakdown ceases (V_{off}) was taken to be 0 V (Fig. 4.2) for all three cases for positive the cycle only.

Table 4.2: Calculated Elements of the Improved Capacitive Model

	R_v and Z_a (mm)		
	0.5	1	1.5
C_1 (F)	$6.91\text{x}10^{-15}$	$4.38\text{x}10^{-14}$	$2.56\text{x}10^{-13}$
R_1 (Ω)	$2.89\text{x}10^{15}$	$4.56\text{x}10^{14}$	$7.82\text{x}10^{13}$
C_v (F)	$9.5\text{x}10^{-15}$	$1.08\text{x}10^{-14}$	$2.55\text{x}10^{-14}$
R_v (Ω)	$4.0\text{x}10^{16}$	$2.00\text{x}10^{16}$	$1.33\text{x}10^{16}$
C_2 (F)	$2.085\text{x}10^{-15}$	$9.23\text{x}10^{-15}$	$2.31\text{x}10^{-14}$
R_2 (Ω)	9.59e15	$2.16\text{x}10^{15}$	$8.66\text{x}10^{14}$
R_{diss} (average) (Ω)	1000	520	350
$R_{dis\ s}$(minimum) (Ω)	840	420	280
R_{diss} (maximum) (Ω)	1400	700	470

4.4 The Model of Void Based on the Induced Charge Concept

The electrical model of the void based on the induced charge concept, is utilised as element void (sub-circuit) in Fig. 4.1 and is presented in detailed in Fig. 4.3.

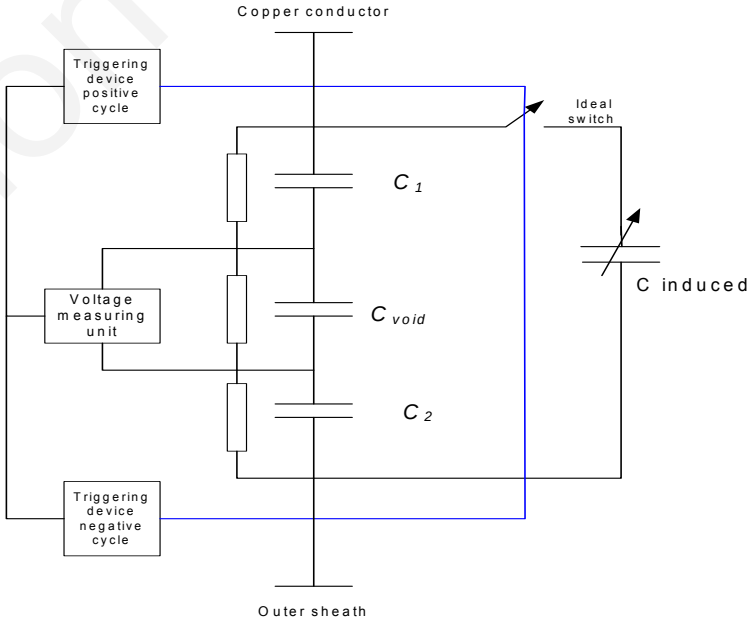

Fig. 4.3. The model of void based on the induced charge concept

The circuits included in element 'void' were calculated in MATLAB (as presented in Appendix A,) by utilizing (3.13), (3.41), (3.46), (3.51) for cylindrical voids of various radii (R_v) and length of Z_a. The value of $C_{induced}$ was calculated using (3.54). For all cases the void is supposed to be located in the middle of the distance between the core and the outer sheath of the cable at 3 km away from the origin of the cable.

In Table 4.3 all elements of Fig. 4.3 are presented for cylindrical voids of radii and length of 0.5 mm, 1 mm and 1.5 mm respectively.

The minimum voltage level (V_{on}) required to initiate the discharge was taken to be 3 kV (negative cycle only), 3.5 kV (positive cycle only), 4 kV (positive cycle only) for void diameter of 0.5 mm, 1 mm, and 1.5 mm and the voltage level across the void where breakdown ceases (V_{off}) was taken to be 0 V (Fig. 4.2) for all three cases.

Table 4.3: Calculated Elements of the Induced Charge Model

	R_V and Z_a (mm)		
	0.5	1	1.5
C_1 (F)	$6.91\text{x}10^{-15}$	$4.38\text{x}10^{-14}$	$2.56\text{x}10^{-13}$
R_1 (Ω)	$2.89\text{x}10^{15}$	$4.56\text{x}10^{14}$	$7.82\text{x}10^{13}$
C_v (F)	$9.5\text{x}10^{-15}$	$1.08\text{x}10^{-14}$	$2.55\text{x}10^{-14}$
R_v (Ω)	$4.0\text{x}10^{16}$	$2.00\text{x}10^{16}$	$1.33\text{x}10^{16}$
C_2 (F)	$2.085\text{x}10^{-15}$	$9.23\text{x}10^{-15}$	$2.31\text{x}10^{-14}$
R_2 (Ω)	9.59e15	$2.16\text{x}10^{15}$	$8.66\text{x}10^{14}$
$C_{induced}$ (F)	2.11e-20	1.19e-19	3.29e-19

4.5 The Advanced Capacitive Model of Void

The electrical model of void based on lumped capacitors (as the classical capacitive model of void) was enhanced by two more factors: the deployment of charges for anode directed streamers and the conductivity of the streamer channel itself is utilized as element void (sub-circuit) in Fig. 4.1 and is presented in detail in Fig. 4.4.

The circuits included in element 'void' were calculated in MATLAB (as presented in Appendix A,) by utilizing (3.13), (3.41), (3.46), (3.51) for cylindrical voids for various radii (R_v) and length of Z_a. The elements C_{dipole} and R_{stream} are calculated by utilizing (3.76), (3.64), and (3.63) respectively. For all cases the void is supposed to be located in

the middle of the distance between the core and the outer sheath of the cable at 3 km away from the origin of the cable.

In Table 4.4 all elements of Fig. 4.4 are presented for cylindrical void of radius and length of 0.5 mm, 1 mm and 1.5 mm respectively. The minimum voltage level (V_{on}) required to initiate the discharge (stage (I)) was taken to be 2.4 kV, 4 kV, 5 kV for void diameters of 0.5 mm, 1mm, and 1.5 mm and the voltage level across the void where breakdown ceases (V_{off}) was taken to be 0 V (Fig. 4.2) for all three cases for negative cycle only. The stage (II) discharge process time delayed was set to $1x10^{-9}$ s for all three cases.

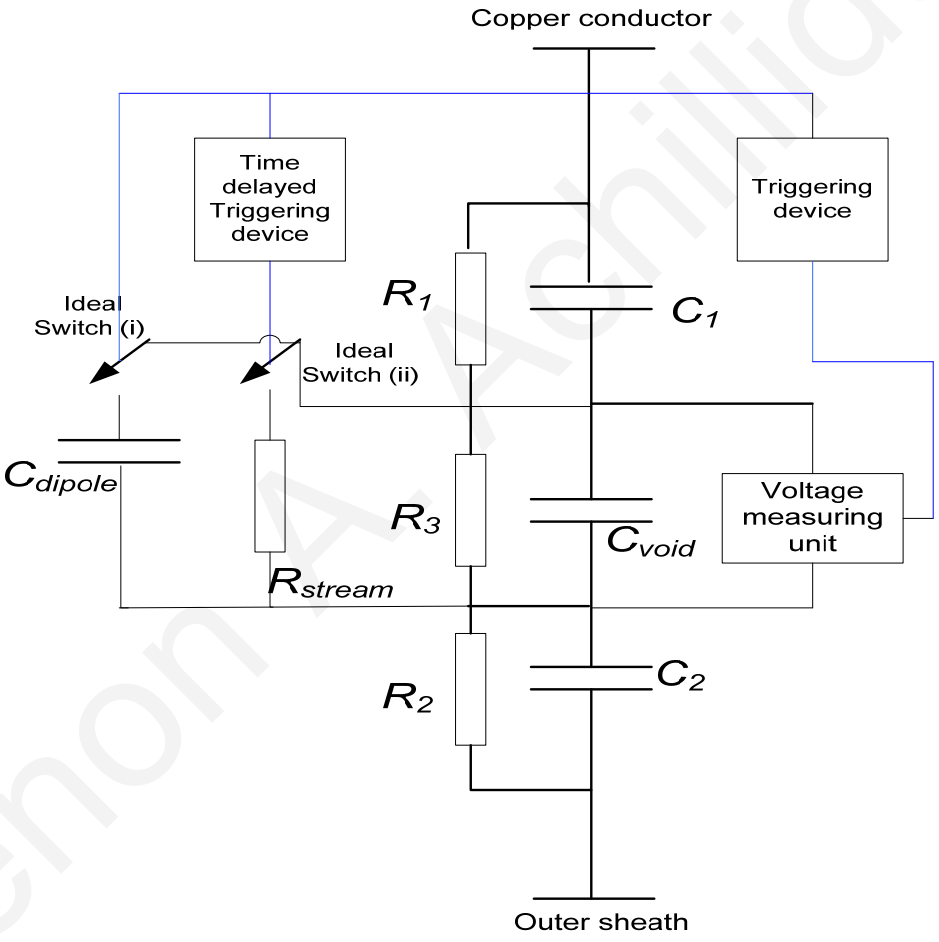

Fig. 4.4. The advanced capacitive model of void

Table 4.4: Calculated Elements of the Advanced Capacitive Model

	R_V and Z_a (mm)		
	0.5	1	1.5
C_1 (F)	6.91×10^{-15}	4.38×10^{-14}	2.56×10^{-13}
R_1 (Ω)	2.89×10^{15}	4.56×10^{14}	7.82×10^{13}
C_v (F)	9.5×10^{-15}	1.08×10^{-14}	2.55×10^{-14}
R_v (Ω)	4.0×10^{16}	2.00×10^{16}	1.33×10^{16}
C_2 (F)	2.085×10^{-15}	9.23×10^{-15}	2.31×10^{-14}
R_2 (Ω)	9.59×10^{15}	2.16×10^{15}	8.66×10^{14}
C_{dipole} (F)	$4.42e \times 10^{-15}$	8.85×10^{-15}	1.33×10^{-15}
$R_{streamer2}$ (Ω)	1000	520	350
$R_{streamer1}$ (Ω)	105×10^{3}	110×10^{3}	116×10^{3}

CHAPTER 5

SIMULATION RESULTS

In this Chapter the simulated transients generated by a breakdown void, as well as their propagation and attenuation along a medium voltage cable, are presented for the classical capacitive model of void and the three proposed models are going to be presented and discussed, for cylindrical voids of radius of 0.5 mm, 1 mm, and 1.5 mm respectively.

5.1 The Classical Capacitive Model of Void

The transients generated by a breakdown void, as well as their traveling and attenuation along a medium voltage cable, are presented in this sub-section for the classical capacitive model. These results are based on the case study described in Chapter 4. The model utilized to replicate the transients of the classical capacitive model, is the model presented in Fig. 4.2 with $R_{diss} = 0.01\ \Omega$.

5.1.1 Void of radius 0.5 mm

The simulated results of a cylindrical void of radius and length of 0.5 mm are presented. The void is located in the middle of the distance between the core and the outer sheath of the cable at 3 km away from the origin of the cable.

The minimum voltage level (V_{on}) required to initiate the discharge was taken to be 2 kV and the voltage level across the void where breakdown ceases (V_{off}) was taken to be 0 V (Fig. 4.2), both values for the positive cycle only.

Fig. 5.1 shows the high frequency voltage superimposed on the 50 Hz power frequency waveform caused by a breakdown void at the point where the void is located. In Fig. 5.2 the waveform of the spike of Fig. 5.1 is shown in detail. The spike has a duration of a fraction of picoseconds (ps) and reaches a maximum amplitude of 1500 V.

Fig. 5.3 shows the high frequency current-spike flowing from the external circuit to the breakdown void. The spike has a duration of a fraction of picoseconds (ps) and reaches a maximum amplitude of 170 A.

Fig. 5.4 shows the attenuated voltage spike observed at the receiving end of the cable located 3 km from the breakdown void. The spike's duration has increased to the order of microseconds (μS) and its maximum amplitude drops to 2.5 mV.

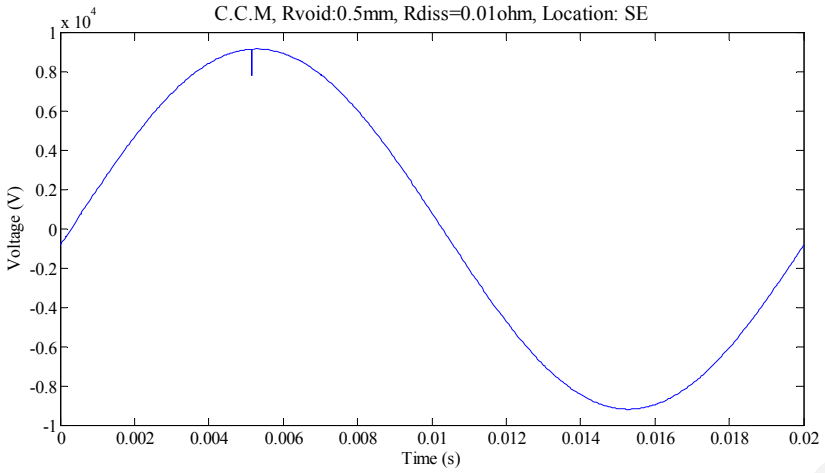

Fig. 5.1. High frequency voltage spike superimposed on the 50 Hz power frequency waveforms generated by a breakdown void at the point where the void is created

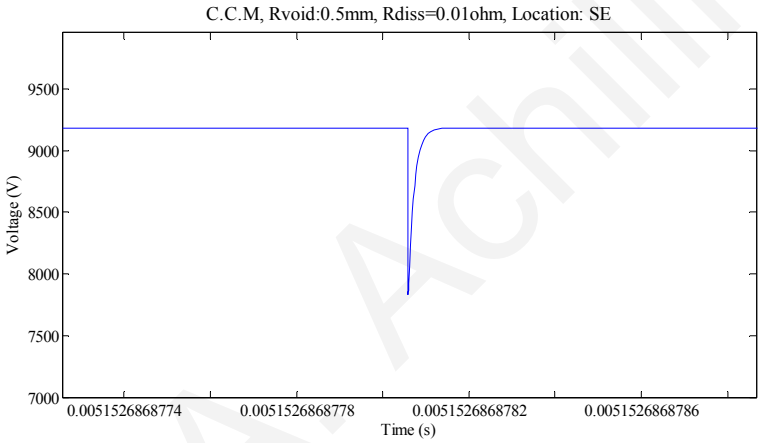

Fig. 5.2. Detailed view of voltage waveforms at the point of the spike (zoomed in from Fig. 5.1).

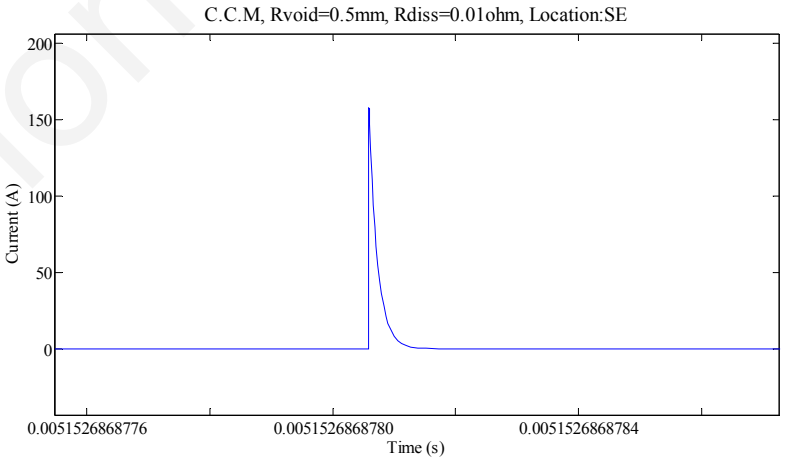

Fig. 5.3. Detailed view of current waveforms flowing from external circuit to breakdown void

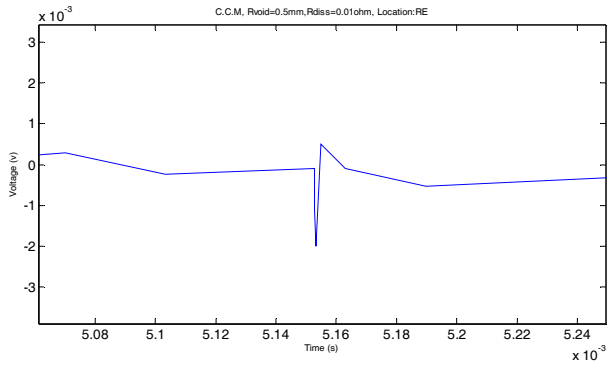

Fig. 5.4. Voltage spike at the receiving end of the 11 kV cable, (HF model) 3 km away from the breakdown void

5.1.2 Void of radius 1 mm

The simulated results of a cylindrical void of radius and length of 1 mm are presented. The void is located in the middle of the distance between the core and the outer sheath of the cable at 3 km away from the origin of the cable. The minimum voltage level (V_{on}) required to initiate the discharge was taken to be 3 kV and the voltage level across the void where breakdown ceases (V_{off}) was taken to be 0 V (Fig.4.2), both values for the positive cycle only.

Fig. 5.5 shows the high frequency voltage superimposed on the 50 Hz power frequency waveform caused by a breakdown void at the point where the void is located. In Fig. 5.6 the waveform of the spike of Fig. 5.5 is shown in detail. The spike has a duration of a fraction of picoseconds (ps) and reaches a maximum amplitude of 4000 V.

Fig. 5.7 shows the high frequency current-spike flowing from the external circuit to the breakdown void. The spike has a duration of a fraction of picoseconds (ps) and reached maximum amplitude of a 500 A.

Fig. 5.8 shows the attenuated voltage spike observed at the receiving end of the cable located 3 km from the breakdown void. The spike's duration has increased to the order of microseconds (μS) and its maximum amplitude drops to 0.8 mV.

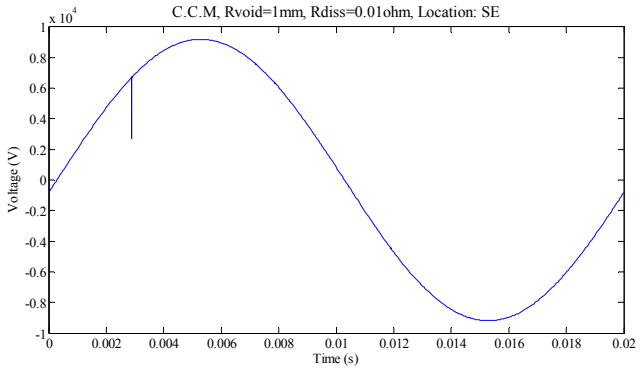

Fig. 5.5. High frequency voltage spike superimposed on the 50 Hz power frequency waveform generated by a breakdown void at the point where the void is created

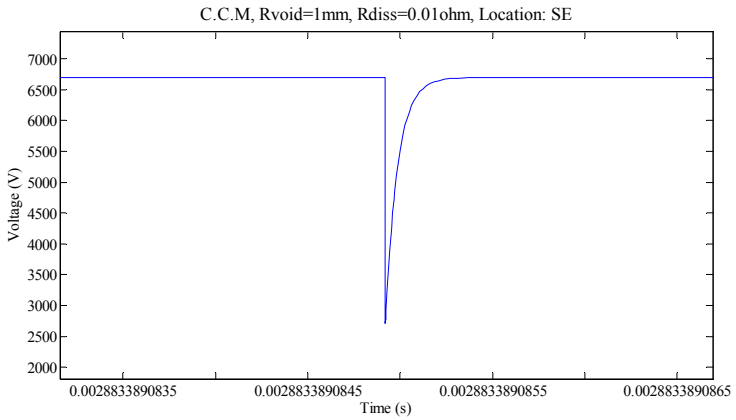

Fig. 5.6. Detailed view of voltage waveforms at the point of the spike (zoomed in from Fig. 5.5)

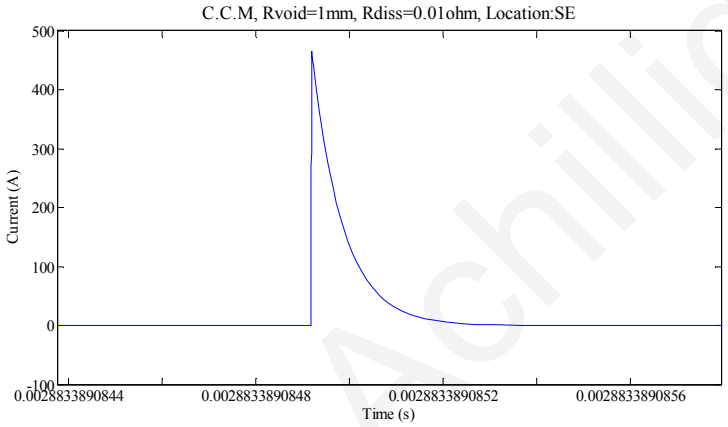

Fig. 5.7. Detailed view of current waveforms flowing from external circuit to breakdown void

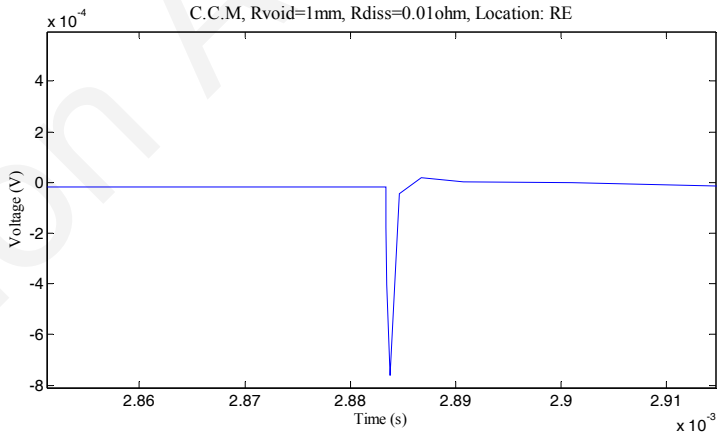

Fig. 5.8. Voltage spike at the receiving end of the 11 kV cable, (HF model) 3 km away from the breakdown void

5.1.3 Void of radius of 1.5 mm

The simulated results of a cylindrical void of radius and length of 1.5 mm are presented. The void is located in the middle of the distance between the core and the outer sheath of the cable at 3 km away from the origin of the cable. The minimum

voltage level (V_{on}) required to initiate the discharge was taken to be 5 kV and the voltage level across the void where breakdown ceases (V_{off}) was taken to be 0 V (Fig.4.2), both values for the positive cycle only.

Fig. 5.9 shows the high frequency voltage superimposed on the 50 Hz power frequency waveform caused by a breakdown void at the point where the void is located. In Fig. 5.10 the waveform of the spike of Fig. 5.9 is shown in detail. The spike has a duration of a fraction of picoseconds (ps) and reached a maximum amplitude of 5000 V.

Fig. 5.11 shows the high frequency current-spike flowing from the external circuit to the breakdown void. The spike has a duration of a fraction of picoseconds (ps) and reached maximum amplitude of 600 A.

Fig. 5.12 shows the attenuated voltage spike observed at the receiving end of the cable located 3 km from the breakdown void. The spike's duration has increased to the order of microseconds (μS) and its maximum amplitude drops to 0.2 mV.

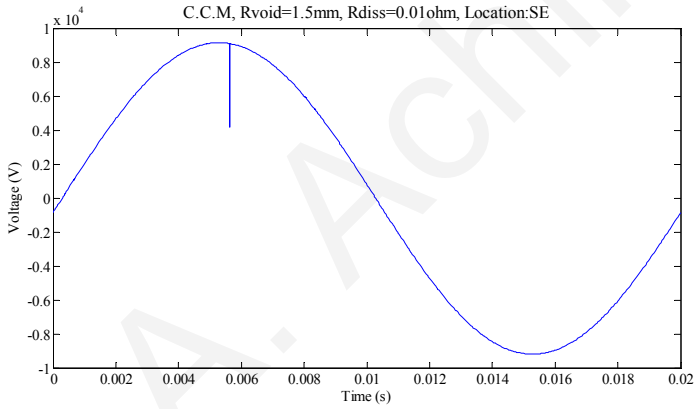

Fig. 5.9. High frequency voltage spike superimposed on the 50 Hz power frequency waveforms generated by a breakdown void at the point where the void is created

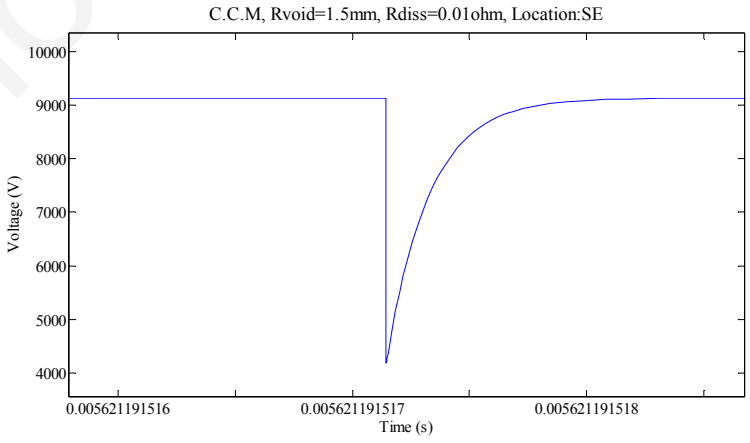

Fig. 5.10. Detailed view of voltage waveforms at the point of the spike (zoomed in from Fig. 5.9)

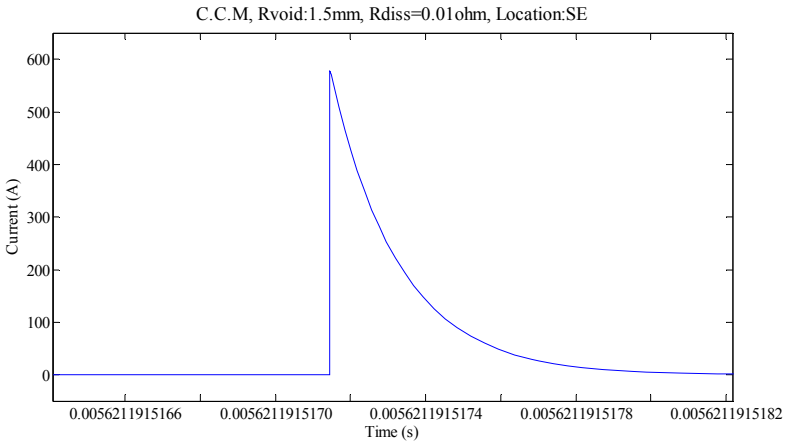

Fig. 5.11. Detailed view of current waveforms flowing from external circuit to breakdown void

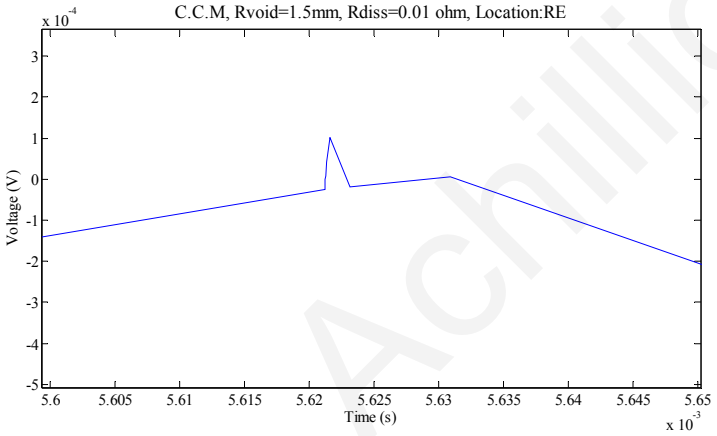

Fig. 5.12. Voltage spike at the receiving end of the 11 kV cable, (HF model) 3 km away from the breakdown void

5.2 The Improved Capacitive Model of Void

The transients generated by a breakdown void, as well as their traveling and attenuation along a medium voltage cable, are presented in this sub-section for the improved capacitive model. These results are based on the case study described in Chapter 4.

5.2.1 Void of radius of 0.5 mm

The simulated results of a cylindrical void of radius and length of 0.5 mm are presented for three distinct cases: for ionized resistance path, (R_{diss}) of a) 1400 Ω, b) 1000 Ω and c) 840 Ω respectively. The void (for all three cases) is located in the middle of the distance between the core and the outer sheath of the cable at 3 km away from the origin of the cable.

The minimum voltage level (V_{on}) required to initiate the discharge was taken to be 2 kV and the voltage level across the void where breakdown ceases (V_{off}) was taken to be 0 V (Fig. 4.2), both values for the positive cycle only.

a. Void of radius of 0.5 mm – R_{diss} =1400 Ω

Fig. 5.13 shows the high frequency voltage superimposed on the 50 Hz power frequency waveform caused by a breakdown void at the point where the void is located. In Fig. 5.14 the waveform of the spike of Fig. 5.13 is shown in detail. The spike has a duration of a fraction of nanoseconds (ns) and reaches a maximum amplitude of 1 V.

Fig. 5.15 shows the high frequency current-spike flowing from the external circuit to the breakdown void. The spike has a duration of fraction of nanoseconds (ns) and reaches maximum amplitude of 0.15 A.

Fig. 5.16 shows the attenuated voltage spike observed at the receiving end of the cable located 3 km from the breakdown void. The spike's duration has increased to the order of microseconds (μs) and its maximum amplitude drops to 3.0 mV.

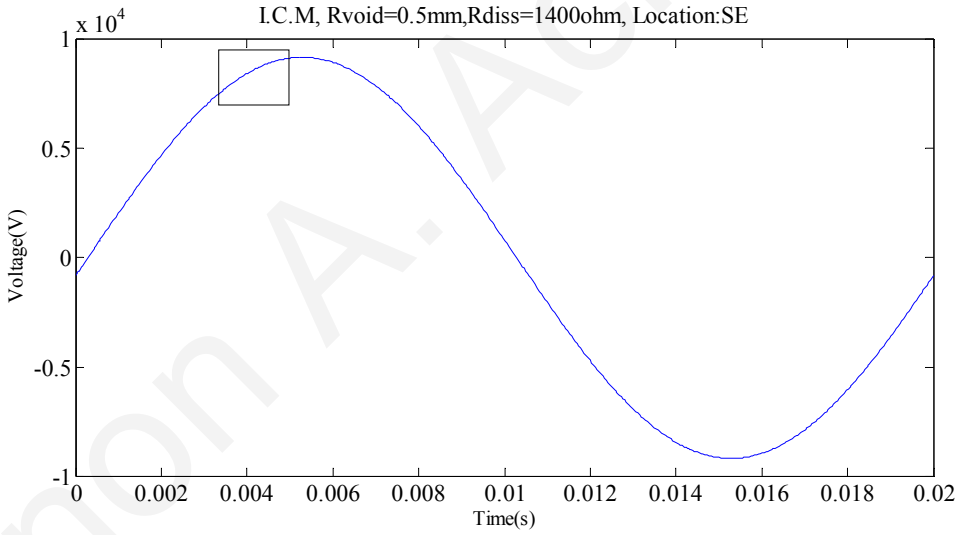

Fig. 5.13. High frequency voltage spike superimposed on the 50 Hz power frequency waveforms generated by a breakdown void at the point where the void is created

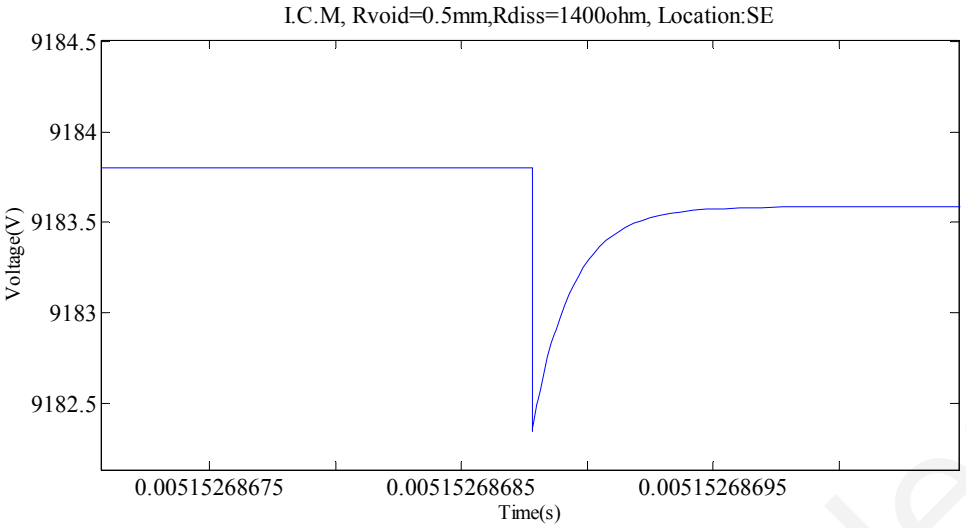

Fig. 5.14. Detailed view of voltage waveforms at the point of the spike (zoomed in from Fig. 5.13)

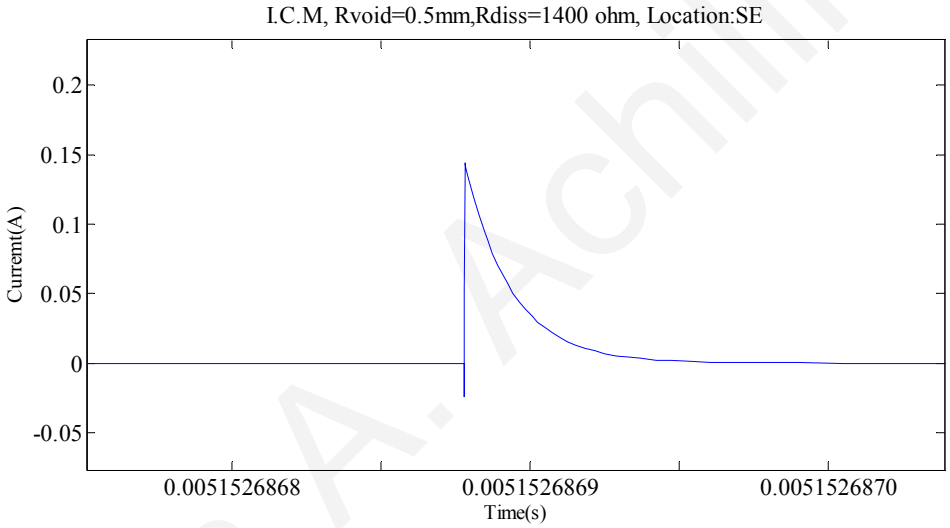

Fig. 5.15. Detailed view of current waveforms flowing from the external circuit to the breakdown void

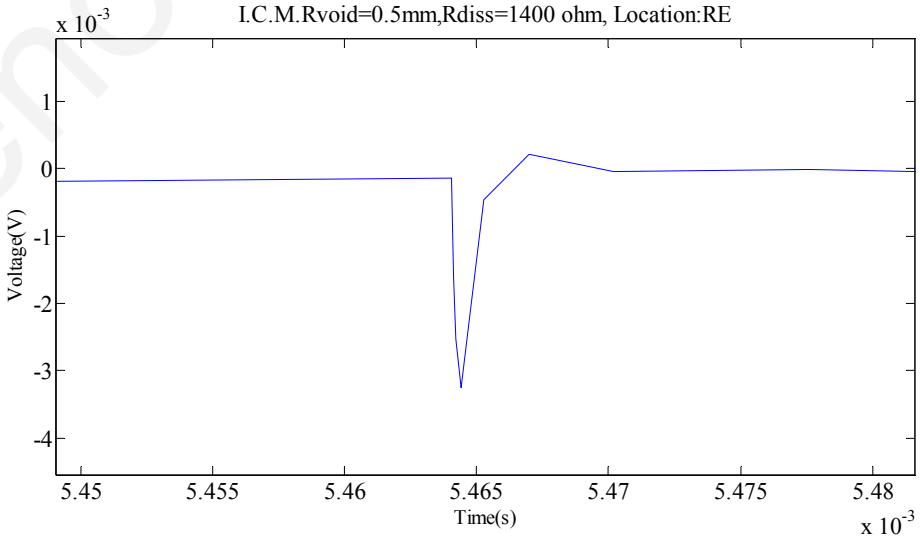

Fig. 5.16. Voltage spike at the receiving end of the 11 kV cable, (HF model) 3 km away from the breakdown void

b. Void of radius of 0.5 mm – R_{diss} = 1000 Ω

Fig. 5.17 shows the high frequency voltage superimposed on the 50 Hz power frequency waveform caused by a breakdown void at the point where the void is located. In Fig. 5.18 the waveform of the spike of Fig. 5.17 is shown in detail. The spike has duration of a fraction of nanoseconds (ns) and reaches a maximum amplitude of 2 V.

Fig. 5.19 shows the high frequency current-spike flowing from the external circuit to the breakdown void. The spike has a duration of a fraction of nanoseconds (ns) and reaches a maximum amplitude of 0.2 A.

Fig. 5.20 shows the attenuated voltage spike observed at the receiving end of the cable located 3 km from the breakdown void. The spike's duration has increased to the order of microseconds (μS) and its maximum amplitude drops to 2.5 mV.

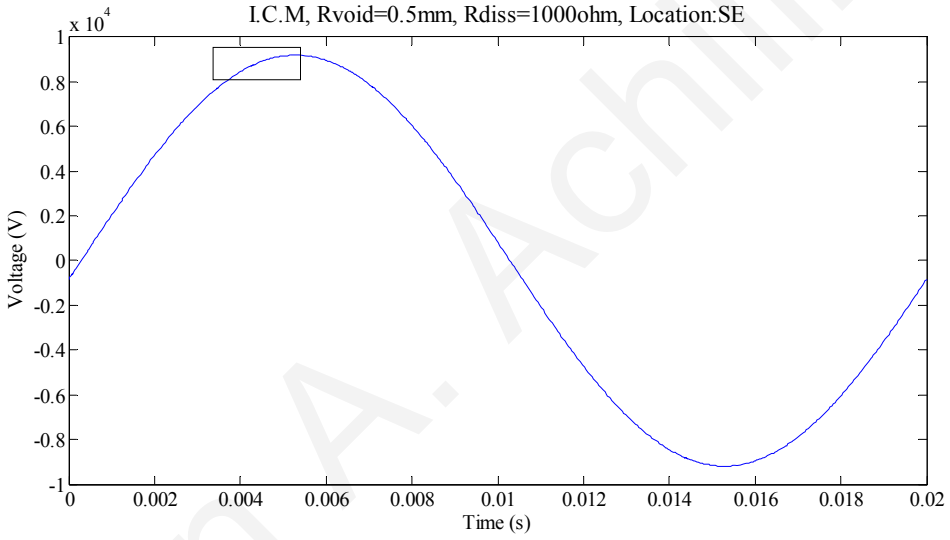

Fig. 5.17. High frequency voltage spike superimposed on the 50 Hz power frequency waveforms generated by a breakdown void at the point where the void is created

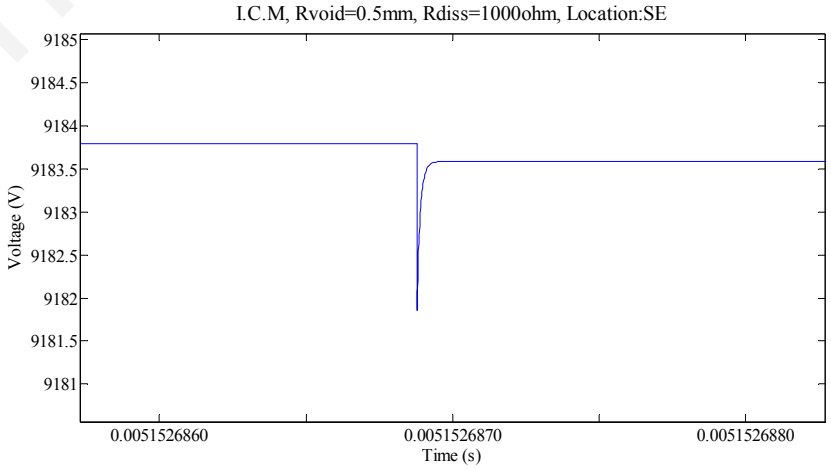

Fig. 5.18. Detailed view of voltage waveforms at the point of the spike (zoomed in from Fig. 5.17)

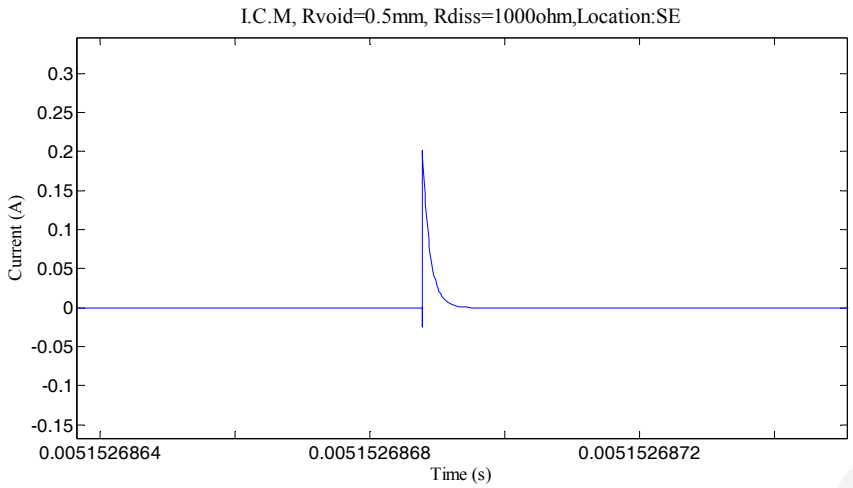

Fig. 5.19. Detailed view of current waveforms flowing from external circuit to breakdown void

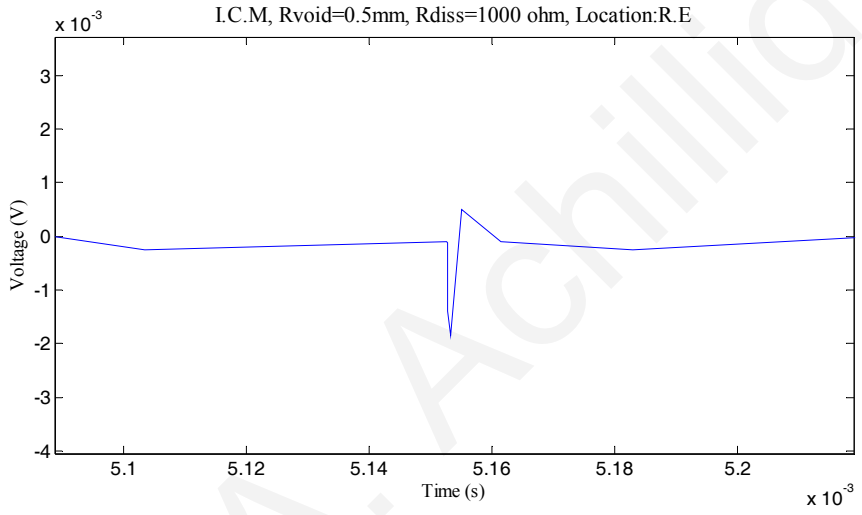

Fig. 5.20. Voltage spike at the receiving end of the 11 kV cable, (HF model) 3 km away from the breakdown void

c. Void of radius of 0.5 mm – R_{diss} = 840 Ω

Fig. 5.21 shows the high frequency voltage superimposed on the 50 Hz power frequency waveform caused by a breakdown void at the point where the void is located. In Fig. 5.22 the waveform of the spike of Fig. 5.21 is shown in detail. The spike has duration of a fraction of nanoseconds (ns) and reaches a maximum amplitude of 1 V.

Fig. 5.23 shows the high frequency current-spike flowing from the external circuit to the breakdown void. The spike has a duration of a fraction of nanoseconds (ns) and reaches maximum amplitude of 0.3 A.

Fig. 5.24 shows the attenuated voltage spike observed at the receiving end of the cable located 3 km from the breakdown void. The spike's duration has increased to order of microseconds (μS) and its maximum amplitude drops to 3.0 mV.

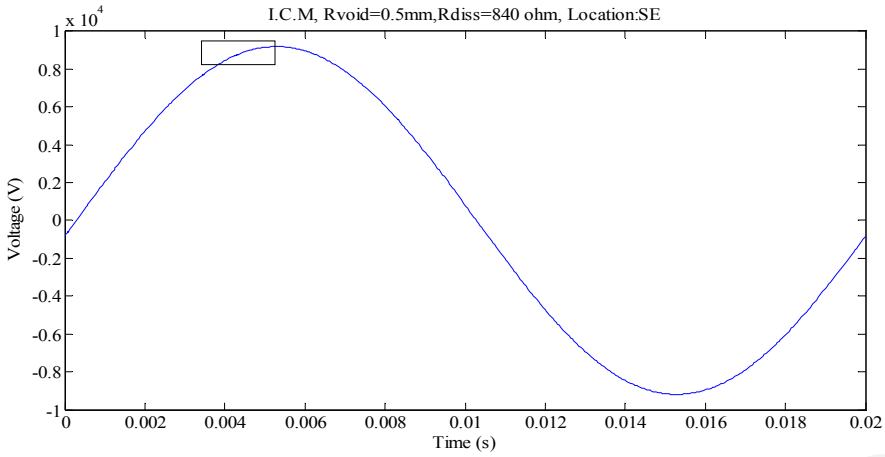

Fig. 5.21. High frequency voltage spike superimposed on the 50 Hz power frequency waveforms generated by a breakdown void at the point where the void is created

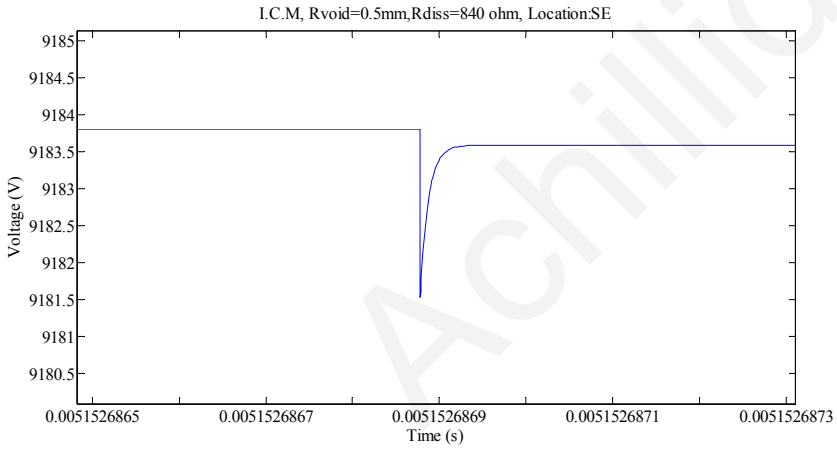

Fig. 5.22. Detailed view of voltage waveforms at the point of the spike (zoomed in from Fig. 5.21)

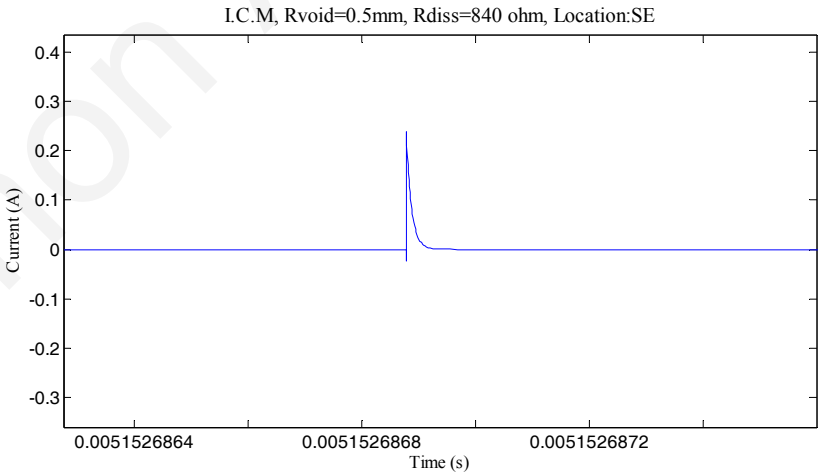

Fig. 5.23. Detailed view of current waveforms flowing from external circuit to breakdown void

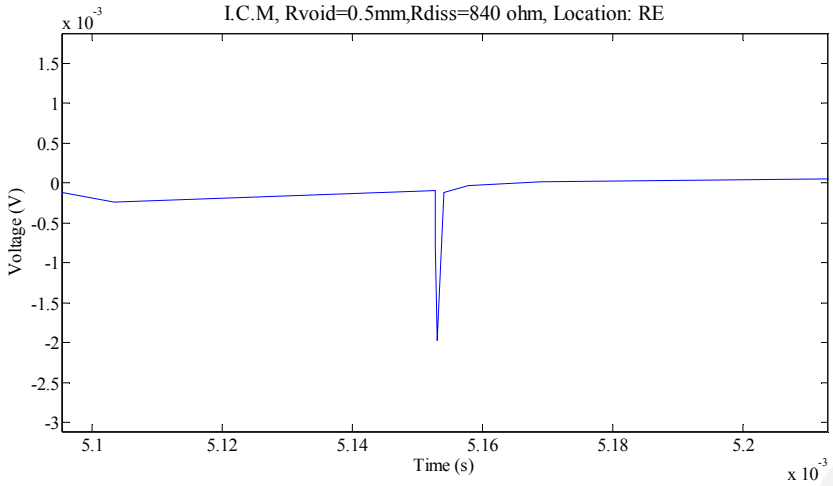

Fig. 5.24. Voltage spike at the receiving end of the 11 kV cable, (HF model) 3 km away from the breakdown void

5.2.2 Void of radius of 1 mm

The simulated results of a cylindrical void of radius and length of 1 mm are presented for three distint cases: for ionized resistance path, (R_{diss}) of a) 700 Ω, b) 520 Ω and c) 420 Ω respectively. The void (for all three cases) is located in the middle of the distance between the core and the outer sheath of the cable at 3 km away from the origin of the cable.

The minimum voltage level (V_{on}) required to initiate the discharge was taken to be 3 kV and the voltage level across the void where breakdown ceases (V_{off}) was taken to be 0 V (Fig.4.2) both values for the positive cycle only.

a. Void of radius of 1 mm – R_{diss}= 700 Ω

Fig. 5.25 shows the high frequency voltage superimposed on the 50 Hz power frequency waveform caused by a breakdown void at the point where the void is located. In Fig. 5.26 the waveform of the spike of Fig. 5.25 is shown in detail. The spike has duration of a fraction of nanoseconds (ns) and reaches maximum amplitude of 25 V.

Fig. 5.27 shows the high frequency current-spike flowing from the external circuit to the breakdown void. The spike has a duration of a fraction of nanoseconds (ns) and reaches maximum amplitude of 2.5 A.

Fig. 5.28 shows the attenuated voltage spike observed at the receiving end of the cable located 3 km from the breakdown void. The spike's duration has increased to a few microseconds (μS) and its maximum amplitude drops to 0.6 mV.

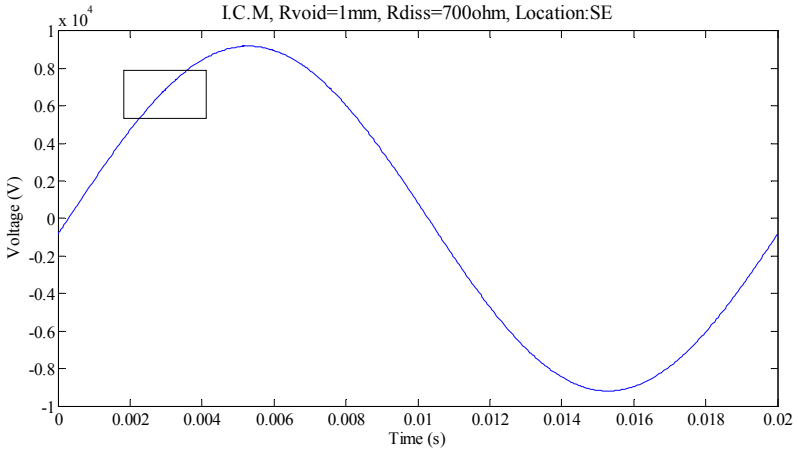

Fig. 5.25. High frequency voltage spike superimposed on the 50 Hz power frequency waveforms generated by a breakdown void at the point where the void is created

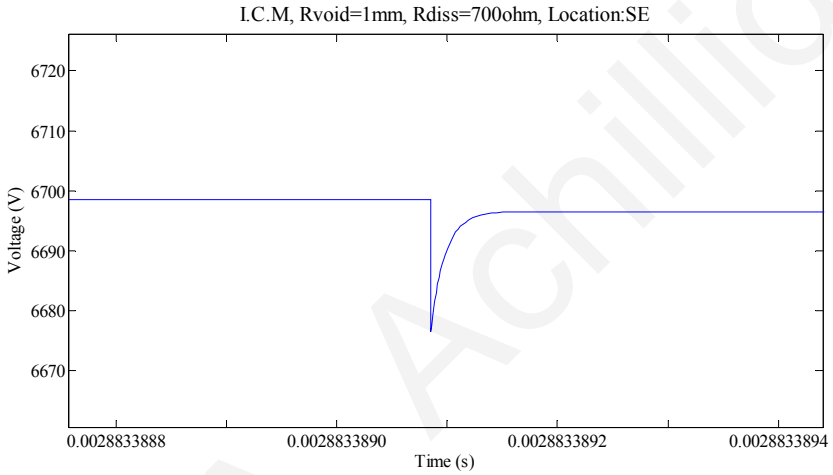

Fig. 5. 26. Detailed view of voltage waveforms at the point of the spike (zoomed in from Fig. 5..25)

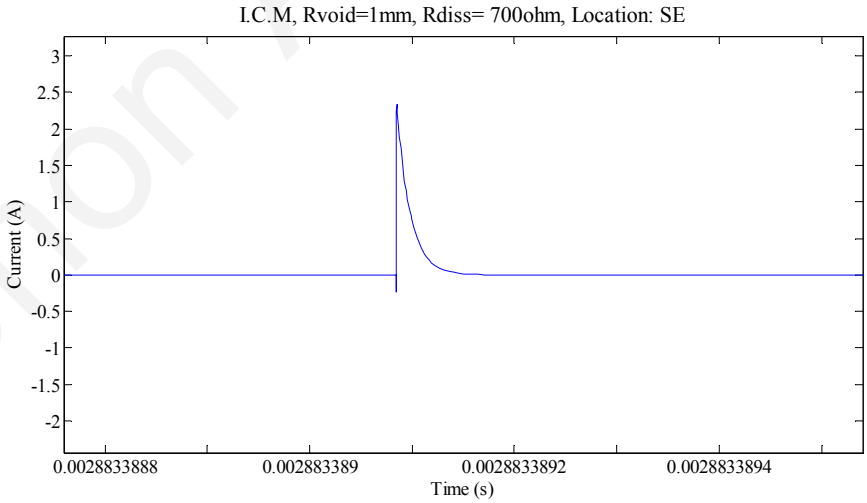

Fig. 5.27. Detailed view of current waveforms flowing from external circuit to breakdown void

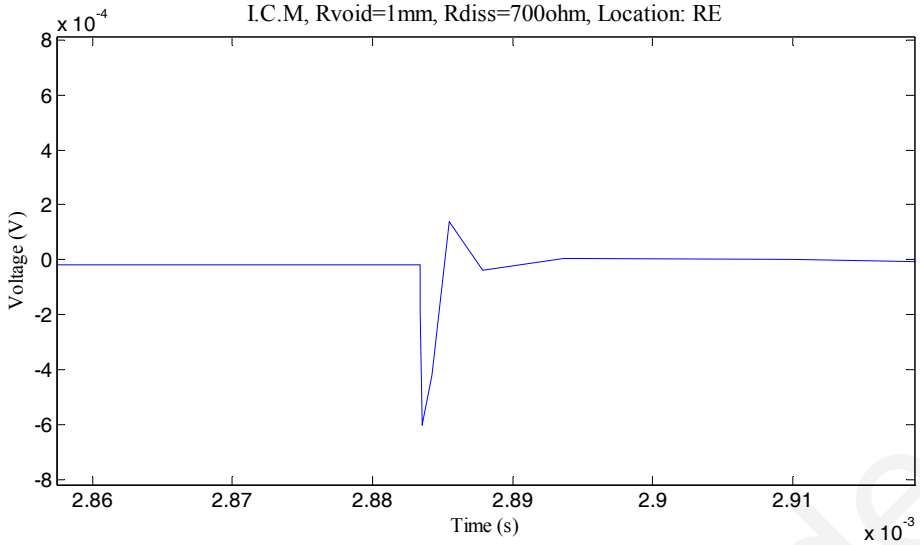

Fig. 5.28. Voltage spike at the receiving end of the 11 kV cable, (HF model) 3 km away from the breakdown void

b. Void of radius of 1 mm – R_{diss}= 520 Ω

Fig. 5.29 shows the high frequency voltage superimposed on the 50 Hz power frequency waveform caused by a breakdown void at the point where the void is located. In Fig. 5.30 the waveform of the spike of Fig. 5.29 is shown in detail. The spike has a duration of a fraction of nanoseconds (ns) and reaches a maximum amplitude of 30 V.

Fig. 5.31 shows the high frequency current-spike flowing from the external circuit to the breakdown void. The spike has a duration of a fraction of nanoseconds (ns) and reaches maximum amplitude of 4 A.

Fig. 5.32 shows the attenuated voltage spike observed at the receiving end of the cable located 3 km from the breakdown void. The spike's duration has increased to the order of microseconds (μS) and its maximum amplitude drops to 1.0 mV.

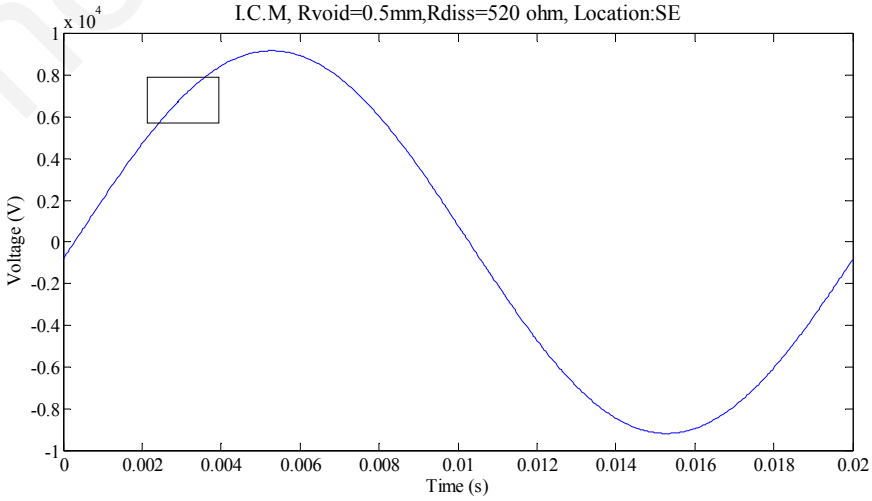

Fig. 5.29. High frequency voltage spike superimposed on the 50 Hz power frequency waveforms generated by a breakdown void at the point where the void is created

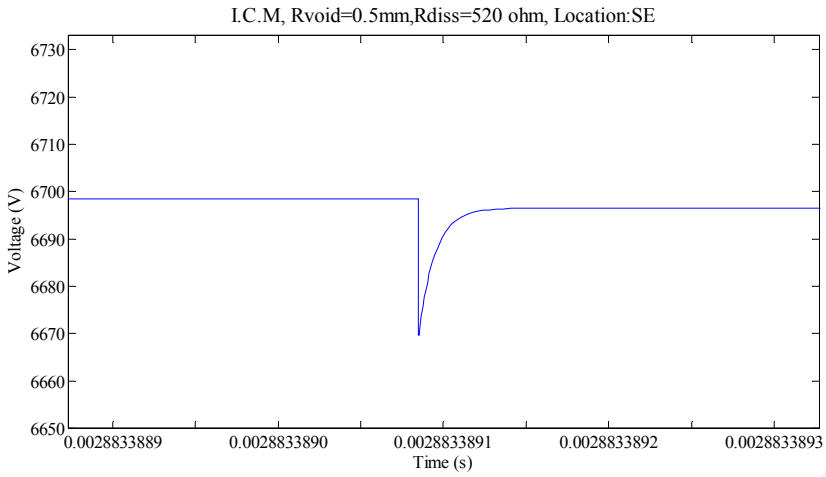

Fig. 5. 30. Detailed view of voltage waveforms at the point of the spike (zoomed in from Fig. 5.29)

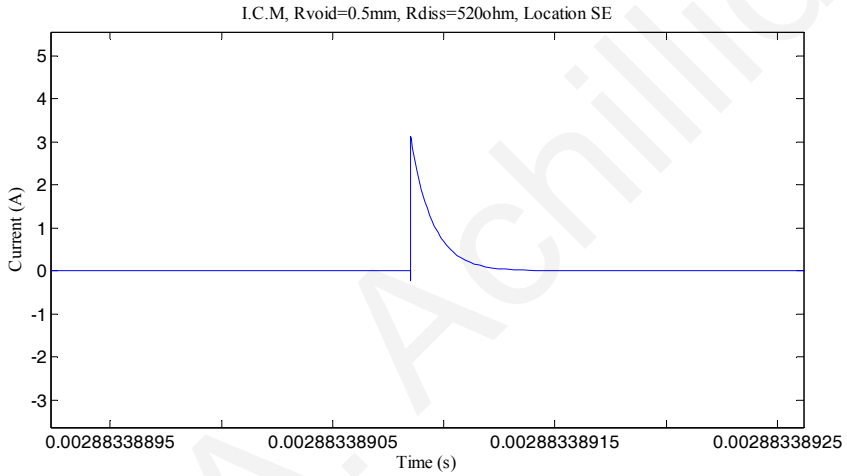

Fig. 5.31. Detailed view of current waveforms flowing from external circuit to breakdown void

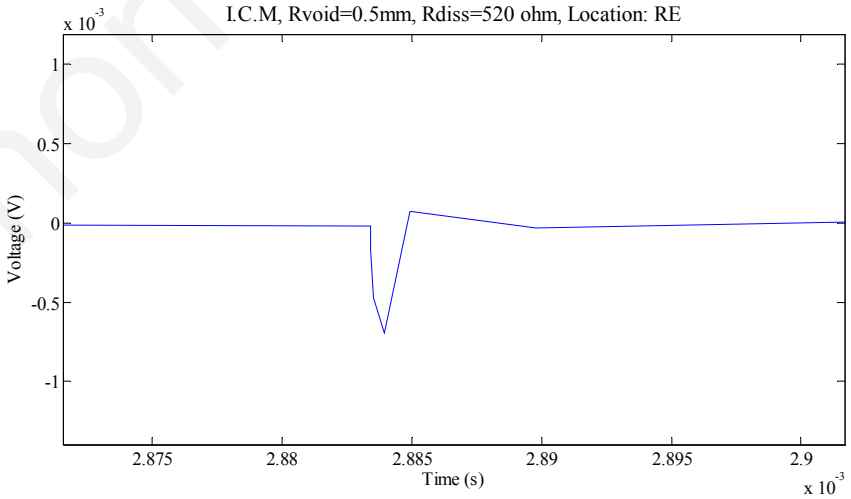

Fig. 5.32. Voltage spike at the receiving end of the 11 kV cable, (HF model) 3 km away from the breakdown void.

c. Void of radius of 1 mm – R_{diss}= 420 Ω

Fig. 5.33 shows the high frequency voltage superimposed on the 50 Hz power frequency waveform caused by a breakdown void at the point where the void is located. In Fig. 5.34 the waveform of the spike of Fig. 5.33 is shown in detail. The spike has a duration of a fraction of nanoseconds (ns) and reaches a maximum amplitude of 40 V.

Fig. 5.35 shows the high frequency current-spike flowing from the external circuit to the breakdown void. The spike has duration of a fraction of nanoseconds (ns) and reaches a maximum amplitude of 4.5 A.

Fig. 5.36 shows the attenuated voltage spike observed at the receiving end of the cable located 3 km from the breakdown void. The spike's duration has increased to order of microseconds (μS) and its maximum amplitude drops to 0.6 mV.

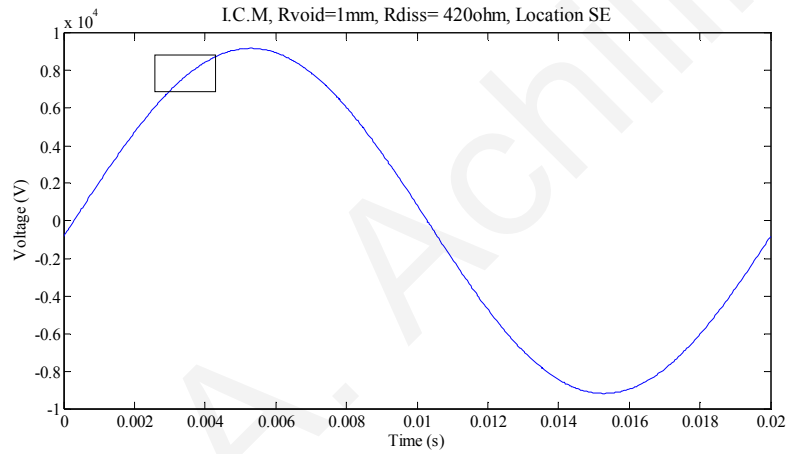

Fig. 5.33. High frequency voltage spike superimposed on the 50 Hz power frequency waveforms generated by a breakdown void at the point where the void is created

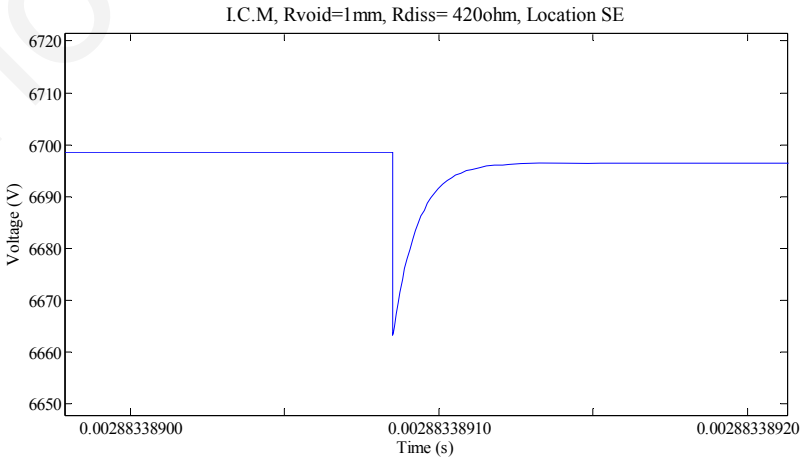

Fig. 5.34. Detailed view of voltage waveforms at the point of the spike (zoomed in from Fig. 5.33)

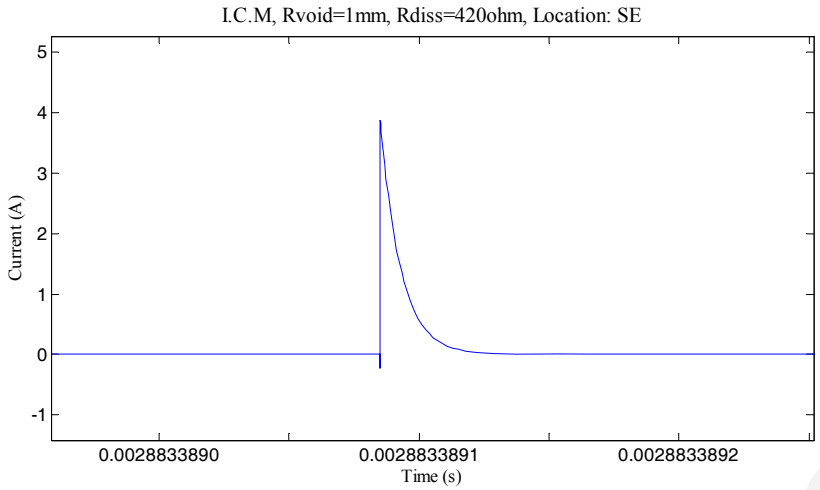

Fig. 5.35. Detailed view of current waveforms flowing from external circuit to breakdown void

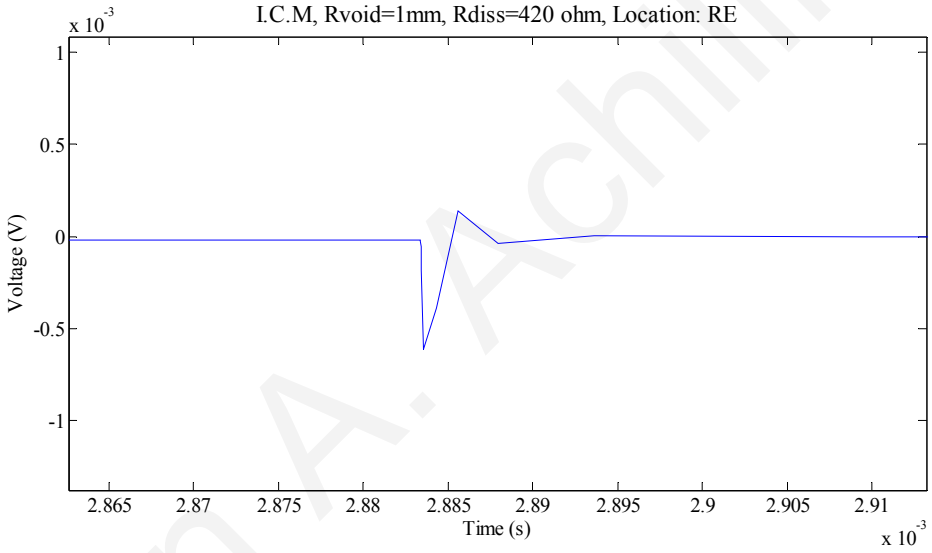

Fig. 5.36. Voltage spike at the receiving end of the 11 kV cable, (HF model) 3 km away from the breakdown void

5.2.3 Void of radius of 1.5 mm

The simulated results of a cylindrical void of radius and length of 1.5 mm are presented for three distinct cases: for ionized resistance path (R_{diss}), of a) 470 Ω, b) 350 Ω and c) 280 Ω respectively. The void (for all three cases) is located in the middle of the distance between the core and the outer sheath of the cable at 3 km away from the origin of the cable.

The minimum voltage level (V_{on}) required to initiate the discharge was taken to be 3 kV and the voltage level across the void where breakdown ceases (V_{off}) was taken to be 0 V (Fig.4.2), both values for the positive cycle only.

a. Void of radius of 1.5 mm – R_{diss}= 470 Ω

Fig. 5.37 shows the high frequency voltage superimposed on the 50 Hz power frequency waveform caused by a breakdown void at the point where the void is located. In Fig. 5.38 the waveform of the spike of Fig. 5.37 is shown in detail. The spike has a duration of a fraction of nanoseconds (ns) and reaches maximum amplitude of 40 V.

Fig. 5.39 shows the high frequency current-spike flowing from the external circuit to the breakdown void. The spike has a duration of a fraction of nanoseconds (ns) and reaches a maximum amplitude of 5 A.

Fig. 5.40 shows the attenuated voltage spike observed at the receiving end of the cable located 3 km from the breakdown void. The spike's duration has increased to the order of microseconds (μS) and its maximum amplitude drops to 0.15 mV.

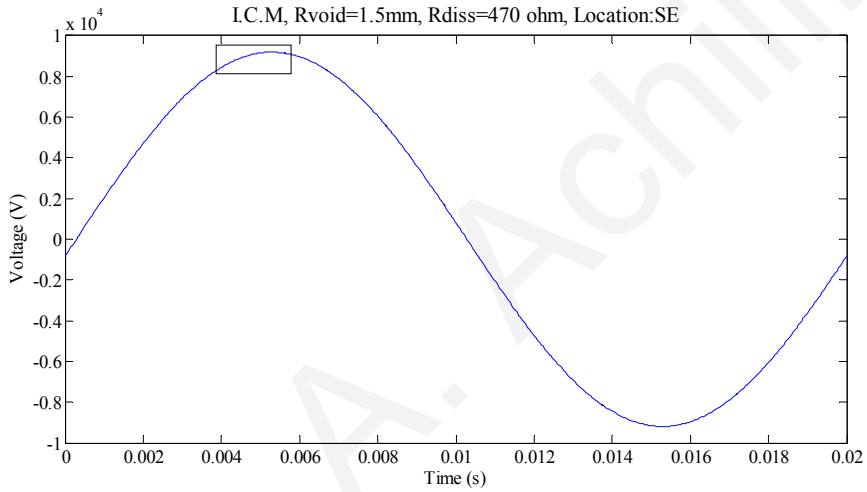

Fig. 5.37. High frequency voltage spike superimposed on the 50 Hz power frequency waveforms generated by a breakdown void at the point where the void is created

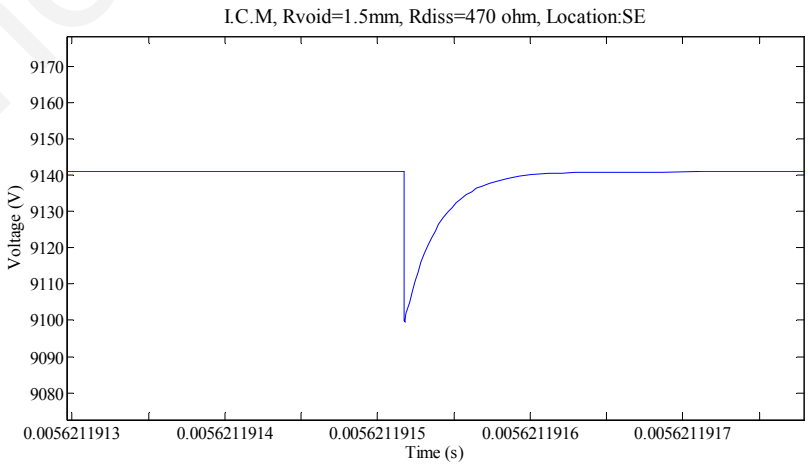

Fig. 5. 38. Detailed view of voltage waveforms at the point of the spike (zoomed in from Fig. 5.37)

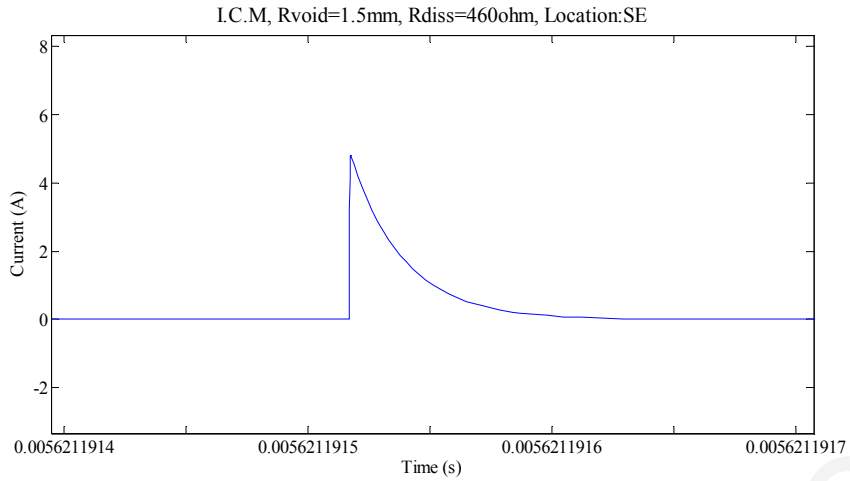

Fig. 5.39. Detailed view of current waveforms flowing from external circuit to breakdown void

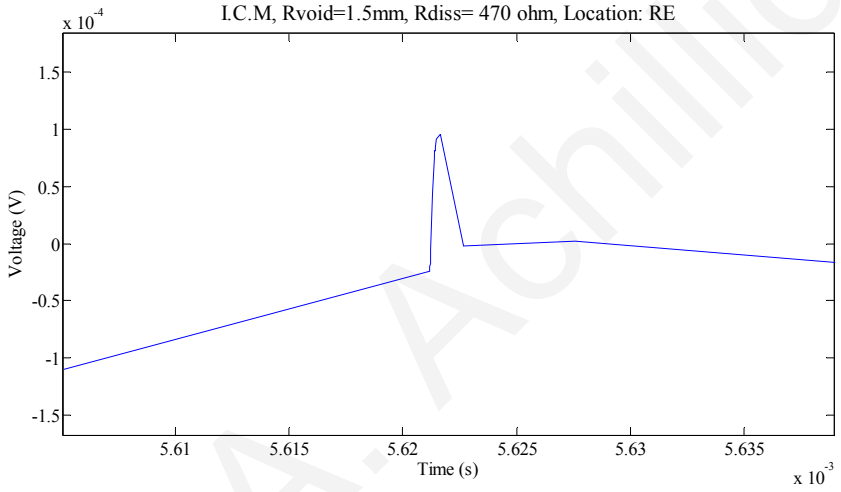

Fig. 5.40. Voltage spike at the receiving end of the 11 kV cable, (HF model) 3 km away from the breakdown void

b. Void of radius of 1.5 mm – R_{diss}= 350 Ω

Fig. 5.41 shows the high frequency voltage superimposed on the 50 Hz power frequency waveform caused by a breakdown void at the point where the void is located. In Fig. 5.42 the waveform of the spike of Fig. 5.41 is shown in detail. The spike has a duration of a fraction of nanoseconds (ns) and reaches a maximum amplitude of 50 V.

Fig. 5.43 shows the high frequency current-spike flowing from the external circuit to the breakdown void. The spike has a duration of a fraction of nanoseconds (ns) and reaches a maximum amplitude of 6 A.

Fig. 5.44 shows the attenuated voltage spike observed at the receiving end of the cable located 3 km from the breakdown void. The spike's duration has increased to the order of microseconds (μS) and its maximum amplitude drops to 0.15 mV.

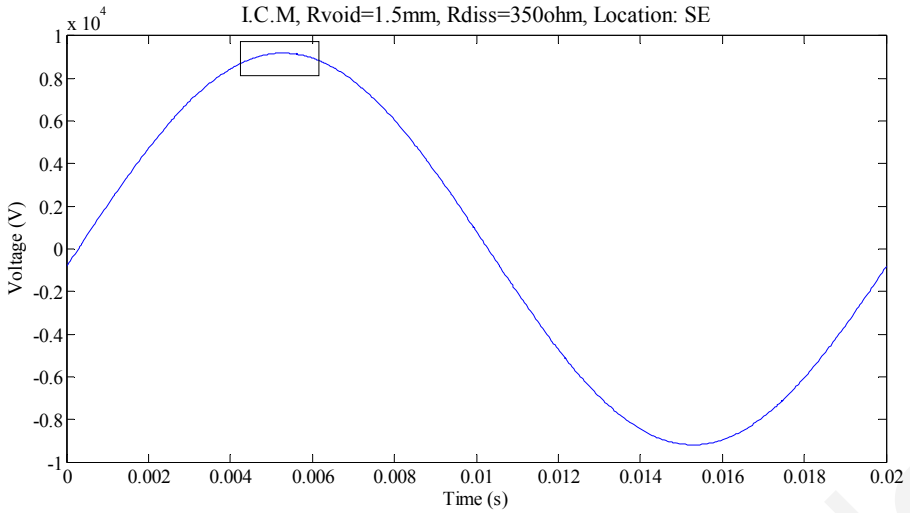

Fig. 5.41. High frequency voltage spike superimposed on the 50 Hz power frequency waveforms generated by a breakdown void at the point where the void is created

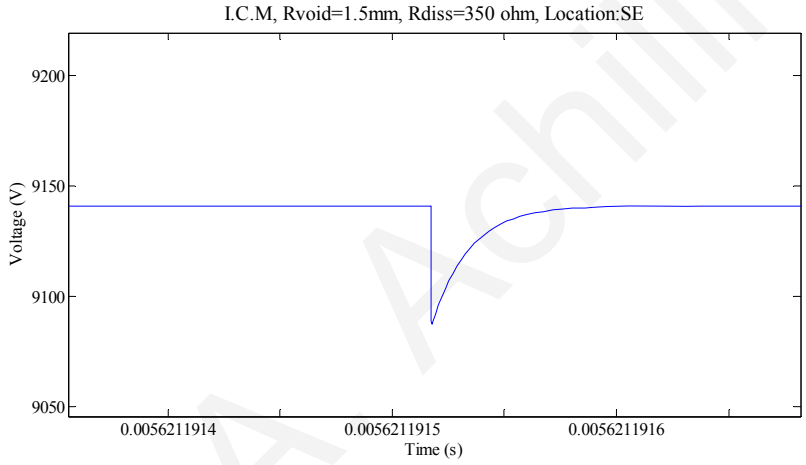

Fig. 5.42. Detailed view of voltage waveforms at the point of the spike (zoomed in from Fig. 5.41)

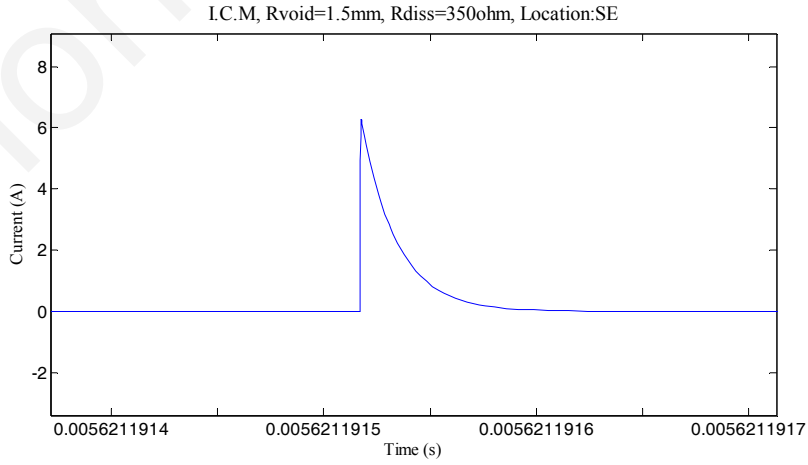

Fig. 5.43. Detailed view of current waveforms flowing from external circuit to breakdown void

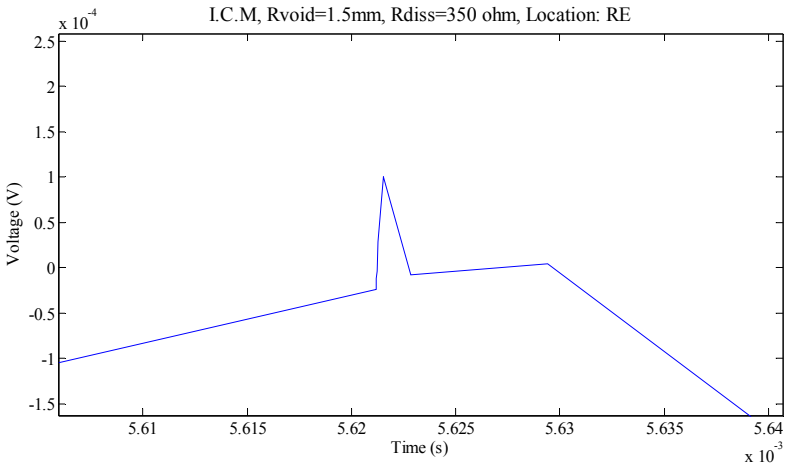

Fig. 5.44. Voltage spike at the receiving end of the 11 kV cable, (HF model) 3 km away from the breakdown void

c. Void of radius of 1.5 mm – R_{diss}= 280 Ω

Fig. 5.45 shows the high frequency voltage superimposed on the 50 Hz power frequency waveform caused by a breakdown void at the point where the void is located. In Fig. 5.46 the waveform of the spike of Fig. 5.45 is shown in detail. The spike has a duration of a fraction of nanoseconds (ns) and reaches a maximum amplitude of 80 V.

Fig. 5.47 shows the high frequency current-spike flowing from the external circuit to the breakdown void. The spike has a duration of a fraction of nanoseconds (ns) and reaches a maximum amplitude of 10 A.

Fig. 5.48 shows the attenuated voltage spike observed at the receiving end of the cable located 3 km from the breakdown void. The spike's duration has increased to the order of microseconds (μS) and its maximum amplitude drops to 0.2 mV.

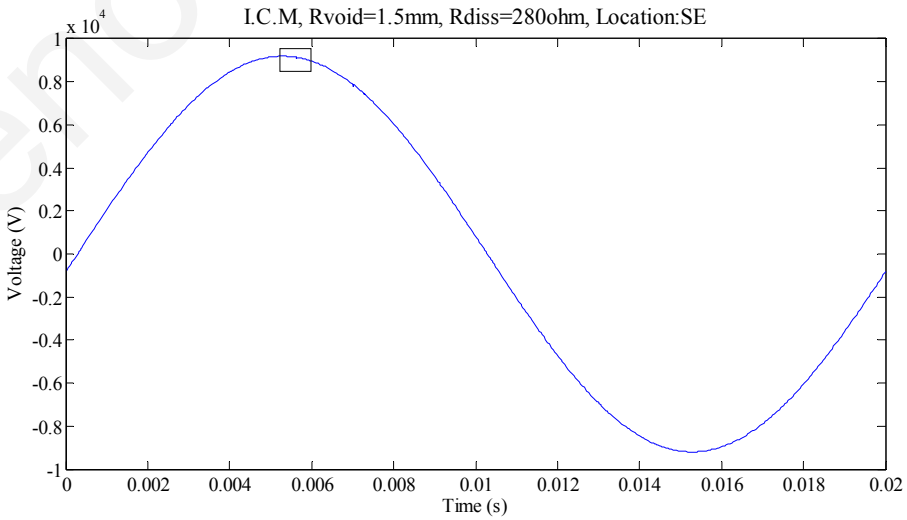

Fig. 5.45. High frequency voltage spike superimposed on the 50 Hz power frequency waveforms generated by a breakdown void at the point where the void is created

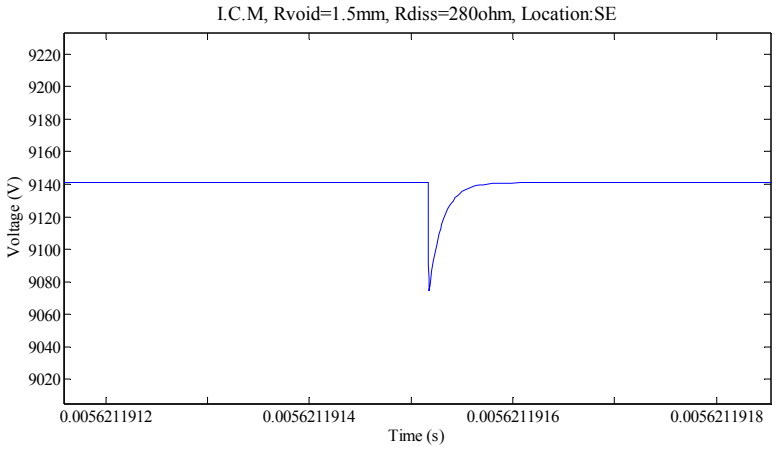

Fig. 5.46. Detailed view of voltage waveforms at the point of the spike (zoomed in from Fig. 5.45)

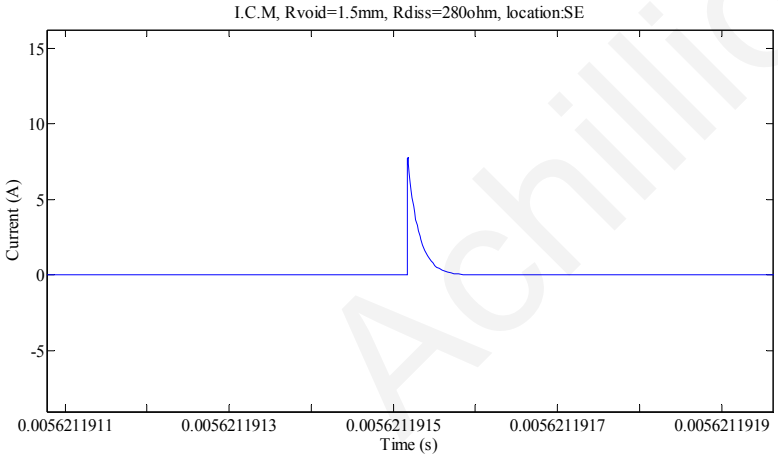

Fig. 5.47. Detailed view of current waveforms flowing from external circuit to breakdown void

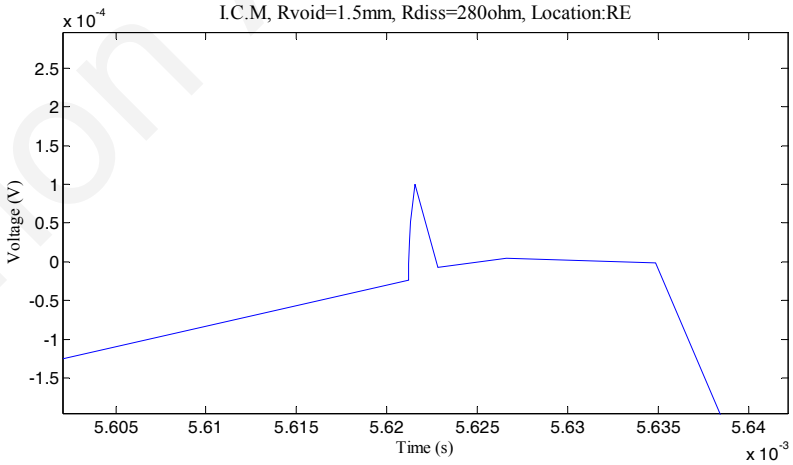

Fig. 5.48. Voltage spike at the receiving end of the 11 kV cable, (HF model) 3 km away from the breakdown void

5.3 The Capacitive Model of Void Based on the Induced Charge Concept

The transients generated by a breakdown void, as well as their traveling and attenuation along a medium voltage cable, are presented in this sub-section for the capacitive model based on the induced charge concept. These results are based on the case study described in Chapter 4.

5.3.1 Void of radius of 0.5 mm

The simulated results of a cylindrical void of radius and length of 0.5 mm are presented. The void is located in the middle of the distance between the core and the outer sheath of the cable at 3 km away from the origin of the cable.

The minimum voltage level (V_{on}) required to initiate the discharge was taken to be 2 kV and the voltage level across the void where breakdown ceases (V_{off}) was taken to be 0 V (Fig.4.3) both values for the negative cycle only.

Fig. 5.49 shows the high frequency voltage superimposed on the 50 Hz power frequency waveform caused by a breakdown void at the point where the void is located. In Fig. 5.50 the waveform of the spike of Fig. 5.49 is shown in detail. The spike has a duration of a fraction of picoseconds (ps) and reaches a maximum amplitude of 0.13 V.

Fig. 5.51 shows the high frequency current-spike flowing from the external circuit to the breakdown void. The spike has a duration of a fraction of picoseconds (ps) and reaches maximum amplitude of 0.01 A.

Fig. 5.52 shows the attenuated voltage spike observed at the receiving end of the cable located 3 km from the breakdown void. The spike's duration has increased to order of microseconds (μS) and its maximum amplitude drops to 0.4 mV.

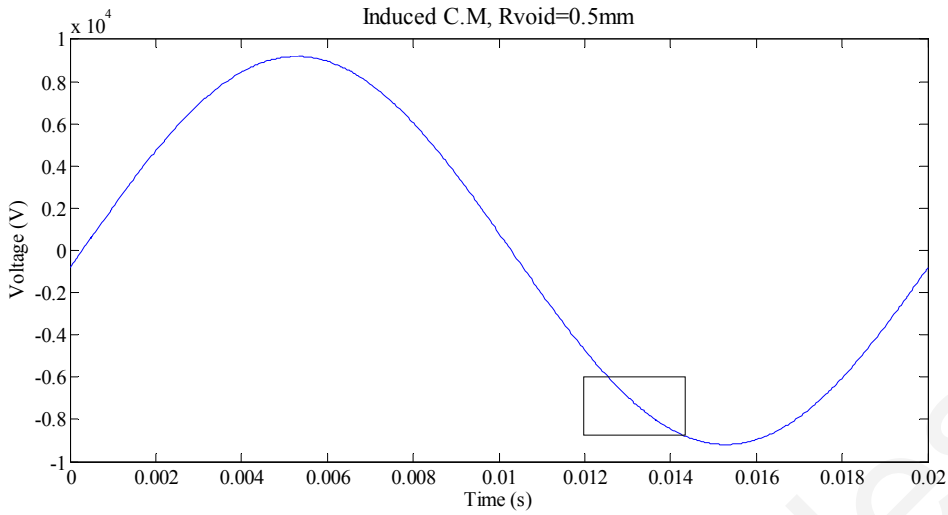

Fig. 5.49. High frequency voltage spike superimposed on the 50 Hz power frequency waveforms generated by a breakdown void at the point where the void is created

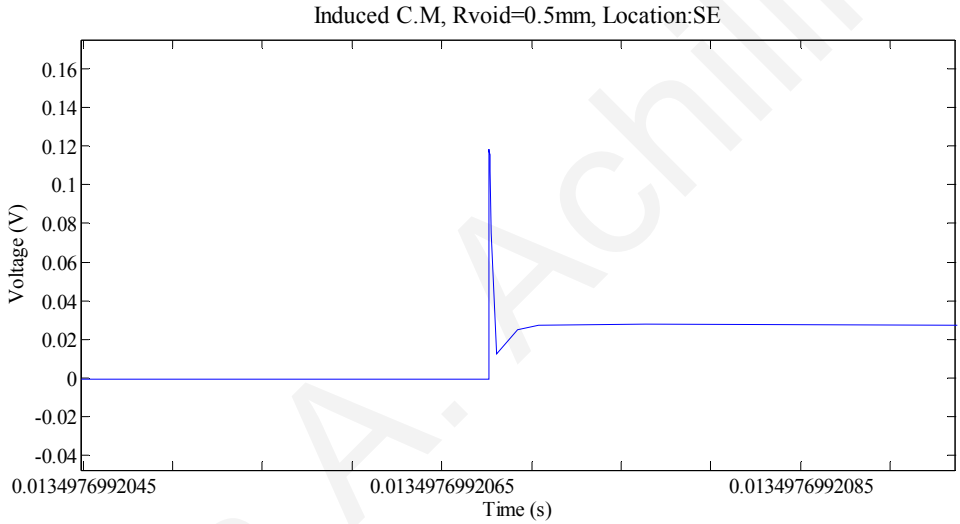

Fig. 5.50. Detailed view of voltage waveforms at the point of the spike (zoomed in from Fig.5.49)

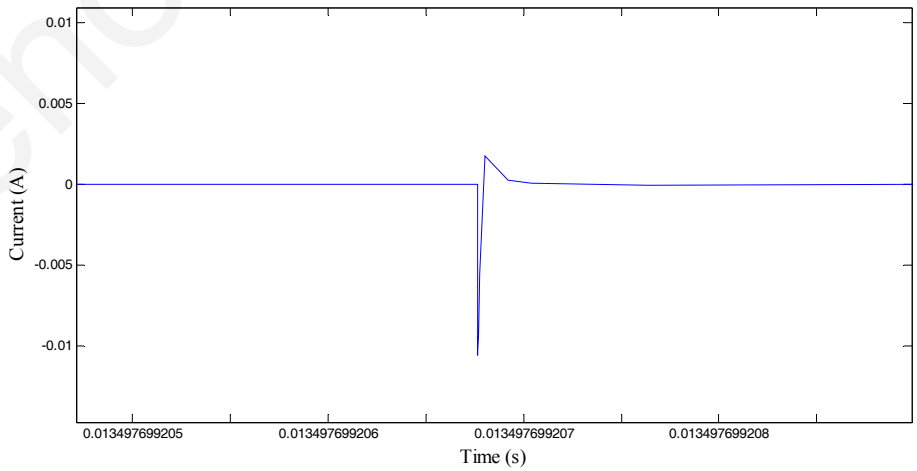

Fig. 5.51. Detailed view of current waveforms flowing from external circuit to breakdown void

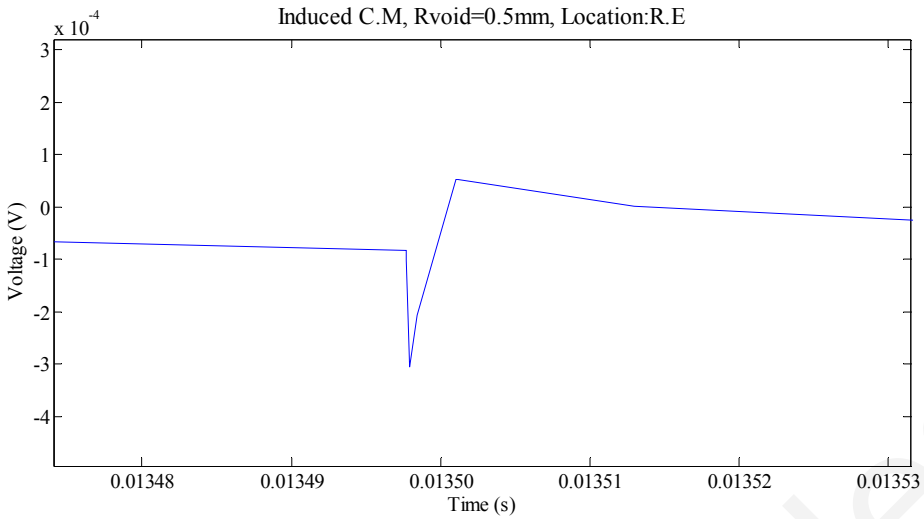

Fig. 5.52. Voltage spike at the receiving end of the 11 kV cable, (HF model) 3 km away from the breakdown void

5.3.2 Void of radius of 1 mm

The simulated results of a cylindrical void of radius and length of 1 mm are presented. The void is located in the middle of the distance between the core and the outer sheath of the cable at 3 km away from the origin of the cable.

The minimum voltage level (V_{on}) required to initiate the discharge was taken to be 3 kV and the voltage level across the void where breakdown ceases (V_{off}) was taken to be 0 V (Fig. 4.3) both values for the positive cycle only.

Fig. 5.53 shows the high frequency voltage superimposed on the 50 Hz power frequency waveform caused by a breakdown void at the point where the void is located. In Fig. 5.54 the waveform of the spike of Fig. 5.53 is shown in detail. The spike has a duration of a fraction of picoseconds (ps) and reaches a maximum amplitude of 2.5 V.

Fig. 5.55 shows the high frequency current-spike flowing from the external circuit to the breakdown void. The spike has a duration of a fraction of picoseconds (ps) and reaches a maximum amplitude of 0.03 A.

Fig. 5.56 shows the attenuated voltage spike observed at the receiving end of the cable located 3 km from the breakdown void. The spike's duration has increased to the order of microseconds (μS) and its maximum amplitude drops to 10 μV.

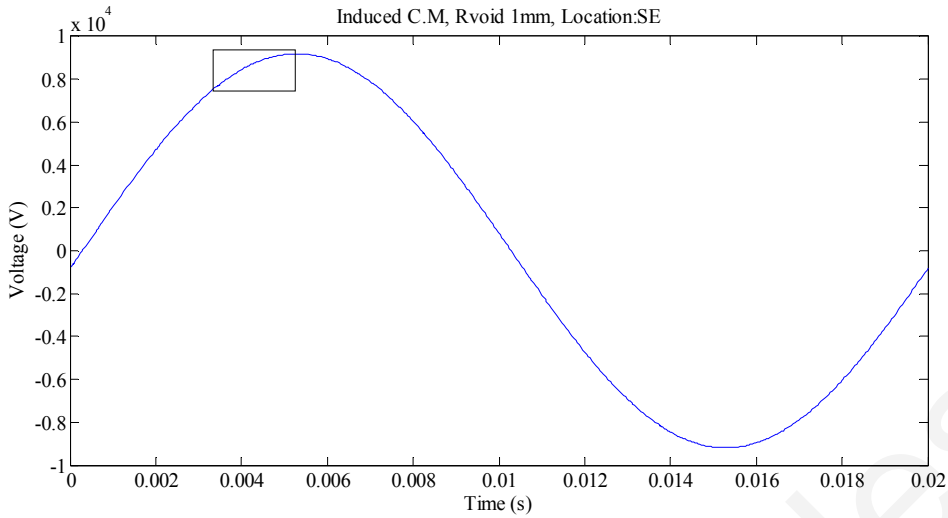

Fig. 5.53. High frequency voltage spike superimposed on the 50 Hz power frequency waveforms generated by a breakdown void at the point where the void is created

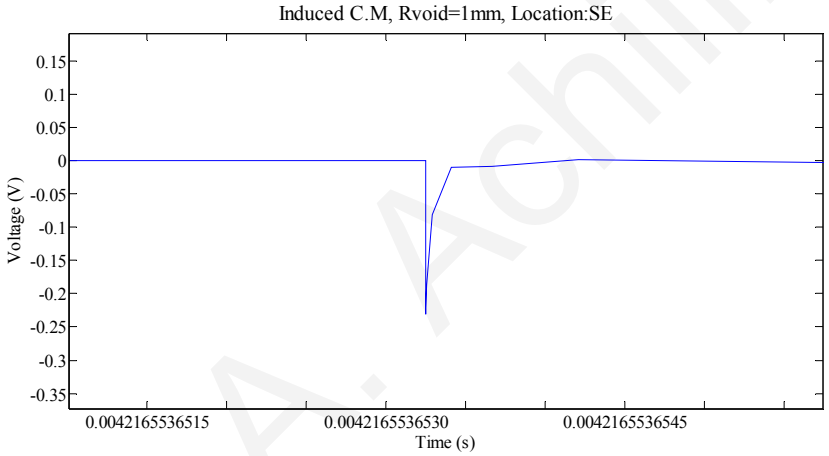

Fig. 5.54. Detailed view of voltage waveforms at the point of the spike (zoomed in from Fig.5.53)

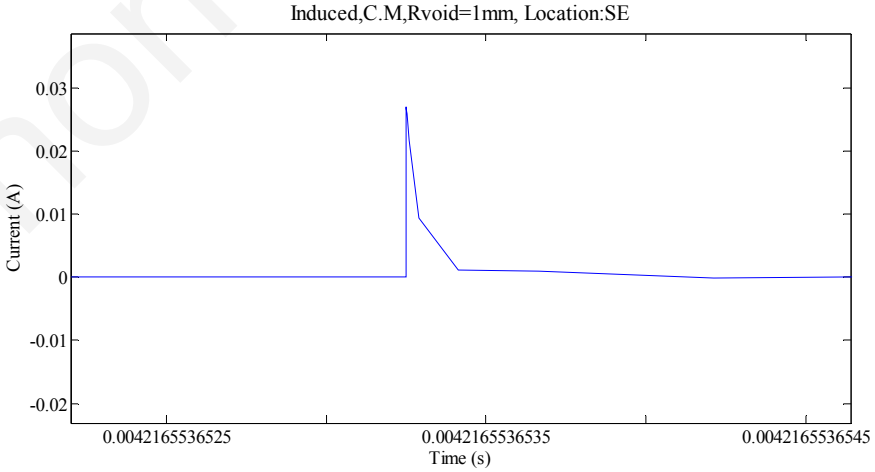

Fig.5.55. Detailed view of current waveforms flowing from external circuit to breakdown void

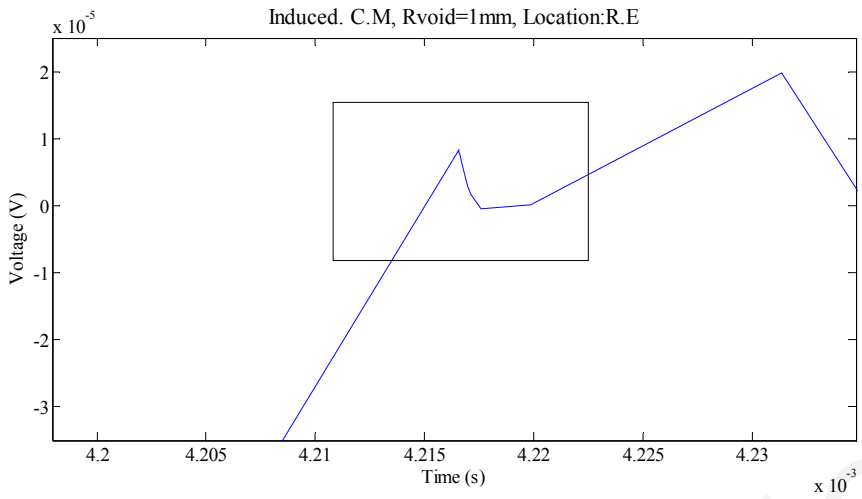

Fig. 5.56. Voltage spike at the receiving end of the 11 kV cable, (HF model) 3 km away from the breakdown void

5.3.3 Void of radius of 1.5 mm

The simulated results of a cylindrical void of radius and length of 1.5 mm are presented. The void is located in the middle of the distance between the core and the outer sheath of the cable at 3 km away from the origin of the cable.

The minimum voltage level (V_{on}) required to initiate the discharge was taken to be 5 kV and the voltage level across the void where breakdown ceases (V_{off}) was taken to be 0 V (Fig. 4.3), both values for the positive cycle only.

Fig. 5.57 shows the high frequency voltage superimposed on the 50 Hz power frequency waveform caused by a breakdown void at the point where the void is located. In Fig. 5.58 the waveform of the spike of Fig. 5.57 is shown in detail. The spike has a duration of a fraction of picoseconds (ps) and reaches a maximum amplitude of 0.3 V.

Fig. 5.59 shows the high frequency current-spike flowing from the external circuit to the breakdown void. The spike has a duration of a fraction of picoseconds (ps) and reaches a maximum amplitude of 0.03 A.

Fig. 5.60 shows the attenuated voltage spike observed at the receiving end of the cable located 3 km from the breakdown void. The spike's duration has increased to the order of microseconds (μS) and its maximum amplitude drops to 2.5 mV.

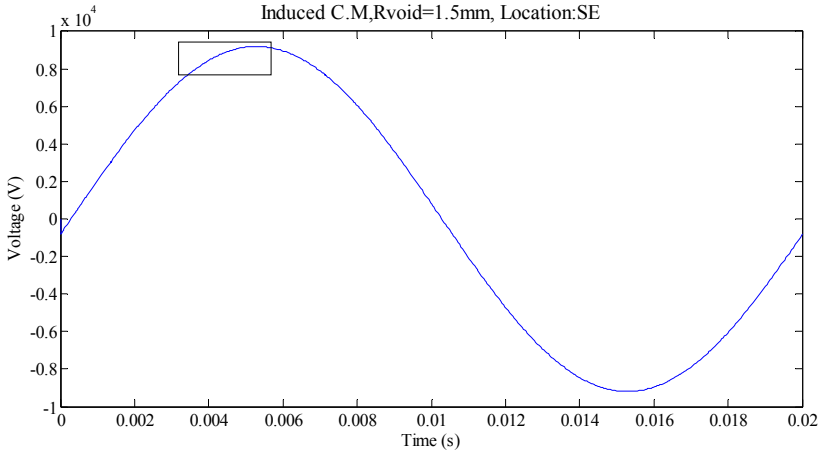

Fig. 5.57. High frequency voltage spike superimposed on the 50 Hz power frequency waveforms generated by a breakdown void at the point where the void is created

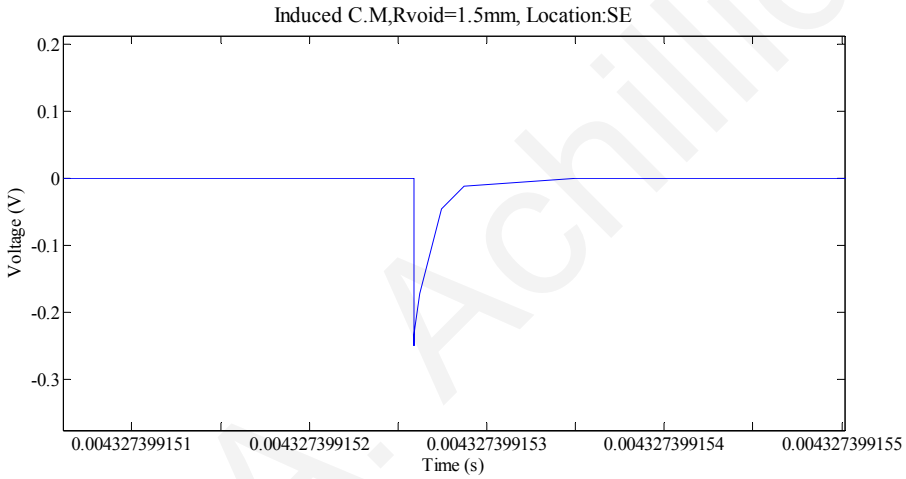

Fig. 5.58. Detailed view of voltage waveforms at the point of the spike (zoomed in from Fig.5.57)

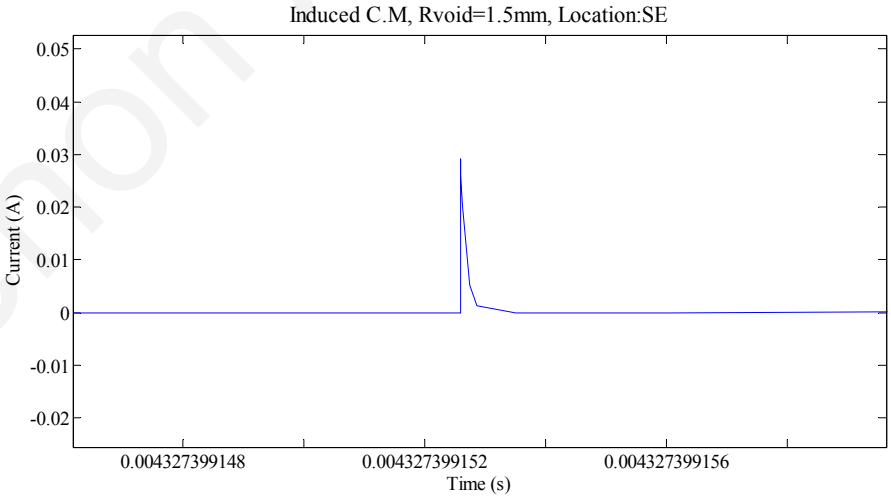

Fig. 5.59. Detailed view of current waveforms flowing from external circuit to breakdown void

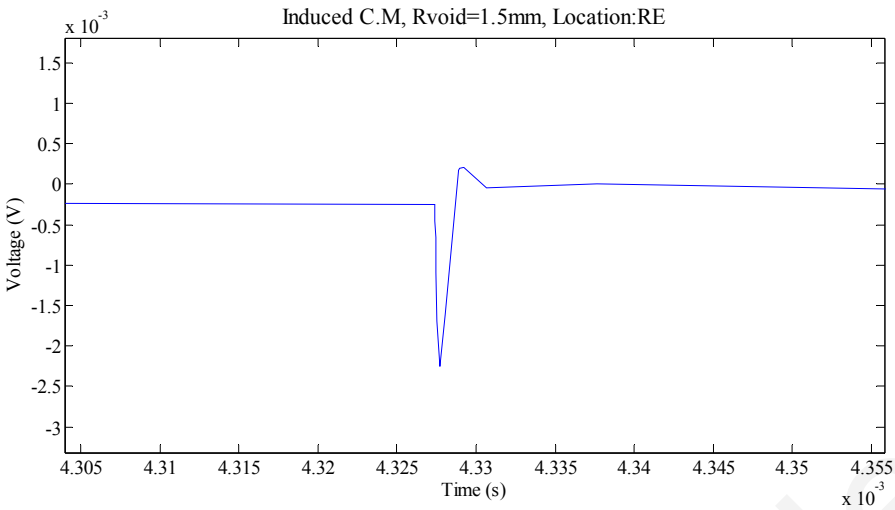

Fig. 5.60. Voltage spike at the receiving end of the 11 kV cable, (HF model) 3 km away from the breakdown void

5.4 The Advanced Capacitive Model of Void

The transients generated by a breakdown void, as well as their traveling and attenuation along a medium voltage cable, are presented in this sub-section for the advanced capacitive model. As already discussed in Chapter 2 this is a two stage breakdown model and eventually two simulated induced transients are expected to be generated.

5.4.1 Void of radius of 0.5 mm

The simulated results of a cylindrical void of radius and length of 0.5 mm are presented. The void is located in the middle of the distance between the core and the outer sheath of the cable at 3 km away from the origin of the cable.

The minimum voltage level (V_{on}) required to initiate the discharge was taken to be 2 kV and the voltage level across the void where breakdown ceases (V_{off}) was taken to be 0 V (Fig. 4.4), both values for the negative cycle only.

Fig. 5.61 shows the high frequency voltage superimposed on the 50 Hz power frequency waveform caused by a breakdown void at the point where the void is located. Fig. 5.62 shows the simulated induced transients on the core of the cable generated by breakdown stage I. The transient reaches a peak magnitude of 800 V and has a duration of a fraction of picosecond (ps) Fig. 5.63 shows the simulated induced transients on the core of the cable generated by breakdown stage II. The transient reaches a peak magnitude of 1.5 V and has a duration of the order of nanosecond (ns)

Fig. 5.64 shows the attenuated voltage spike observed at the receiving end of the cable located 3 km from the breakdown void. The spike's duration has increased to the order of microseconds (μs) and its maximum amplitude drops to 0.8 mV.

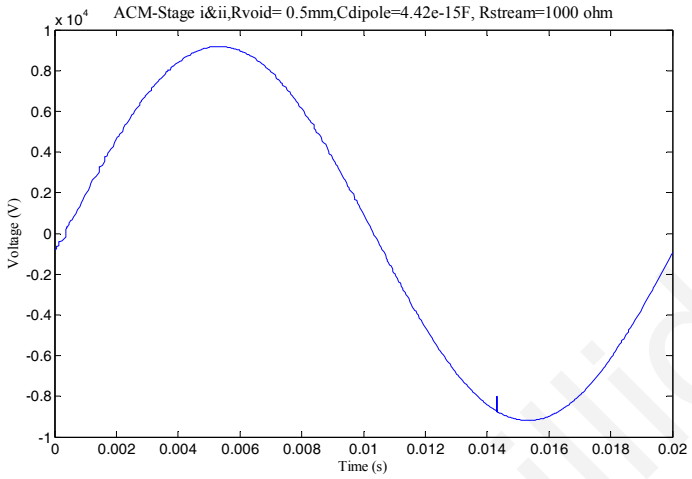

Fig. 5.61. High frequency voltage spike superimposed on the 50 Hz power frequency waveforms generated by a breakdown void at the point where the void is created

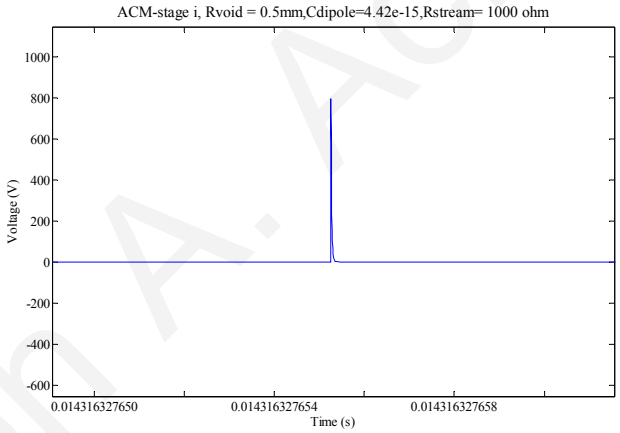

Fig. 5.62. Detailed view of voltage waveforms at the point of the spike (zoomed in from Fig.5.61) for breakdown stage-I

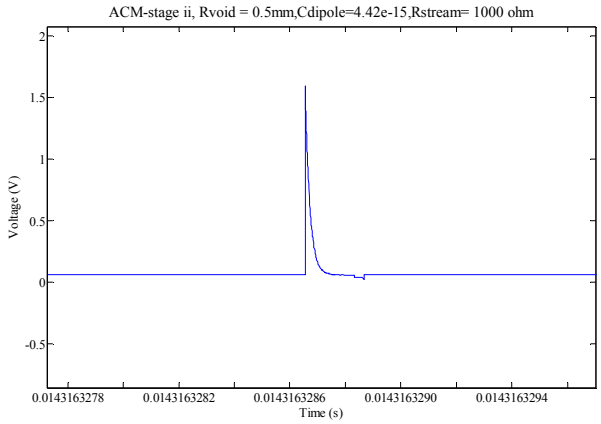

Fig. 5.63. Detailed view of voltage waveforms at the point of the spike (zoomed in from Fig.5.61) for breakdown stage-II

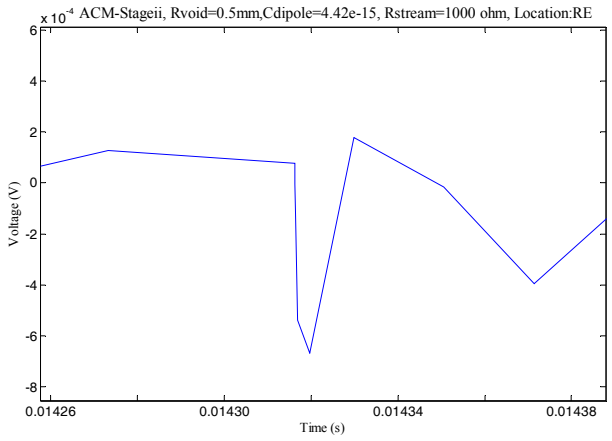

Fig. 5.64. Voltage spike at the receiving end of the 11 kV cable, (HF model) 3 km away from the breakdown void

5.4.2 Void of radius of 1 mm

The simulated results of a cylindrical void of radius and length of 1 mm are presented. The void is located in the middle of the distance between the core and the outer sheath of the cable at 3 km away from the origin of the cable.

The minimum voltage level (V_{on}) required to initiate the discharge was taken to be 3kV and the voltage level across the void where breakdown ceases (V_{off}) was taken to be 0 V (Fig. 4.4) both values for the negative cycle only.

Fig. 5.65 shows the high frequency voltage superimposed on the 50 Hz power frequency waveform caused by a breakdown void at the point where the void is located. Fig. 5.66 shows the simulated induced transients on the core of the cable generated by breakdown stage I. The transient reaches a peak magnitude of 2000 V and has a duration of a fraction of picosecond (ps). Fig. 5.67 shows the simulated induced transients on the core of the cable generated by breakdown stage II. The transient reaches a peak magnitude of 20 V and has a duration of the order of nanosecond (ns).

Fig. 5.68 shows the attenuated voltage spike observed at the receiving end of the cable located 3 km from the breakdown void. The spike's duration has increased to the order of microseconds (μS) and its maximum amplitude drops to 0.05 mV.

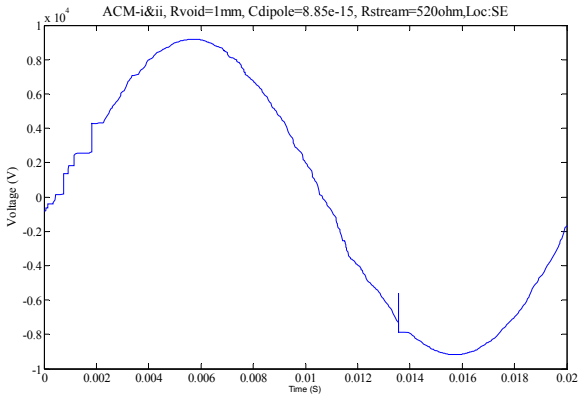

Fig. 5.65. High frequency voltage spike superimposed on the 50 Hz power frequency waveforms generated by a breakdown void at the point where the void is created

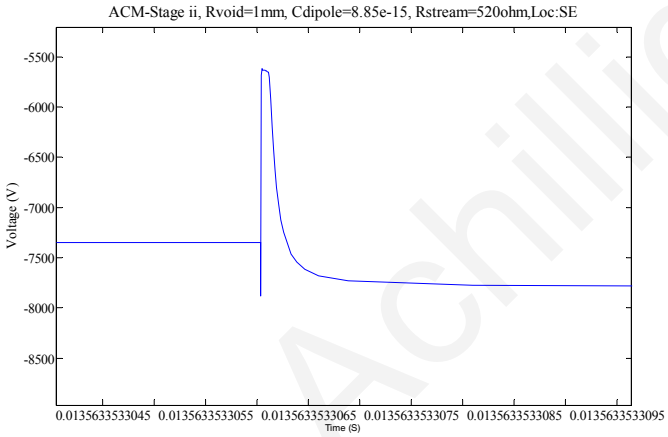

Fig. 5.66. Detailed view of voltage waveforms at the point of the spike (zoomed in from Fig.5.65) for breakdown stage-I

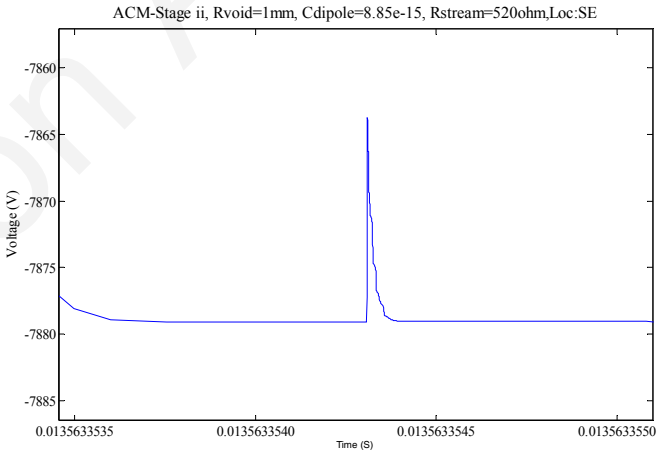

Fig. 5.67. Detailed view of voltage waveforms at the point of the spike (zoomed in from Fig.5.65) for breakdown stage-II

..

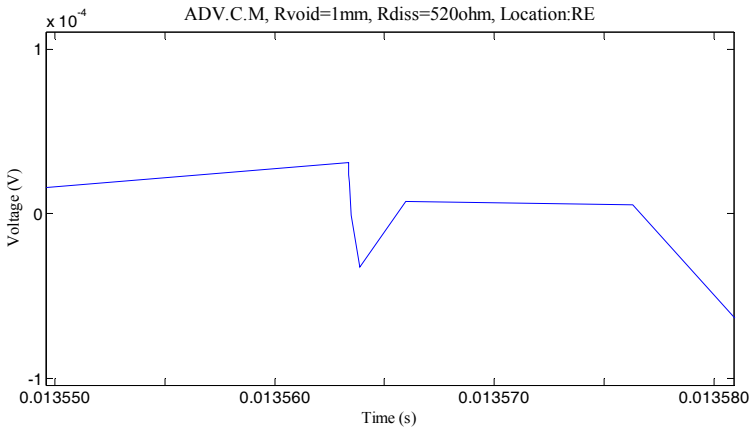

Fig. 5.68. Voltage spike at the receiving end of the 11 kV cable, (HF model) 3 km away from the breakdown void.

5.4.3 Void of radius of 1.5 mm

The simulated results of a cylindrical void of radius and length of 1.5 mm are presented. The void is located in the middle of the distance between the core and the outer sheath of the cable at 3 km away from the origin of the cable.

The minimum voltage level (V_{on}) required to initiate the discharge was taken to be 4 kV and the voltage level across the void where breakdown ceases (V_{off}) was taken to be 0 V (Fig. 4.4) both values for the negative cycle only.

Fig. 5.69 shows the high frequency voltage superimposed on the 50 Hz power frequency waveform caused by a breakdown void at the point where the void is located. Fig. 5.70 shows the simulated induced transients on the core of the cable generated by breakdown stage I. The transient reaches a peak magnitude of 2200 V and has a duration of a fraction of picosecond (ps). Fig. 5.71 shows the simulated induced transients on the core of the cable generated by breakdown stage II. The transient reaches a peak magnitude of 40 V and has a duration of the order of nanosecond (ns).

Fig. 5.72 shows the attenuated voltage spike observed at the receiving end of the cable located 3 km from the breakdown void. The spike's duration has increased to the order of microseconds (μS) and its maximum amplitude drops to 0.3 mV.

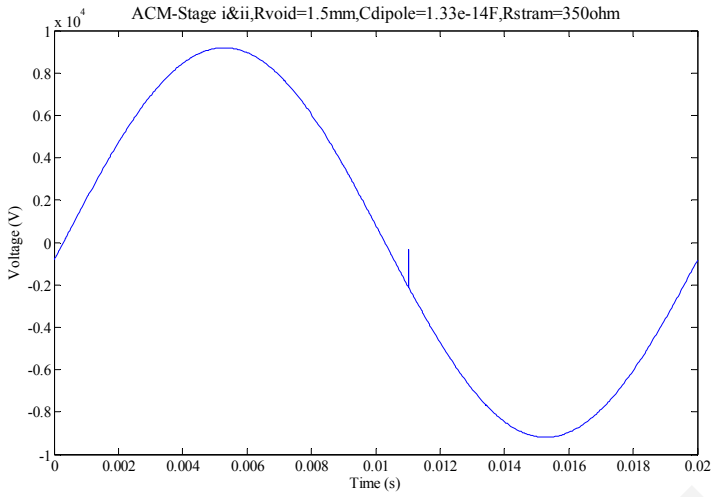

Fig. 5.69. High frequency voltage spike superimposed on the 50 Hz power frequency waveforms generated by a breakdown void at the point where the void is created

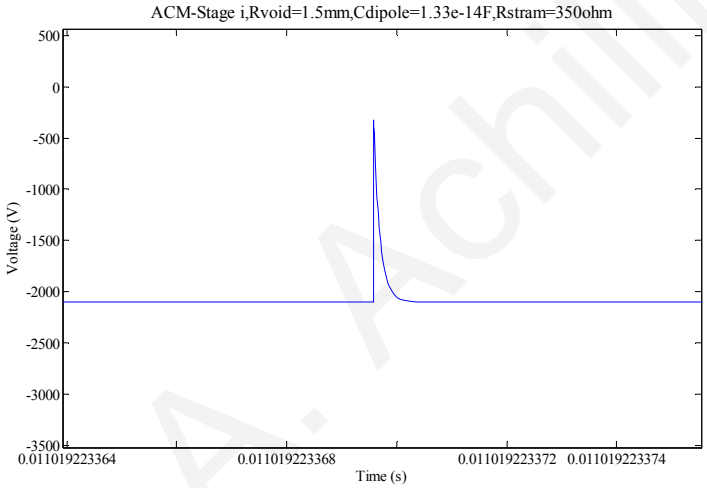

Fig. 5.70. Detailed view of voltage waveforms at the point of the spike (zoomed in from Fig.5.69) for breakdown stage-I

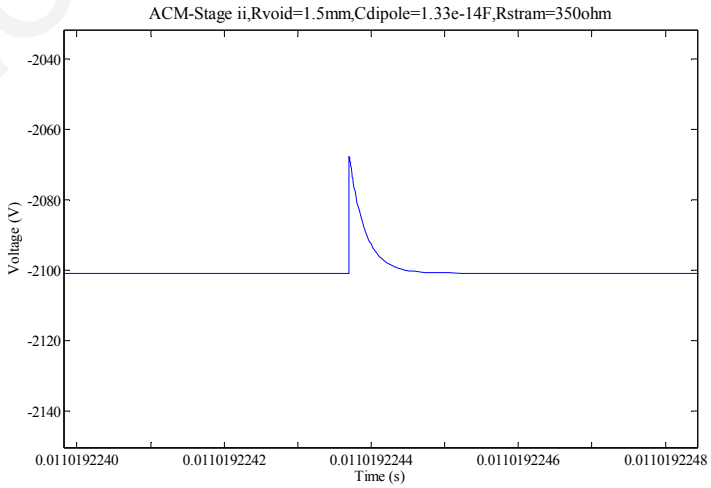

Fig. 5.71. Detailed view of voltage waveforms at the point of the spike (zoomed in from Fig.5.69) for break down stage-II

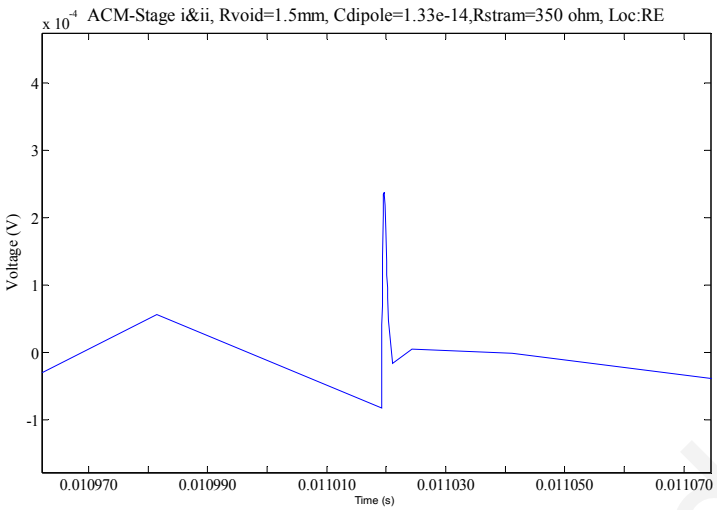

Fig. 5.72. Voltage spike at the receiving end of the 11 kV cable, (HF model) 3 km away from the breakdown.

CHAPTER 6

THEORETICAL DISCUSSION

This Chapter provides a theoretical discussion of the results obtained. More specifically, the theoretical performance of all three proposed models are evaluated and discussed by relating the principle of operation of each model and the induced transients on the core of the cable under investigation. The high frequency and low frequency characteristics of XLPE medium voltage cables for PD propagation are evaluated. Further the simulating performances of the models are investigated. Finally the general conclusions of this work are going to be presented.

6.1 Theoretical Performance of the Proposed Models and Associated Induced Transients

6.1.1 Classical Capacitive Model Against Improved Capacitive Model

a. ***The significance of the calculated components***

The simulated induced transients on the core of the cable generated by a breakdown void is directly related to model components as presented in Chapter 2 and calculated in Chapters 3 and 4. The importance of these components in relation to the induced transient can be justified as follows:

A simplified model of Fig. 4.2 (associated with the distributed impedance of the cable) is presented in Figs. 6.1 and 6.2.

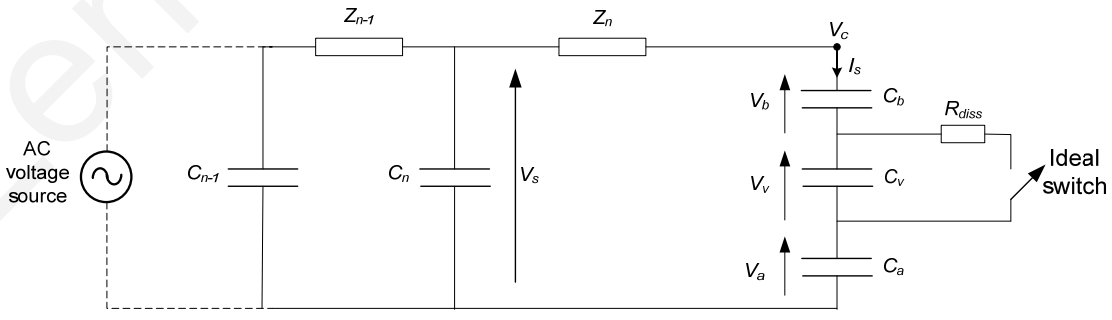

Fig. 6.1. Simplified model of void (prior breakdown)

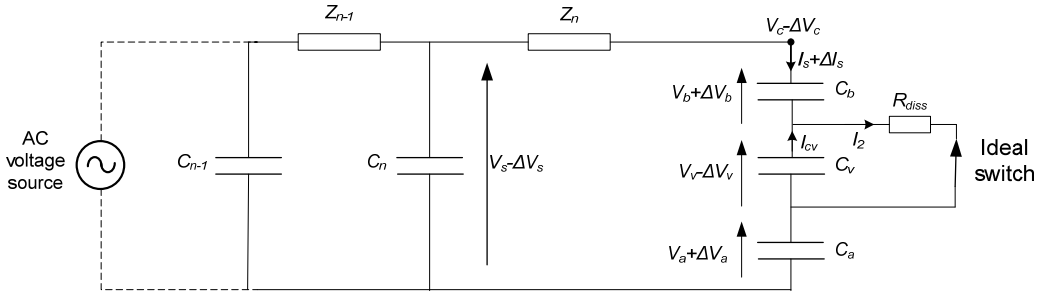

Fig. 6.2. Simplified model of void (during breakdown)

With reference to Figs. 6.1 and 6.2, Z_n and C_n represent the distributed series impedance and shunt capacitance of the n^{th} element of the cable respectively, C_a and C_b represent the healthy part of the insulation and C_v represents the capacitance of the void.

Voltages V_s, V_c, V_b, V_a and V_v represents the source voltage, the cable's core voltage, the voltage of the healthy part and defect of the test object. Fig. 6.1 represents the condition prior to breakdown, whereas Fig 6.2 represents the condition during breakdown.

With reference to Fig. 6.1 and by utilizing Kirchhoff's circuit laws:

$$V_c = V_a + V_b + V_v . \tag{6.1}$$

With reference to Fig. 6.2, ΔI_s, represent the increase in the core current (apparent current), ΔV_c, ΔV_a and ΔV_b represent the decrease and increase in voltage across the core of cable and capacitances C_a and C_b respectively, after closing the switch across the capacitor C_v. I_{cv} represents the discharge current flowing through the ionized path resistor R_{diss} during the simulated breakdown.

By applying Kirchhoff's circuit laws to Fig. 6.2 we have:

$$V_c - \Delta V_c = (I_{cv} + I_s + \Delta I_s)R_{diss} + \Delta V_a + \Delta V_b + V_a + V_b . \tag{6.2}$$

By subtracting (5.2) from (5.1) we get:

$$\Delta V_c = V_v - (I_{cv} + I_s + \Delta I_s)R_{diss} - \Delta V_a - \Delta V_b . \tag{6.3}$$

By switching (6.3) to the s-domain and by substituting to (5.3) $\Delta V_a = \Delta I_s * Z_a$ and $\Delta V_b = \Delta I_s * Z_b$ we get:

$$\Delta V_c = V_v - (I_{cv} + I_s + \Delta I_s)R_{diss} - \Delta I_s (Z_a + Z_b) . \tag{6.4}$$

From Fig.5.2 ΔI_s can be calculated as follows:

$$I_s + \Delta I_s = \frac{V_s - \Delta V_s - (V_c - \Delta V_c)}{Z_n} . \tag{6.5}$$

Also by taking into consideration that I_s is very small and eventually V_s is almost equal to V_c then (6.4) and (6.5) will become:

$$\Delta V_c = V_v - (I_{cv})R_{diss} - \Delta I_s(Z_a + Z_b + R_{diss}). \tag{6.6}$$

$$\Delta I_s = \frac{\Delta V_c - \Delta V_s}{Z_n}. \tag{6.7}$$

The outcome of (6.6) and (6.7) represents two equations coupled together, ΔV_c and ΔI_c represent the expected recorded (induced) voltage and current transients (spike) respectively at the core of the cable for a simulated breakdown of a void at the point where the void is supposed to be created. The outcome of (6.6) and (6.7) indicates that the recorded transients are related to: a) the upper and lower capacitance of the healthy part of insulation C_a *and* C_b respectively, b) the capacitance C_v the, voltage across void V_v, the resistance of the ionized path R_{diss}, and the nature of discharge current I_{cv}, and c) the wave impedance of the external circuit (Z_n).

b. Performance of the proposed model

The significance of the resistance of the ionized path (R_{diss}) in relation to the performance of the proposed model and to the induced voltage transients ΔV_c is demonstrated analytically in this section. For simplicity of this analysis, the maximum possible induced transient will be considered. This maximum transient can be recorded when ΔV_a and ΔV_b of (6.3) are set to a very small value. This is the case just after closing the switch (Fig. 6.2) and eventually before the current ΔI_s (flowing from the external circuit to the void circuitry) reaches a significant value.

Substituting ΔV_a and ΔVb equal to zero this leads to $I_{cv} >> \Delta I_s > I_s$ and eventually (6.3) becomes:

$$\Delta V_c = V_v - (I_{cv})R_{diss}. \tag{6.8}$$

Based on Fig. 6.2 and by tanking into consideration the assumptions stated above, then the discharge current I_{cv} (in time domain) is given below:

$$I_{cv} = \frac{V_v e^{-\frac{t}{C_v R_{diss}}}}{R_{diss}}. \tag{6.9}$$

By further substituting (6.2) to (6.8) we get:

$$\Delta V_c = V_v(e^{-\frac{t}{C_v R_{diss}}} - 1). \tag{6.10}$$

The outcome of (6.10) can be utilised in order to analyse and eventually compare the two models at the initial state of the discharge process. Based on the outcome of (6.10) three cases will be discussed: (i) Resistance of the ionized path R_{diss} with infinite value

(ii) Resistance of the ionized path R_{diss} with zero value, and (iii) Resistance of the ionized path R_{diss} with value as calculated in this thesis.

b1. Resistance of the ionized path R_{diss} with infinite value

By equating R_{diss} to infinity value then practically there is no breakdown and eventually nothing is expected to be induced on the core of the cable. By substituting R_{diss} = infinity in (6.10) this will lead to

$$\Delta V_c = 0 \tag{6.11}$$

The outcome of (6.11) indicates that there is no induced transient on the core of the cable (as naturally expected) and eventually justifies the truthfulness of (6.10). The simulated results of this case are presented in Fig. 6.3.

b2. Resistance of the ionized path (R_{diss}) with zero value

By equating R_{diss} to zero the model switches from the improved capacitive to the classical capacitive model. By substituting this value ($R_{diss}=0$) to (6.10) then we have:

$$\Delta V_c = -V_v. \tag{6.12}$$

Also, by taking into consideration that the relative permittivity of air (within the void) is lower than the relative permittivity of the insulating medium of the cable, then, as a result, a large percentage of the system operating voltage is expected to emerge across the void (V_v). The outcome of (6.12) indicates that this large percentage of the system operating voltage (V_v) is expected to be induced as a transient at the core of the cable. Furthermore the time constant of (6.10) tends to zero and eventually leads to extremely fast transients. The simulated result of this case is presented in Fig. 6.4.

b3. Resistance of the ionized path (R_{diss}) with value as calculated in this thesis

By utilising the $R_{diss} = 840\ \Omega$ (as calculated in Chapter 3 and presented in Chapter 4), then the time constant of (6.10) is not infinity and eventually the maximum induced transient is directly controlled by: a) the value of R_{diss}, b) the capacitance of the void, C_v, c) the voltage prior to the discharge across the void and d) the time duration (t) of the discharge (6.10). The simulated result of this case is presented in Fig. 6.5.

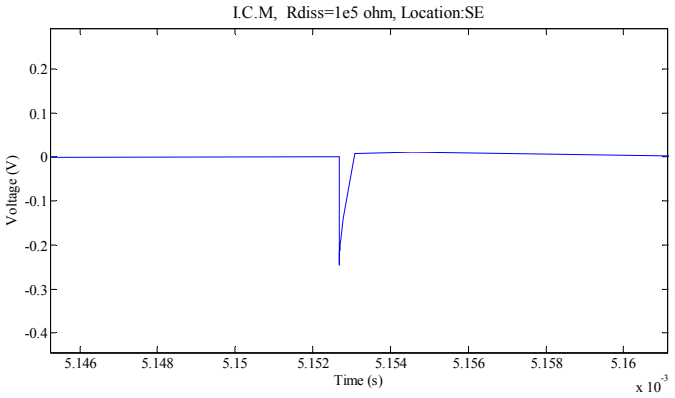

Fig. 6.3. Improved Capacitive Model: Resistance of the ionized path (R_{diss}) with infinite value

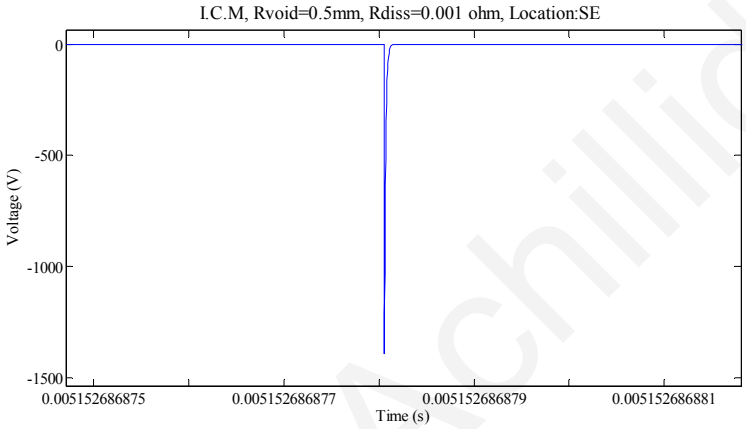

Fig. 6.4. Improved Capacitive Model: Resistance of the ionized path (R_{diss}) with zero value

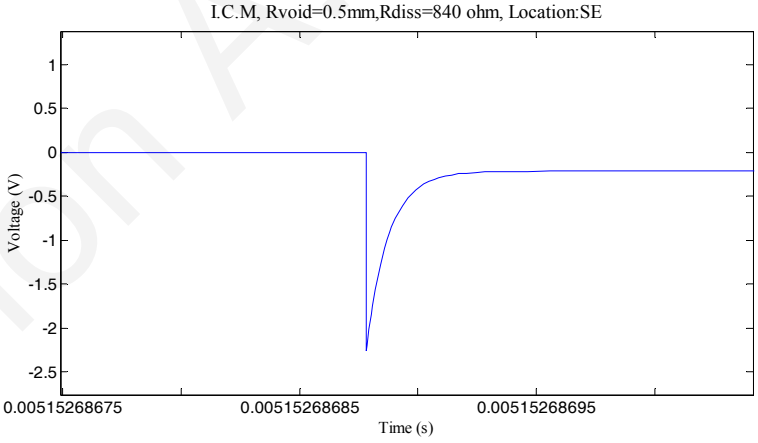

Fig. 6.5. Improved Capacitive Model: Resistance of the ionized path (R_{diss}) with value as calculated in the thesis

6.1.2. The Model of Void Based on the Induced Charge Concept

a. The significance of the calculated components

These simulated induced transient on the core of the cable generated by a breakdown void is directly related to model components as presented in section 2 and calculated in

sections 3 and 4. The importance of these components in relation to the induced transient can be justified based on energy concepts and the principle of conservation of energy, as follows:

A simplified model of Fig. 4.3 (associated with distributed impedance of cable) is presented in Fig(s). 6.6 and 6.7 below:

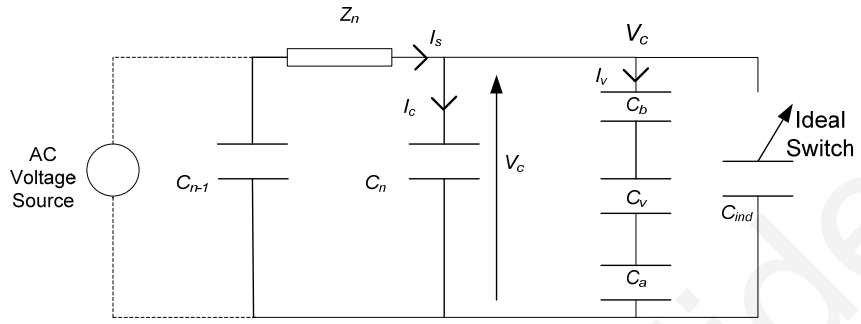

Fig. 6.6. Simplified model of void (prior break down)

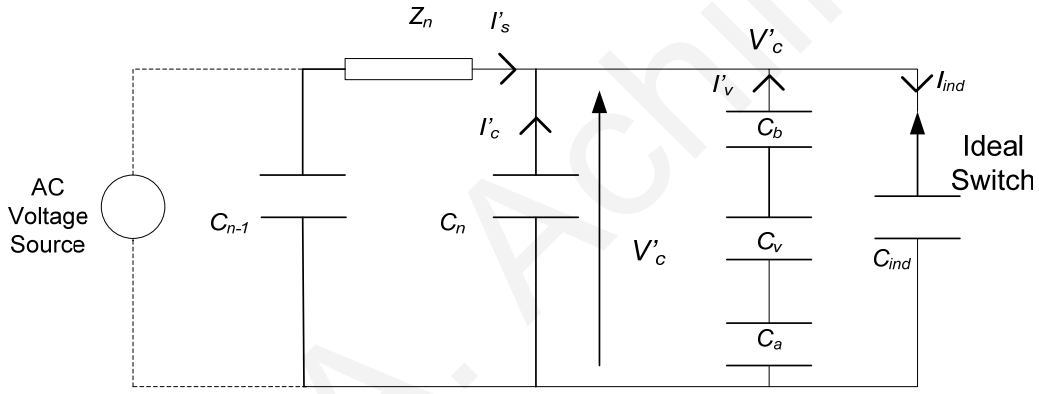

Fig. 6.7. Simplified model of void (during break down)

With reference to Figs. 6.6 and 6.7, Z_n and C_n represent the distributed series impedance and shunt capacitance of the n^{th} element of the cable respectively, C_a and C_b represent the healthy part of the insulation, C_v represents the capacitance of the void, and C_{ind} represents the capacitance due to the induced charge concept [13].Voltages V_c and $V_c^{'}$ are the cable's core voltage, before and during breakdown conditions. Fig. 6.6 represents the condition prior to breakdown, whereas Fig 6.7 represents the condition during breakdown.

With reference to Fig. 6.6, the energy stored in the capacitances adjacent to the defect (void), just prior to the simulated breakdown is given by:

$$E = \frac{1}{2}(C_n + C_T)V_c^{\,2} \tag{6.13}$$

where E is the total energy stored in the capacitors C_n and C_T, C_n is the distributed cable capacitance in the vicinity of the void, and C_T is the total capacitance composed of capacitances C_a , C_b, and C_v in parallel.

With reference to Fig. 6.7 the energy stored in the capacitances adjacent to the defect (void), during simulated breakdown is given by:

$$E' = \frac{1}{2}(C_n + C_T + C_{ind})V_c'^2 \tag{6.14}$$

where E' and V_c' is the energy stored and the voltage across the capacitors C_n, C_T and C_{ind} just after closing the ideal switch of Fig. 6.7. With reference to Fig. 6.7 and just after closing the ideal switch, the discharge process will start and capacitors C_n and C_T will start to pump up current (and energy) to capacitor $C_{induced}$.Furthermore, the distributed capacitor C_{n-1} (Fig. 6.7) will start to discharge towards capacitor C_n and through the series distributed impedance Z_n.

The maximum discharge of capacitors C_n and C_T will take place when there is a minimum flow of current (and energy) for the cable's distributed capacitor C_{n-1}. These maximum discharge processes will eventually produce the maximum possible recorded transient across the cable's core. Furthermore, by taking into account the principle of conservation of energy just before and after closing the ideal switch of Figs. 6.6 and 6.7 and eventually by equating (6.13) and (6.14) we obtain:

$$V_c' = \sqrt{\frac{C_n + C_T}{C_n + C_T + C_{ind}}}V_c \tag{6.15}$$

The recorded transient (ΔV) is defined as follows:

$$\Delta V = V_c - V_c' \tag{6.16}$$

By substituting (6.15) to (6.16) we get:

$$\Delta V = V_c(1 - \sqrt{\frac{C_n + C_T}{C_n + C_T + C_{ind}}}) \tag{6.17}$$

The outcome of (6.17) indicates that the recorded (induced) transients of the induced capacitive model are related to: C_T (which is composed of the upper and lower capacitance of the healthy part of insulation C_a and C_b) and the capacitance of the void itself (C_v), the voltage across the cable prior to the simulated discharge (V_c), the distributed capacitance of cable (C_n), and the capacitance of the induced charge (C_{ind}).

b. Performance of the proposed model

The outcome of (6.17) can be utilised in order to analyse and evaluate the

performance of the model on a theoretical basis. For this reason, three cases are to be discussed: (i) C_{ind} with zero value, (ii) C_{ind} with infinite value, and (iii) C_{ind} with value as calculated in this thesis.

b1. C_{ind} with zero value

By equating C_{ind} to zero, in practice there is no breakdown and eventually nothing is expected to be induced on the core of the cable. By substituting C_{ind} = 0 to (6.17) this leads to:

$$\Delta V = 0 \tag{6.18}$$

The outcome of (6.18) is interpreted as no induced transient on the core of the cable (as expected) and eventually justifies the truthfulness of (6.17). The simulated result of this case is presented in Fig. 6.8.

b2. C_{ind} with infinite value

The effect of equating C_{ind} to an infinite value is similar to connecting a very large capacitor as a load to the cable (Fig 6.7). A very large capacitor (load) requires a large amount of energy to be charged up. This energy is going to be provided by capacitors C_T and C_n, but due to the limited stored energy in these capacitors, (the capacitance C_n and C_T are very small) then, an the unavoidable energy drainage will take place leaving the two capacitors with almost zero energy and eventually at almost zero voltage.

By substituting (V'_c= 0) to (6.16), then a large transient is expected to be recorded as shown in (6.19).

$$\Delta V = V_c . \tag{6.19}$$

Also by substituting C_{ind} = infinity in (6.17) then right hand side of (6.17) will become zero and eventually (6.17) will become:

$$\Delta V = V_c . \tag{6.20}$$

The outcome of (6.20) is equal to (6.19) as expected. The outcome of (6.20) indicates that a large percentage of the system operating voltage (V_c) is expected to be induced as a transient at the core of the cable. The simulated results of this case are presented in Fig. 6.9.

b3. Value of C_{ind} as calculated in this thesis

By utilising the value of C_{ind} as calculated in this thesis then the nature of the recorded transient will be controlled by the magnitude of C_{ind} and the magnitude of the

rest of the capacitances as presented by (6.17). The simulated results of this case are presented in Fig. 6.10.

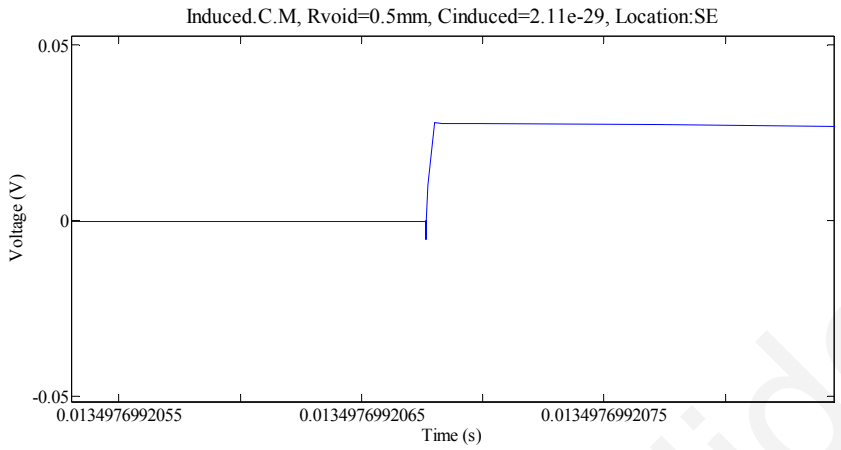

Fig. 6.8. Induced Charge Capacitive Model: $C_{induced}$ with zero value

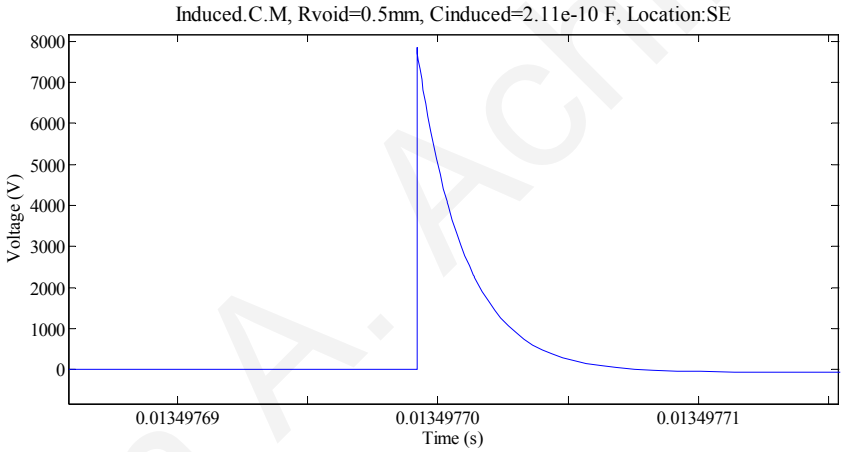

Fig. 6.9. Induced Charge Capacitive Model: $C_{induced}$ with infinite value

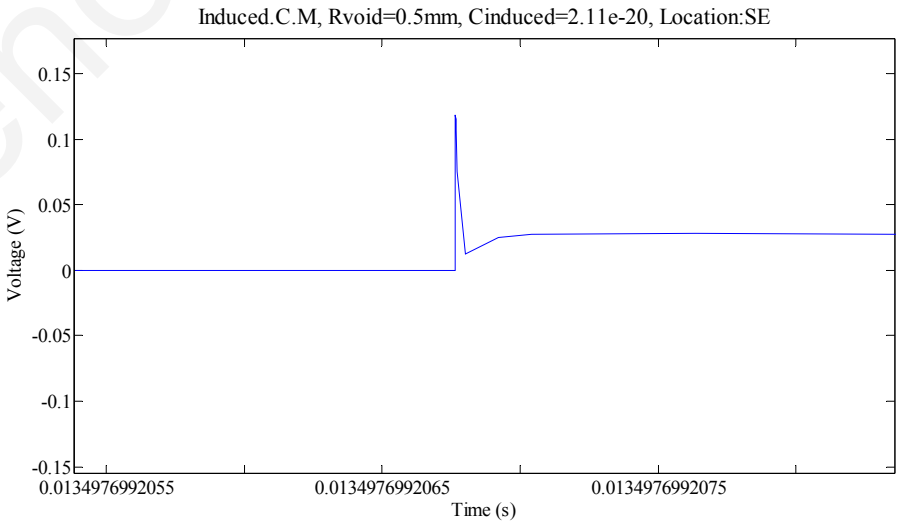

Fig. 6.10. Induced Charge Capacitive Model: $C_{induced}$ as calculated in this thesis

6.1.3. The Advanced Capacitive Model of Void

a. The significance of the calculated components

The simulated induced transient on the core of the cable generated by a breakdown void is directly related to model components as presented in section 2 and calculated in sections 3 and 4. The importance of these components in relation to the induced transient can be justified based on energy concepts and the principle of conservation of energy as follows:

A simplified model of Fig. 4.4 (associated with distributed impedance of cable) is presented in Figs. 6.11, 6.12 and 6.13 below:

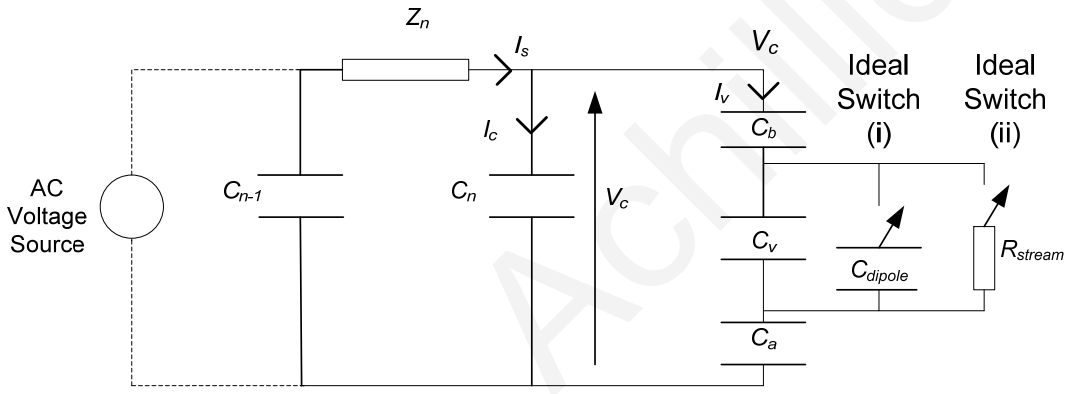

Fig. 6.11. Simplified model of void (prior breakdown)

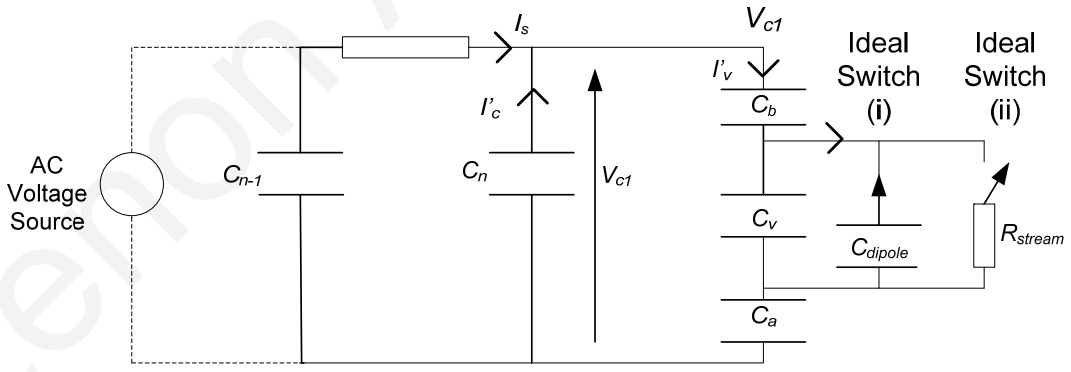

Fig. 6.12. Simplified model of void (during breakdown - stage (I))

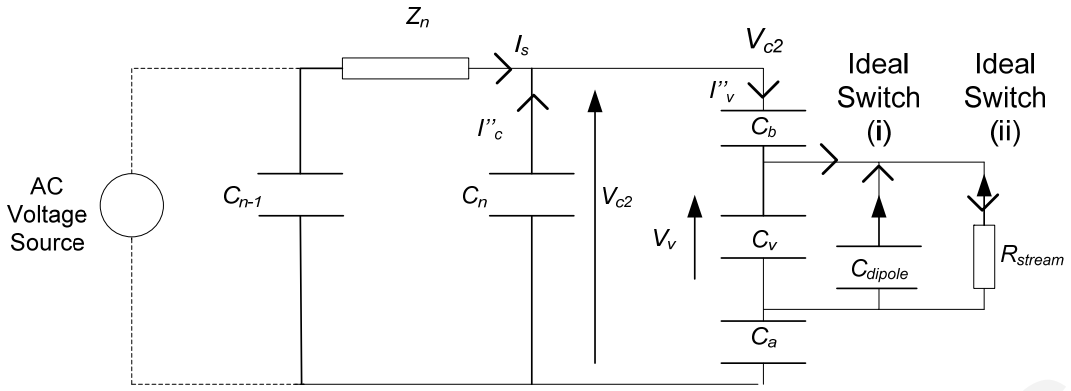

Fig. 6.13 Simplified model of void (during breakdown - stage (II))

With reference to Figs. 6.11, 6.12 and 6.13, Z_n and C_n represent the distributed series impedance and shunt capacitance of the n^{th} element of the cable respectively, C_a *and* C_b represent the healthy part of the insulation and C_v represents the capacitance of the void. C_T is the total capacitance composed of capacitances C_a // C_b // C_v and C'_T is the total capacitance composed of capacitances $C_a//C_b//(C_v+C_{dipole})$. C_{dipole} and $R_{streamer}$ represent the capacitance and resistance due to charge separation and neutralization as described in section 2.

Voltages V_c, V_{c1}, and V_{c2} are the cable's core voltage, before and during breakdown conditions at stage i and stage ii respectively. Fig. 6.11 represents the condition prior to breakdown whereas Figs. 6.12 and 6.13 represents the breakdown condition stage I and II.

With reference to Fig. 6.11, the energy store at the capacitances adjacent to the defect (void), just prior to the simulated breakdown is given by:

$$E = \frac{1}{2}(C_n + C_T)V_c^2 \tag{6.21}$$

b. Energy concepts: Break downstage (I)

With reference to Fig. 6.12 the simulated breakdown (Stage I) is achieved by closing the ideal switch (i). The energy stored in the capacitances adjacent to the defect (void), is given by:

$$E' = \frac{1}{2}(C_n + C'_T)V_{c1}^2 \tag{6.22}$$

where E' and V_{c1} is the energy and the voltage across the capacitors C_n and C'_T just after closing the ideal switch (Stage I) of Fig. 6.12. With reference to Fig.6.12 and at the time just after closing the ideal switch, the discharge process will start and capacitor C_v will

start to pump up current (and energy) to capacitor $C_{dipole.}$ The discharge process of C_v will lead to the pumping up of current (and energy) from distributed capacitor C_n (Fig. 6.13) towards capacitor $C'_{T.}$. Furthermore, the distributed capacitor C_{n-1} will start to pump current (and energy) towards capacitor C_n through the distributed impedance $Z_{n.}$

Maximum discharge, of capacitor C_n will take place when there is a minimum flow of current (and energy) through the cable's distributed capacitor $C_{n-1.}$ These maximum discharge processes will eventually produce the maximum possible recorded transient across the cable's core. Furthermore, by taking into account the principle of conservation of energy just before and after closing the ideal switch of Figs 6.12 and 6.13 respectively and eventually by equating (6.21) and (6.22) we obtain:

$$V_{c1} = \sqrt{\frac{(C_n + C'_T)}{C_n + C_T}} V_c \tag{6.23}$$

c. Energy concepts: Breakdown stage (II)

With reference to Fig. 6.13 the simulated breakdown (stage II) is achieved by closing the ideal switch (ii). At that time, the energy stored in capacitors C_v and C_{dipole} will be dissipated in the resistor R_{stream} and capacitor C_n will start to pump up current (and energy) to capacitor C_a ,C_b and $C_{v.}$ Furthermore, the distributed capacitor C_{n-1} (Fig. 6.13) will start to discharge towards capacitor C_n and through the series distributed impedance Z_n.

The maximum discharge of capacitor C_n will take place when there is a minimum flow of current (and energy) for the cable's distributed capacitor $C_{n-1.}$ These maximum discharge processes will eventually produce the maximum possible recorded transient across the cable's core. Furthermore, by taking into account the principle of conservation of energy just before and after closing the ideal switch (ii) of Figs. 6.12 and 6.13 respectively we obtain:

$$E' = E'' + E_L\,, \tag{6.24}$$

where E'' is the energy remaining stored in the capacitance of the system and E_L is the energy lost in the resistor (R_{stream}) as heat in the following way: Just before closing ideal switch (ii) the energy stored in the system, is given by (6.22). Just after closing ideal switch (ii) the capacitors C_V and C_{dipole} will start to discharge through resistor R_{stream} until almost all the energy stored will be drained out. This energy drainage will lead to the collapse of the voltage across capacitors C_V and C_{dipole} (V_v =0 in Fig. 6.13) and will

produce a voltage transient (V_{c2} in Fig. 6.13) as discussed in [13]. Basically at the initial time of the discharge process ($t=0$) all the energy will be stored in an electrostatic form (i.e, $E'=E''$), but as the time passes some of this energy will be dissipated in the resistance R_{stream}, resulting in (6.24).

By combining all the above concepts together and by substituting (6.22) to (6.24), then (6.24) yields to:

$$\frac{1}{2}(C_n + C'_T)V_{c1}{}^2 = \frac{1}{2}(C_n + C'_T)V(t)_{c2}{}^2 + \int_0^t I(t)^2 R_{stream}\, dt\,, \tag{6.25}$$

where $V(t)_{c2}$ represents the change of voltage at the core of the cable (Fig. 6.13) as a function of time, and the second part of the right hand side of (6.25) represents the energy lost across resistor R_{stream} in an integral form. The current $I(t)$, in (6.25) represents the discharge current from capacitors C_v and C_{dipole} towards resistor $R_{streamer}$ so current $I(t)$, can be replaced in (6.25) as follows:

$$\frac{1}{2}(C_n + C'_T)V_{c1}{}^2 = \frac{1}{2}(C_n + C'_T)V(t)_{c2}{}^2 + \int_0^t \frac{V_V{}^2}{R_{diss}} e^{-\frac{2t}{CR_{diss}}} dt\,, \tag{6.26}$$

where V_v represents the voltage across capacitors C_V and C_{dipole} just before closing the ideal switch (ii), and C the sum of the capacitors C_V and $C_{dipole.}$. By further expanding (6.26) we get:

$$\frac{1}{2}(C_n + C'_T)V_{c1}{}^2 = \frac{1}{2}(C_n + C'_T)V(t)_{c2}{}^2 - \frac{1}{2}[V_v{}^2 C(e^{-\frac{2t}{CR_{diss}}} - 1)]\,, \tag{6.27}$$

Equation (6.27) predicts the expected change of voltage on the core of the cable $V(t)_{c2}$ in relation to the simulated breakdown condition stage II, by taking into consideration energy conservation concepts.

The truthfulness of (6.27) can be verified in the following manner: by substituting $t=0$ to (6.27) we get:

$$\frac{1}{2}(C_n + C'_T)V_{c1}{}^2 = \frac{1}{2}(C_n + C'_T)V(t)_{c2}{}^2\,, \tag{6.28}$$

and eventually (6.28) turns as follows:

$$V(t)_{c2} = V_{c1} \tag{6.29}$$

The outcome of (6.29) indicates that at $t=0$ there is no voltage change on the core of the cable due to the simulated breakdown activity –stage (II), as naturally expected, and of course all the energy is stored in the system and no energy is dissipated as heat. Furthermore, by substituting t = infinite to (6.27) we obtain:

$$\frac{1}{2}(C_n + C'_T){V_{c1}}^2 = \frac{1}{2}(C_n + C'_T){V_{c2}}^2 + \frac{1}{2}{V_v}^2 C \tag{6.30}$$

The left hand side of (6.30) represents the energy stored in the system just prior to the closing of the ideal switch (ii) (Fig. 6.12). The first part of the right hand side of (6.30), represents the final energy that remains stored in the system after closing the ideal switch (ii) (Fig.6.13) and when the system reaches steady-state conditions. The second part of (6.30), basically represents the energy lost as heat in the system, which in fact is the part of the system's energy stored in electrostatic form across capacitors C_V and C_{dipole} (just prior to closing ideal switch (ii) (Fig. 6.13)). This energy is expected to be dissipated as heat across resistor R_{diss} after closing ideal switch (ii).

d. Induced Transients: Simulated breakdown stage (I)

The simulated induced transients on the core of the cable for breakdown stage (I) can be calculated by subtracting the expected voltage on the core of the cable (V_c) prior to closing the ideal switch (i) (Fig. 6.11) from the expected recorded voltage on the core of the cable (V_{c1}) after closing the ideal switch (i) (Fig. 6.12) as follows:

$$\Delta V_{c1} = V_c - V_{c1}, \tag{6.31}$$

where ΔV_{c1} is the expected recorded induced transients on the core of the cable for simulated condition breakdown stage (i). Furthermore by substituting (6.23) to (6.31) we obtain:

$$\Delta V_{c1} = V_c\left(1 - \sqrt{\frac{C_n + C'_T}{C_n + C_T}}\right) \tag{6.32}$$

The truthfulness of (6.32) can be justified as follows: If no space charge exists within the void, then, no charge separation is possible (as discussed in Chapter 2), giving $C_{dipole} = 0$ and this leads to $C_T = C_T'$ and which makes the second part of the right hand side of (6.32) equal to one and finally (6.32) equal to zero, resulting in no induced transients as expected.

e. Induced Transients: Simulated breakdown stage (II)

The simulated induced transients on the core of the cable for simulated breakdown stage (II) can be calculated in the following way:

The amount of voltage across capacitors C_V and C_{dipole} (Fig. 6.12) is given below:

$$V_v = V_{c1}\frac{C_a \,//\, C_b}{C_a \,//\, C + C_V} \tag{6.33}$$

By letting the product on the right hand side of V_{c1} of (6.33) equal to A and by substituting (6.33) to (6.27) we get:

$$V(t)_{c2}{}^2 = V_{c1}{}^2(1-\frac{A^2C}{B}(e^{-\frac{2t}{CR_{diss}}}-1)), \tag{6.34}$$

where B is equal to $C_n+C_T^{'}$.

The simulated induced transients on the core of the cable for breakdown stage (II) can be calculated by subtracting the expected voltage on the core of the cable (V_{c1}) prior to closing the ideal switch (ii) (Fig. 6.12) from the expected recorded voltage on the core of the cable (Vc_2) after closing the ideal switch (ii) (Fig. 6.13)) as follows:

$$\Delta V_{c2} = V_{c1} - V(t)_{c2}, \tag{6.35}$$

where $\Delta V(t)_{c2}$ is the simulated induced transient on the core of the cable. By substituting (6.34) in (6.35) and by letting K equal to constants on the right hand side of (6.34) we obtain:

$$\Delta V_{c2} = V_{c1}[1-\sqrt{(1-K(e^{-\frac{2t}{CR_{diss}}}-1))}] \tag{6.36}$$

Equation (6.36) represents the expected induced transients on the core of the cable for simulated breakdown condition stage (II).

g. Performance of the proposed model

By substituting (6.23) to (6.36), then the expected induced transients on the core of the cable for simulated breakdown condition stage (II) under the influence of the breakdown stage (II) can be predicted as follows:

$$\Delta V_{c2} = V_c\sqrt{\frac{(C_n+C^{'}{}_T)}{C_n+C_T}}[1-\sqrt{(1-K(e^{-\frac{2t}{CR_{diss}}}-1))}] \tag{6.37}$$

The first part of the right hand side of (6.37) represents the influence of breakdown stage (I) to the simulated induced transient: a time independent variable, whereas, the second part of the right hand side of (6.37) represents the influence of the simulated breakdown stage (II) on the expected simulated induced transient on the core of the cable: a time dependent variable.

Further evaluation of (6.37) can be implemented by considering different operating conditions as follows:

g1. t= 0

By substituting t =0 in (6.37), then (6.37) turns to zero and eventually no transient is expected to be induced on the core of the cable as expected:

$$\Delta V_{c2} = 0 \tag{6.38}$$

g2. C_{dipole}*= 0*

By equating C_{dipole} = 0, then $C_T = C'_T$ and C=C_v. This eventually will lead to no influence of breakdown stage (I) on the expected induced transient on the core of the cable and the time constant of the expected induced transient is going to be reduced as follows and of course will rely only on the simulated breakdown stage (II) as follows:

$$\Delta V_{c2} = V_c[1 - \sqrt{(1 - K(e^{-\frac{2t}{C_{dipole}R_{diss}}} - 1)}] \tag{6.39}$$

g3. $R_{diss} = 0$

By letting R_{diss}=*0* the exponential part of (6.37) will reach infinity and eventually (6.37) to a time independent function (a very fast induced transient) in the following manner:

$$\Delta V_{c2} = V_c\sqrt{\frac{(C_n + C'_T)}{C_n + C_T}}[1 - \sqrt{(1+K)}] \tag{6.40}$$

g4. R_{diss} = *infinite*

By letting R_{diss} = infinite then the exponential part of (6.37) will be close to one and eventually (6.37) will turn to zero, and finally no transient is expected to be induced on the core of the cable as naturally expected.

$$\Delta V_{c2} = 0 \tag{6.41}$$

6.2 PD Propagation along an XLPE Medium Voltage Cable

One of the scopes of this work was to attempt to propagate PD simulated transients, along an MV XLPE cable. Since cables have many components, these can contribute differently on the propagation loss and eventually on the PD attenuation and waveshape deformation [42]. In Chapter 5 of this work, PD propagation results were presented for the three proposed models and the classical capacitive model by utilizing a high frequency (HF) XLPE cable model as discussed in [36,37] and calculated in 'Appendix A' of this work.

In this section by utilizing wave equations and simulated results, the HF-10 MHz characteristics will be compared against Low Frequency-50 Hz (LF) characteristics (as given by the manufacture's data sheets [34]) of an MV XLPE cable.

6.2.1 Propagation Characteristics in Lines/Cables

The general wave equation in term of phasor voltage is given below:

$$\frac{d^2V_s}{dz^2} = (R + j\omega L)(G + j\omega C)V_s \tag{6.42}$$

where V_s is the phasor voltage, z is the cable length and the *R-L-C-G* parameters are the resistance, inductance, capacitance and conductance of the line/cable under investigation. The voltage along any transmission line in the time domain is given by [11]:

$$V_T(z,t) = V_o^+ e^{-az}\cos(\omega t - \beta z) + V_o^- e^{+az}\cos(\omega t + \beta z) \tag{6.43}$$

where $V_T(z,t)$ is the propagated voltage along the cable as a function of time *(t)* and length of the cable z, V_o^+ and V_o^- represent the forward and backward propagation wave at t and z equal to zero (i.e., at the point where the signal is created), α and β are the attenuation and phase coefficient respectively, which can be defined as follows [30]:

$$\alpha = \frac{1}{2}(R\sqrt{\frac{C}{L}} + G\sqrt{\frac{L}{C}}) \tag{6.44}$$

$$\beta = \omega\sqrt{LC}[1 + \frac{1}{8}(\frac{G}{\omega C} - \frac{R}{\omega L})^2] \tag{6.45}$$

These components are frequency dependent components and their characteristics change considerably at higher frequencies of propagation.

PD signals are very fast signals containing high frequency components. This eventually turns the R-L-C-G components of the cable/line to be frequency dependent [35, 36] components and therefore (6.43) and (6.44) become:

$$\alpha(\omega) = \frac{1}{2}(R(\omega)\sqrt{\frac{C(\omega)}{L(\omega)}} + G(\omega)\sqrt{\frac{L(\omega)}{C(\omega)}}) \tag{6.46}$$

$$\beta(\omega) = \omega\sqrt{L(\omega)C(\omega)}[1 + \frac{1}{8}(\frac{G(\omega)}{\omega C(\omega)} - \frac{R(\omega)}{\omega L(\omega)})^2] \tag{6.47}$$

In this work, by utilizing data given in [35-36], [34] and code (as presented in Appendix A) the R-L-C-G components (and eventually the α and β coefficients) of an MV XLPE cable are calculated for two distinct frequencies: 50 Hz (LF) and 10MHz (HF). The attenuation coefficient at 50 Hz and 10 MHz (per km) were calculated to be α = 0.0084 and α = 3.11 respectively.

6.2.2 High Frequency Against Low Frequency Characteristics of MV Cable

In the following discussion, by utilizing simulation results, the performance of the HF against the LF propagation characteristics of the XLPE MV cable under investigation will be examined, by accommodating and propagating the PD signals as generated by the three proposed models.

a. The Improved Capacitive Model

The simulated propagated PD signals for the improved capacitive model along an MV XLPE cable are presented.

Fig. 6.14 shows the PD signal at its birth point (sending end). The spike has duration of a fraction of nanoseconds (ns) and reaches maximum amplitude of 3 V.

Fig. 6.15 shows the attenuated voltage spike observed at the receiving end of the cable located 3 km from the breakdown void by utilizing the HF model. The spike's duration has increased to the order of microseconds (μs) and its maximum amplitude drops to 0.2 mV.

Fig. 6.16 shows the attenuated voltage spike observed at the receiving end of the cable located 3 km from the breakdown void by utilizing the LF model. The spike's duration has increased to the order of microseconds (μS) and its maximum amplitude drops to 0.3 V.

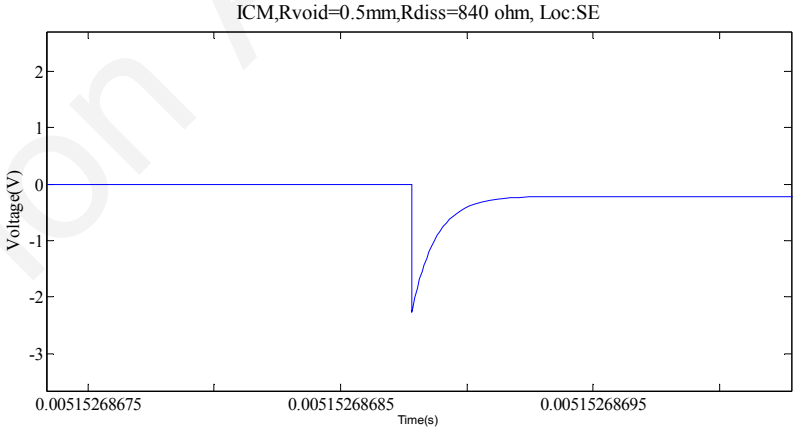

Fig. 6.14. PD simulated signal, Location: Sending end

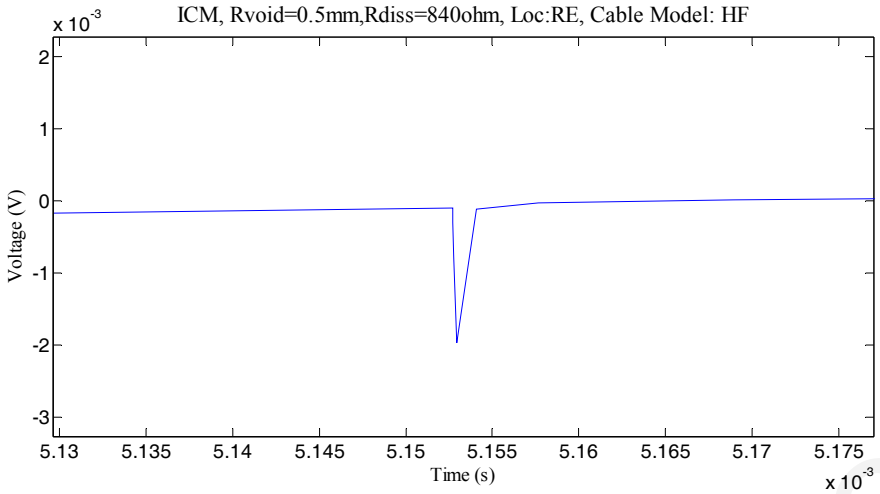

Fig. 6.15. PD simulated signal, Location: Receiving end, Model: HF

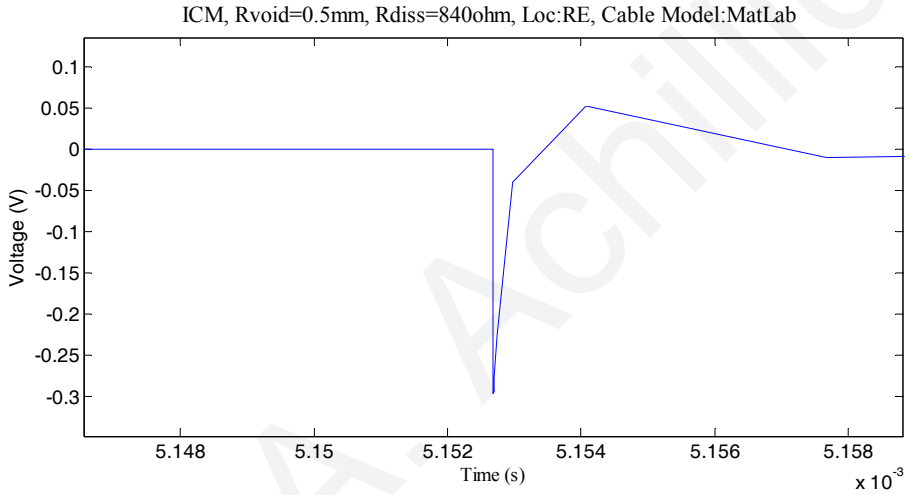

Fig. 6.16. PD simulated signal, Location: Receiving end, Model: LF

b. The Induced Charge Capacitive Model

The simulated propagated PD signals for the induced charge capacitive model along an MV XLPE cable are presented.

Fig. 6.17 shows the PD signal at its birth point (sending end). The spike has duration of a fraction of picoseconds (ps) and reaches a maximum amplitude of 0.15 V.

Fig. 6.18 shows the attenuated voltage spike observed at the receiving end of the cable located 3 km from the breakdown void by utilizing the HF model. The spike's duration has increased to the order of microseconds (μs) and its maximum amplitude drops to 0.3 mV.

Fig. 6.19 shows the attenuated voltage spike observed at the receiving end of the cable located 3 km from the breakdown void by utilizing LF model. The spike's duration has increased to the order of microseconds (μs) and its maximum amplitude drops to 80 mV.

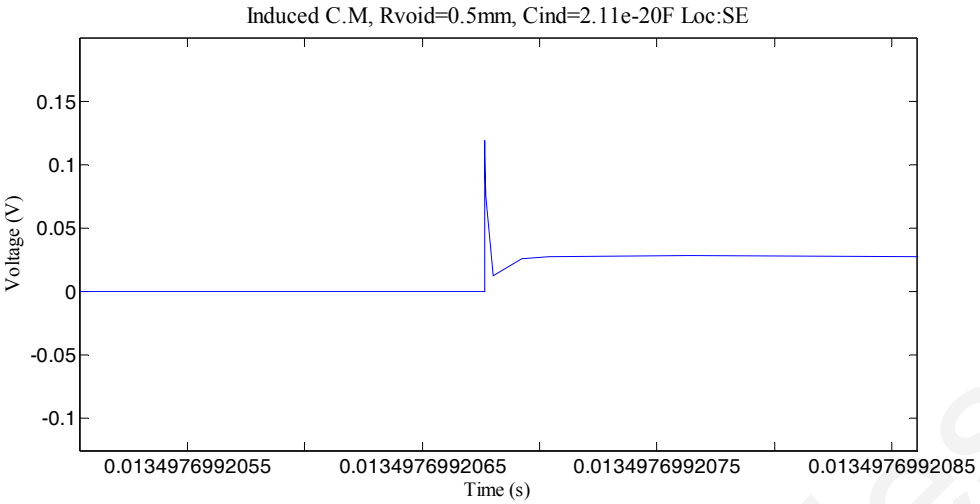

Fig. 6.17. PD simulated signal, Location: Sending end

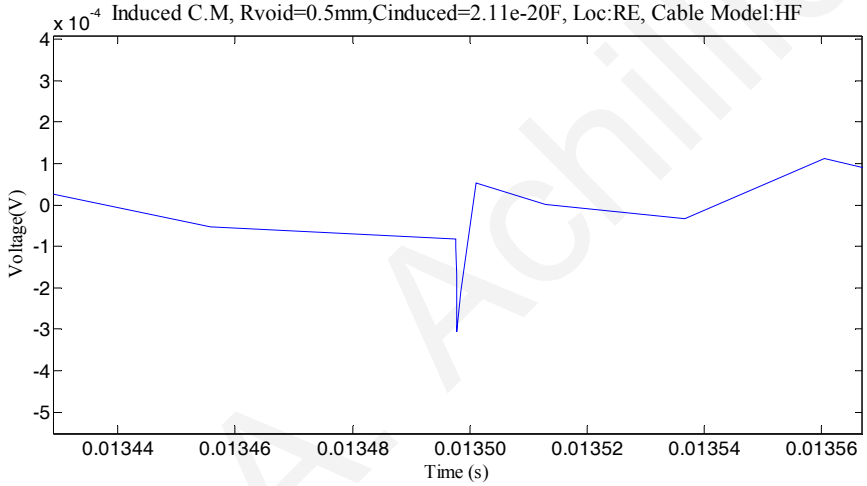

Fig. 6.18. PD simulated signal, Location: Receiving end, Model: HF

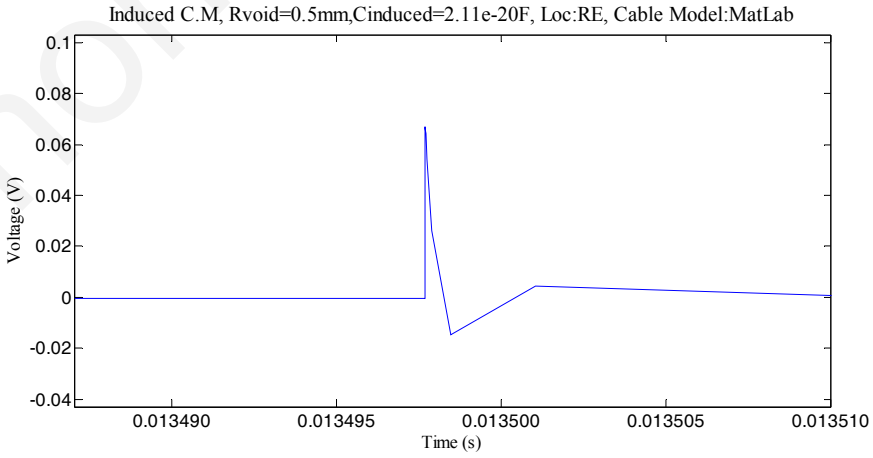

Fig. 6.19. PD simulated signal, Location: Receiving end, Model: LF

c. The Advanced Capacitive Model

The simulated propagated PD signals for the advanced capacitive model along MV XLPE cable are presented for breakdown stage (I).

Fig. 6.20 shows the PD signal at its birth point (sending end). The spike has duration of a fraction of picoseconds (ps) and reaches a maximum amplitude of 800 V.

Fig. 6.21 shows the attenuated voltage spike observed at the receiving end of the cable located 3 km from the breakdown void by utilizing the HF model. The spike's duration has increased to the order of microseconds (μs) and its maximum amplitude drops to 1 mV.

Fig. 6.22 shows the attenuated voltage spike observed at the receiving end of the cable located 3 km from the breakdown void by utilizing the LF model. The spike's duration has increased to the order of microseconds (μS) and its maximum amplitude drops to 0.15V.

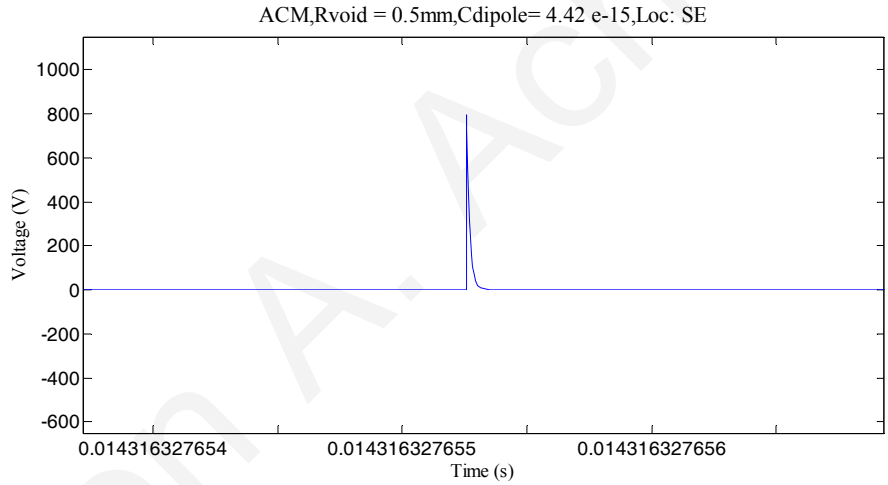

Fig. 6.20. PD simulated signal, Location: Sending end

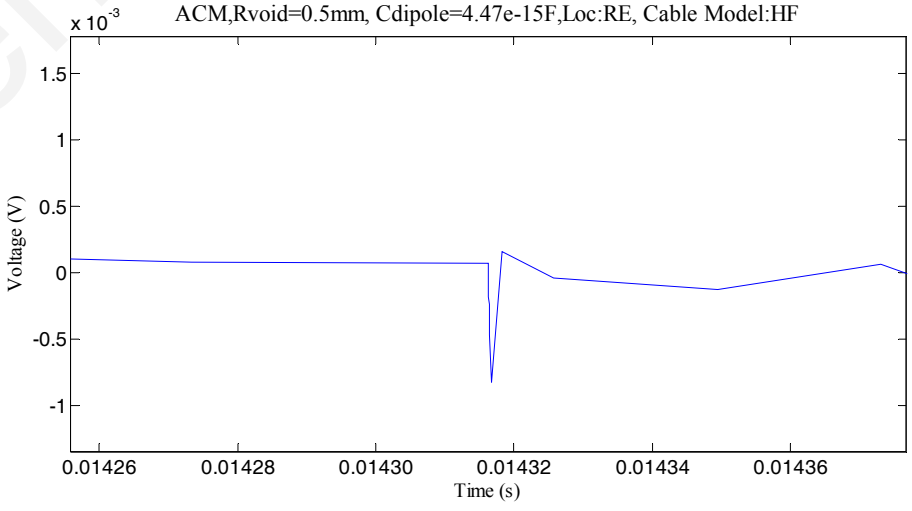

Fig. 6.21. PD simulated signal, Location: Receiving end, Model: HF

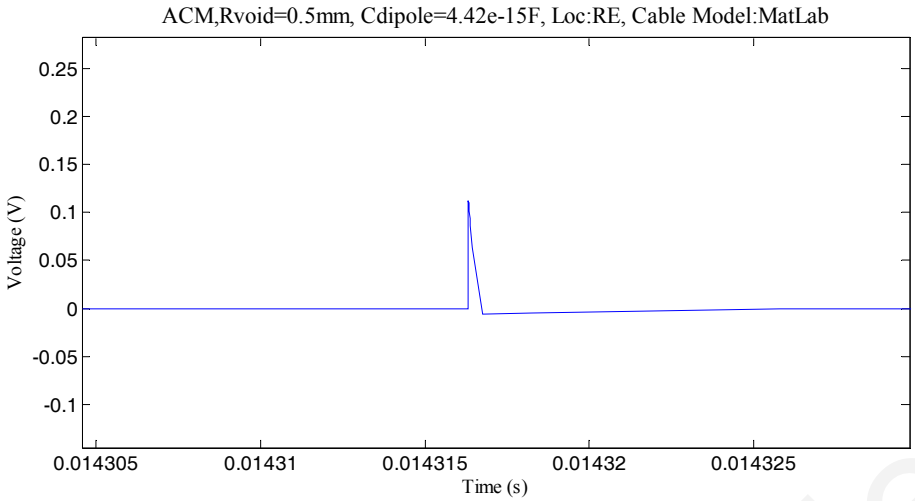

Fig. 6.22. PD simulated signal, Location: Receiving end, Model: LF

6.2.3 Discussion

Based on the discussion of Chapter 6.2.1, the attenuation coefficient (α) of the HF model and LF cable model were calculated to be 3.11 and 0.0084 respectively (Appendix A). This eventually gives an attenuation ratio for the two models of the order of 400. This ratio is reflected in the simulation results as presented in Section 6.2.2.The difference in magnitude of the PD receiving end signals between the HF and LF cable models are more than obvious for all three cases. The HF model attenuates PD signals by 100 times more than the LF model for all three proposed models under investigation. Although this ratio is large enough, it is four times less than the expected theoretical attenuation as calculated at the beginning of section 6.2. The reason for this is that MATLAB/Simulink is capable to adjust the 50 Hz components (partially) by taking into consideration the skin effect, so this eventually increases, the attenuation coefficient (α) by a factor close to four (for this case).

6.3 Discussion on the Simulation Results

In Chapter 5 the simulated results of the PD for the three proposed models and the classical capacitive model have been presented, for cylindrical voids of different diameters and length. In all three cases, void(s) were located in the middle of the insulation between the core and the sheath of the cable under investigation. In the discussion that follows the influence of the diameter and the length of the void for simulating and propagating PD signals will be discussed for each model separately.

6.3.1 The Classical Capacitive Model.

The PD simulated results of the classical capacitive model are presented in Chapter 5.1 for cylindrical voids for three cases, where the diameter and the length of void were 0.5 mm, 1 mm and 1.5 mm.

a. Waveshape

The waveforms of all simulated transients for all three cases are all of a similar nature, following the exponentially charge/discharge transients of capacitors as expected.

b. Time duration of PD simulated signals

The total time duration of the PD simulated transients, as presented in Chapter 5.1, is of the order of a fraction of picoseconds (ps) regardless of the diameter and the length of the cylindrical void under consideration. These results can be justified as follows: Based on (6.10) the expected time constant and the rise time of the simulated PDs are directly related to the product of R_{diss} and C_{void} . The values of C_{void} as given in Table 4.1 are of the order of 10^{-14} F for all the three cases. By further utilizing R_{diss}= 0.01 Ω (instead of zero), then the time constants of the PD simulated signals are similar for all three cases and eventually the time duration of the simulated PD signals are expected to be similar for all three cases. This is verified in the simulation results as presented in Chapter 5.1

c. Voltage magnitude of the PD simulated signals

The peak magnitude of the simulated induced voltage transients are 1500 V, 3500 V and 5000 V for voids of radii of 0.5 mm, 1 mm and 1.5 mm respectively. The main reason for these differences is due to the onset voltage magnitude for simulating the PD signal which was chosen to be 2 kV, 3.5 kV and 5 kV respectively. These simulation results can be justified based on the discussion given in Section 6.1.1, and the outcome of (6.10) as follows: By setting R_{diss} of (6.10) equal to zero (i.e., classical capacitive model) then the recorded transient (ΔV_c) is equal to V_V. V_v is the value of the voltage across the void capacitance C_V (Fig 4.2) just before closing the ideal switch, which in turn is equal to the value of the onset voltage for simulating PDs.

d. PD propagated simulated signals

For the three cases presented in Chapter 5.1 (0.5 mm, 1 mm and 1.5 mm) all simulated PD signals suffer heavy attenuation and energy loss after 3 km of propagation along the MV cable. The main reason for this is the HF components of the MV cables

and eventually the attenuation coefficient (α) -as discussed in Chapter 6.2. The PD simulated signals for all three cases originated (sending end) with a signal magnitude of the order of thousands of volts and with a time duration of a fraction of picoseconds and ended up (receiving end-3 km away) with a magnitude of the order of mV and a time duration of the order of microseconds (μs).

6.3.2 The Improved Capacitive Model

The PD simulated results of the improved capacitive model are presented in Chapter 5.2 for cylindrical voids for three cases, where the diameter and the length of the Voids are of 0.5 mm, 1 mm and 1.5 mm.

a. Waveshape

The waveforms of all simulated transients for all three cases are all of a similar, nature following the exponentially charge/discharge transients of capacitors, as expected.

b. Time duration of PD simulated signals

The total time duration of the PD simulated transients as presented in Chapter 5.2, is of the order of a fraction of nanoseconds (ns) regardless of the diameter and the length of the cylindrical void under consideration. These results can be justified as follows: Based on (6.10) the expected time constant and the rise time of the simulated PDs are directly related to the product of R_{diss} and C_{void}. The product of C_{void} and R_{diss} as given in Table 4.2 is in the range between 10^{-11}- 10^{-12} F for all the three cases. For this reason the time duration of the simulated PD signals are similar for all three cases and are in the order of nanoseconds (ns).

c. Voltage magnitude of the PD simulated signals

The peak magnitude of the simulated induced voltage transients ranging from a few volts to a few hundred of volts for all three cases. These simulation results can be justified based on the discussion given in Section 6.1.1, and the outcome of (6.10) relating the diameter of the void and eventually the capacitance C_V (Fig. 4.2), to the on set voltage magnitude for simulating PD signal V_v, and finally the resistance of the ionized path R_{diss}.

d. PD propagated simulated signal.

For the three cases presented in Chapter 5.2 (0.5 mm, 1 mm and 1.5 mm), all simulated PD signals suffer heavy attenuation and energy loss after 3 km propagation along the MV cable. The main reason for this is the HF components of the MV cables and eventually the attenuation coefficient (α), as discussed in Chapter 6.2. The PD simulated signals for all three cases originated (sending end) with signal magnitude of the order of a few volts to a few hundreds of volts and with a time duration of the fraction of nanoseconds and ended up (receiving end) with a magnitude of the order of mV and time duration in the order of microseconds.

6.3.3 The Induced Charge Capacitive Model

The PD simulated results of the capacitive model of the void based on the induced charge concept are presented in Chapter 5.3 for cylindrical voids for three cases, where the diameter and length of the voids are 0.5 mm, 1 mm and 1.5 mm.

a.Waveshape

The waveforms of all simulated transients for all three cases, are all of a similar nature following the exponentially charge/discharge transients of capacitors as expected.

b. Time duration of PD simulated signals

The total time duration of the PD simulated transients, as presented in Chapter 5.3, are of the order of a the fraction of picoseconds (ps), regardless of diameter and length of the cylindrical void under consideration. These results can be justified as follows: Equation (6.17) represents the expected induced transient on the core of the cable of the proposed model. This equation is composed only by capacitive elements which in turn produces very small time constant and this eventually leads to very narrow rise time of the simulated PDs.

c. Voltage magnitude of the PD simulated signals

The peak magnitude of the simulated induced voltage transients are in the range 0.12 mV, 0.2 mV and 0.3 mV for the three cases respectively. These simulation results can be justified based on the discussion given in Section 6.1.2, and the outcome of (6.17) relating the diameter of the void and eventually the capacitance $C_{induced}$ (Fig 4.3 and Table 4.2) to the induced PD simulated signals.

d. PD propagated simulated signals

For the three cases presented in Chapter 5.3 (0.5 mm, 1 mm and 1.5 mm) all simulated PD signals suffer from a heavy attenuation and energy loss after a 3 km propagation along the MV cable. The main reason for this is the HF components of the MV cables and eventually the attenuation coefficient (α), as discussed in Chapter 6.2. The PD simulated signals for all three cases originated (sending end) with a signal magnitude of the order of few hundred millivolts (mV) and with a time duration of a fraction of picoseconds and ended up (receiving end 3 km away) with a magnitude in the order of hundred of microVolts (μV) and a time duration of the order of microseconds (μs).

6.3.4 The Advanced Capacitive Model

The PD simulated results of the advanced capacitive model are presented in Chapter 5.4 for cylindrical voids for three cases, where the diameter and the length of voids are 0.5 mm, 1 mm and 1.5 mm.

a. Waveshape

The waveforms of all simulated transients for all three cases are all of a similar nature following the exponentially charge/discharge transients of capacitors, as expected.

b. Time duration of PD simulated signals

The total time duration of the PD simulated transients as presented in Chapter 5.4 are of the order of a fraction of nanoseconds (ns) (breakdown stage (II)), regardless of diameter and length of the cylindrical void under consideration. These results can be justified as follows: Based on (6.36), the expected time constant and the rise time of the simulated PDs are directly related to the product of R_{diss} and $C_{void} + C_{dipole}$. The products of C_{void} and R_{diss}, as given in Table 4.4 are in the range of 10^{-11}- 10^{-12} s for all the three cases. For this reason, the time durations of simulated PD signals are similar for all three cases and are of the order of nanoseconds (ns).

c. Voltage magnitude of the PD simulated signals

The peak magnitude of the simulated induced voltage transients are in the range of a few volts to a few tens of volts for the three cases (breakdown stage (II)). These simulation results can be justified based on the discussion given in Section 6.1.3, and the

outcome of (6.36) relating the diameter of the void and eventually the capacitance C_{dipole} (Fig. 4.4 and Table 4.4), and the induced PD simulating signals.

d. PD propagated simulated signals

For the three cases presented in Chapter 5.4 (0.5 mm, 1 mm and 1.5 mm) all simulated PD signals suffer from a heavy attenuation and energy loss after a 3 km propagation along the MV cable. The main reason for this is the HF components of the MV cables and the attenuation coefficient (α), as discussed in Chapter 6.2. The PD simulated signals for all three cases originated (sending end) with a signal magnitude of the order of a few volts to tens of volts and with a time duration of a fraction of nanoseconds (ns) and ended up (receiving end 3 km away) with a magnitude in the order of hundreds of microvolts (μV) and time a duration of the order of microseconds (μs).

6.4 Comparison of the Simulation Results against Laboratory Measurements Obtained from the International Literature

One of the major scopes of this work was to replicate and propagate the PD signals as faithfully as possible. For this reason three new capacitive models have been proposed and utilised in order for this goal to be achieved. In the following discussion the three proposed models and the classical capacitive model are going to be compared against laboratory measurements as obtained from the international literature. The length and magnitude of PD signals as described in literature [44-48], and measured in laboratory work [37-41] range between 0.5-5 millivolts (mV) to volts (V) respectively.

6.4.1 The Models

a. The classical capacitive model of void

The magnitude of the generated PD simulated signals (as presented in Chapter 5.1) range between a few hundred to few a thousand volts and the duration of the signals is in the order of picoseconds.

b. The improved capacitive model of void

The magnitude of the generated PD simulated signals (as presented in Chapter 5.2) range between few a volts to tens of volts and the duration of the signals is in the order of nanoseconds.

c. The capacitive model based on induced charge concept

The magnitude and duration of the generated PD simulated signals (as presented in Chapter 5.3) range between a few tens of millivolts to a hundred of milivolts and the duration of the signals is in the order of picoseconds.

d. The advanced capacitive model of void

The magnitude and duration of the generated PD simulating signals (as presented in Chapter 5.4) range between a few volts to tens of volts and the duration of the signals is in the order of nanoseconds.

6.4.2 Discussion

Regarding the magnitude of PD signals, the capacitive model of the void, based on the induced charge concept, generates PD signals in close similarity with those PD signals presented in laboratory measurements [37-40]. As far as the signal duration of the partial discharge is concerned, the improved capacitive model and the advanced capacitive model generate signals in close similarity with those PD signals presented in laboratory measurements [37-40] as well. As far as the classical capacitive model generates PD signals that are unrealistic. The difference between laboratory results and simulated results as presented in Chapter 5 in this work is explained below:

a. Coupling

For laboratory results, direct measurements on the core of the cable at the point where the defect within the insulation is supposed to be created is not possible. For this reason capacitive or inductive couplers are utilised in order to measure PD signals. Thses couplers have a certain bandwidth limitation (usually less than GHz) which eventually attenuates higher frequency components (if any) composing PD signals. On the other hand PD, simulated signals can be ‘measured’ directly on the core of the cable at close vicinity of the void without any coupling elements.

b. Detection impedance method for measuring PD signals

The laboratory results as discussed in [37-40] are utilising the detection impedance method for the measurement of PD signals. This method utilises an impedance in series with the defect (this method is discussed and evaluated in detail in [41]) and this eventually will alter considerably the circuitry (of all proposed models) as discussed in Chapter 6.1 and eventually the recorded transients.

c. Energy of source

In any laboratory (utilising high voltage equipment) current limiting devices or high impedance voltage source(s) are utilised in order to limit the amount of energy and current that can be drawn from the source for safety reasons. The behaviour of this high impedance source will alter considerably the circuitry (of all proposed models) as discussed in Chapter 6.1 and, eventually the expected recorded transients. On the other hand, in the simulation no safety issue is considered and eventually the impedance of the source is modelled as is in Power network (i.e., low value as described in Chapter 4) and therefore an 'infinite' amount of energy is available at any point on the core of the MV cable under consideration.

d. Void dimensions

The diameter and length of the void (0.5, 1, 1.5 mm) utilised in the simulation results is comparatively large compared to the insulation thickness of the MV cable [34]. This leads to a higher value of capacitances (Tables 4.1-4.4) and eventually higher magnitude induced transients (as discussed in Chapter 6.1).

6.5 MATLAB/Simulink Performance

In this work the software package of MATLAB/Simulink was utilised in order to calculate components of the proposed circuits, and generate, propagate, and attenuate PD simulated signals in the time domain. Due to the complex nature of the system resulting from the coupling between the PD generation models and the cable propagation model this becomes a complex task. During the simulation process sometimes MATLAB/Simulink failed to converge or produced unrealistic results.

To overcome/minimize this problem the variable-step solution 'ode 23tb (stiff/TR-BDF2)' was utilised for all simulation results presented in this work. For even better

results, an attempt was made to decouple the models (void model and cable model) in the following way: First, the PD signals based on the LF components of the cable and the void model were generated and recovered at the point where the void is created. Consequently the MATLABs/Simulinks RF block set 'R-L-C-G Transmission line model' was utilised in order to propagate the PD signals along the 'R-L-C-G Transmission line model'. Finally the signals were attempted to be recovered at the far end of the line. Despite this effort this goal was not achieved.

The MATLABs/Simulinks RF block set 'R-L-C-G Transmission line model' is designed to work in the frequency domain only, so the generated PD signals had to be switched from the time to frequency domain via the FFT conversion block before injected to the 'R-L-C-G Transmission line model'. However due to the variable time step nature of the PD signals that conversion lead to failure. To overcome this problem, an HF model of the transmission line was created and connected in parallel with the LF model of the line (Fig. 4.1). Although by utilising this technique the problem was overcome, but that was not without a price. Another two additional sources of errors were added to the simulation results: (i) The PD generated signal faces two different characteristic impedances (HF and LF) at the same time, so it splits, is reflected and refracted accordingly at the point of coupling, (ii) due to the presence of the HF line an extra distributed capacitance is added to the circuitry and therefore this changes the induced transients (Chapter 6.1, equations (6.17) and (6.36)).

CHAPTER 7

GENERAL DISCUSSION

7.1 General Discussion - Conclusions

The main motivation of this work is to understand the physical process regarding the partial discharge mechanism and improve the existing PD models in order to replicate and estimate the transients generated, traveled and attenuated by PD activity along the core of medium voltage distribution cables. This work also aims at comparing the simulation results against laboratory data obtained from the international literature. For this reason, the relevant Physics, Mathematics and the associated circuit theory related to PD modeling were utilised. An outline of all these concepts and how they merge together in this work is presented below:

The potential and weaknesses of the classical capacitive representation of the void have been exploited, the induced charge concept has been introduced, and the criticism related to the capacitance model has been argued. Also the relationship between the induced charge concept and the change of capacitance has been demonstrated. Further more by utilizing classical electromagnetism, the simulated discharge current (6.9) (as described in Section 6 and predicted by the capacitive model of the void) is correlated with the physical current (2.45) flowing within an insulating medium after the establishment of breakdown conditions and directly related to the conduction of the ionized channel for the streamer breakdown mechanism. This correlation leads to the introduction of the element of the ionized path resistance R_{diss} in the classical capacitive model. As a further step forward to PD modeling, the element of C_{dipole} is introduced, based on streamer concepts. This element reflects partially the physical process regarding charge separation between charges and positive ions as the avalanche propagates towards the anode and further correlated to the increase of the system's capacitance due to the presence of space charges and dipole moments as discussed in Chapter 2.

All the above concepts lead to the proposition of three proposed models of the void: a) an improved capacitive model of the void, b) a capacitive model of the void based on the induced charge concept, and c) an advanced capacitive model of void. These models are based on the low frequency passive elements of the cable under investigation.

Furthermore, an analytical method for calculating all elements of the three proposed models is demonstrated and proposed based on classical electromagnetics. All elements that constitute the proposed models are modeled together with the high frequency

dependent components (R-L-C-G) of the medium voltage cable under investigation, as calculated in this thesis.

One of the scopes of this work is to examine the performance of the three proposed models on a theoretical basis. For this reason, the principle of conservation of energy associated with circuit theory was utilized. It was succefully demonstrated that the induced transients on the cable's core due to the PD activity are directly related to and controlled by the passive components of the cable's insulation and the defect as shown in (6.10), (6.17), (6.33) and (6.35) for all the proposed models.

As a further contribution in this thesis, the high frequency and low frequency propagation characteristics of the MV cable have been compared and discussed based on the components as calculated in this work associated with the simulation results of Chapter 5. As a result of this comparison, the MATLAB/Simulink performance is evaluated for the generation and propagation of PD signals. As a final contribution of this work, the simulation results, as presented in Chapter 5, are compared to and discussed against laboratory measurements obtained from the international literature.

Finally, it can be concluded from the simulation results and the discussion presented throughout the thesis, that the capacitive models of the void, as proposed in this thesis, associated with the HF impedance of the distribution cable are a powerful tool in the hand of the engineers to replicate the PD signals.

7.2 Theoretical assesion of the three proposed models

One of the major contributions of this work is the proposition of three new capacitive models of the void: a) the improved capacitive model of the void, b) the capacitive model of the void based on the induced charge concept and c) the advanced capacitive model of the void. The evaluation performed below is based on the fact that in this work all three models are modeled as a part of an MV distribution cable and the rest of the electrical network as presented and discussed in Chapter 4.

From the theoretical evaluation of the performance of the models as presented and discussed in Chapter 6 and supported by simulation results as presented in Chapter 5, the capacitive model based on the induced charge concept performs poorer among the three of the proposed models. The main reason for this is that the core of the model is composed only by capacitive elements and eventulally this induces very fast simulated PD signals on the core of the cable (in the order of a fraction of picoseconds). This is in contradiction to the common knowledge regarding PD signals. The short duration of the

PD simulated signals is predicted by (6.15) and supported by the simulation results as presented in Section 5.3.

From the theoretical point of view, the advanced capacitive model of the void reflects closer the PD mechanism for streamer concepts compared to the other two proposed models. The simulated PD transients produced by the model and induced on the core of the cable under investigation are predicted by (6.36) and supported by simulation results as presented in Section 5.4, have a time duration in the order of nanoseconds and a magnidute in the order of a volt, which are closer to common kmowledge regarding PD signals based on the laboratory measurements as presented in [37-41]. One of the major disadvantages of the advanced capacitive model is that the simulation of partial discharges is based on a two stage mechanism; this becomes a very complex task and enormous effort is required from the available software package to generate, travel, and attenuate the simulated PD signals (as discussed in detailed in Section 6.5).

The improved capacitive model performs as well as the advanced capacitive model. The simulated PD transients produced by the model and induced on the core of the cable under investigation are predicted by (6.10) and supported by simulation results as presented in Section 5.2. These transients have time duration in the order of nanoseconds and a magnitude in the order of a volt, which are closer to common kmowledge regarding PD signals, based on the laboratory measurements presented in [37-41].

Based on the evaluation given in this section and by taking into account all the aforementioned factors, the improved capacitive model of the void, modeled with the impedance of the cable and the rest of the power network is the most efficient model to appropriately model the partial discharge mechanism.

7.3 Future Work

For PD signal replication, an adequate PD model is required. In this work four models based on lumped capacitors were utilized. The accuracy of this model and eventually the generated PD signals are directly related to the values of the components composing these models, so for this reason and as future work:

(i) The analytical method proposed in this thesis in order to calculate these components may be compared and verified by utilizing an appropriate EMTP software package.

(ii) The software MATLAB/Simulink was utilized for both PD signal generation and propagation, for this reason EMTP propagation software is required so that variable time step signals are created in order to propagate and compare the PD signals with Simulink.

(iii) A frequency domain analysis of the time domain PD simulated signals is more than a necessity. For this reason, the problem of the transformation of discrete time variable step signals to the frequency domain has to be resolved.

(iv) In a real MV network a lot of static and dynamic elements are connected along line/cables so a PD signal during its travel along the cable confronts these elements. For this reason, the HF components of these elements have to be modeled and included in the circuits.

(v) Different geometries and location of voids within the insulation of cables may be modeled to examine whether there is any variation in the generation and propagation of partial discharges.

REFERENCES

[1] A. Pedersen G. C. Crichton and I. W. McAllister, "The theory and measurements of partial discharge transients," *IEEE Trans. Electr. Insul. ,* vol. 26, pp. 487–497, 1991.

[2] A. Gemant and W. V. Philippoff, "Die Funkenstrecke mit Vorkondensator*", Z. Techn. Phys.*, Vol.13, pp. 425–430, 1932.

[3] S. Whitehead, *Dielectric Breakdown of Solid*, Clearendon Press, Oxford, England, 1951.

[4] G. Paolleti and A. Golubev, "Partial discharge theory and applications to electrical systems," *IEEE Pulp and Paper Industry Technical Conf.* , Seattle, WA, USA, pp. 124-138, 21-25 June 1999.

[5] G. C. Crichton, P. W. Karlsson and A. Pedersen, "Partial discharges in ellipsoidal and spheroidal voids", *IEEE Trans. Electr. Insul*., vol. 24, pp. 335–342, 1989.

[6] I. W. McAllister, "Electric field theory and the fallacy of the void capacitance," *IEEE Trans. Electr. Insul. ,* vol. 26, pp. 458–459, 1991.

[7] C. Oatley, *Electric and Magnetic fields. An Introduction*, Cambridge University Press Cambridge, pp. 47-51, 1976.

[8] M. G. Danikas, "Partial discharges in ellipsoidal and spheroidal voids," *IEEE Trans. Electr. Insul,* vol. 26, pp. 537–538, 1991.

[9] M. G. Danikas, "Discharge studies in solid insulation voids," *IEEE Conf. Electr. Insul. Dielectr. Phenomena* (*CEIDP*), pp. 249-254, 1990.

[10] N. P. Kolev, E. D. Gadjeva, M. G. Danikas, and N. R. Gourov, *"*An approach to develop a partial discharge investigation," *IEEE Electr. Insul. Conf. and Electrical Manufacturing and Coil Winding Conf.,* pp. 507-510, 1999.

[11] M. G. Danikas and G. E. Vardakis, "The case of Pedersen's theory to model partial discharges in cavities enclosed in solid insulation: A criticism of some of its aspects from an electrical engineers' and from physicists' point of view," *Journal of Electrical Engineering,* vol. 52, pp. 166–170, 2001.

[12] M. G. Danikas and D. Papagiotopoulos, "Partial discharges in solid insulation cavities: A theoretical analysis and a comparison with experimental results", Facta Universitatis (Ser.: Elec. Energ.), vol. 15, no. 3, pp. 385-398, 2002.

[13] Z. Achillides, G. E. Georghiou and E. Kyriakides "partial discharges and associated transients: the induced charge concept versus capacitive modeling," *IEEE Trans. on Dielect. and Electr. Insul*., vol. 15, no. 6, pp. 1507–1516, Dec. 2008.

[14] W. H. Hayt and J. A. Buck, *Engineering Electromagnetics,* 7th ed. McGraw-Hill, 2005.

[15] P. Y. Chia and A. C. Liew, "Novel approach to partial discharge signals modeling in dielectric insulation void using extension of lumped capacitance model," *IEEE Power System Technology Conf, Perth, WA, Australia*, vol. 3, pp. 1207-1212, 2000.

[16] G. Elert, *The Physics Hypertext book*, 1998-2008. [Online] http://www.hypertextbook.com/physics

[17] L. Niemeyer, "A generalized approach to partial discharge modeling," *IEEE Trans. on Dielect. and Electr. Insul*., vol. 2, no. 4, pp. 510–528, 1995.

[18] G. C. Crichton, P. W. Karlsson, and A. Pedersen, "A theoretical derivation of the transients related to partial discharges in ellipsoidal voids," *IEEE Intern. Sympos. Electr. Insul. (ISEI),* Boston, MA, pp. 238-241, 1988.

[19] P. C. Clemmow, *An Introduction to Electromagnetic Theory*, Cambridge University Press, Cambridge, UK, 1973.

[20] J. Fischer*, Elektrodynamik*, Springer-Verlag, Berlin, Germany, 1976.

[21] D. T. Paris and F. K. Hurd, *Basic Electromagnetic Theory*, McGraw-Hill, New York, USA, pp. 185-186, 1969.

[22] I. W. McAllister and G. C. Crichton "Analysis of the temporal fields in lossy dielectric media," *IEEE Trans. Electr. Insul*., vol. 26, pp. 513–528, 1991.

[23] F. Miller, Jr. *College Physics*, Harcourt Brace Jovanovich, Inc, 5th ed., N.Y, USA, 1982.

[24] M. E. Zaret, *Outline of Electromagnetic Theory*, Sloves & Frey, USA, 1964.

[25] Yu. P. Raizer: *Gas Discharge Physics*, Springer-Verlag Berlin Heidelberd, 1997

[26] J. M. Meek, J. D. Graggs, *Electrical Breakdown of Gases,* John Wiley, 1978

[27] E. Nasser *Fundamentals of Gaseous Ionization and Plasma Electronics*, Wiley-Interscience, 1971.

[28] P. Y. Chia and A. C. Liew, "Novel approach to partial discharge signals modeling in dielectric insulation void using extension of lumped capacitance model," *IEEE Proceedings on Power System Technology*, vol. 3, pp. 1207-1212, Dec. 2000.

[29] E. Carminati, and M. Lazzaroni "A contribution in partial discharge detection", *IEEE Instrumentation and Measurements Technology Conference*, Ottawa, Canada, pp 501- 506, May 19-21, 1997

[30] Z. Achillides, E. Kyriakides and G. E. Georghiou "Partial discharges and induced transients along medium voltage distribution cables" *DEMSEE conference, Nicosia, Cyprus*, paper ref. 139, 22-23 Sep. 2008.

[31] Erwin Kreyszig, *Advanced Engineering Mathematics*, 7th ed. John Wiley & Sons, Inc,1993

[32] M.G Danikas and G Adamidis, "Partial discharges in epoxy resin voids and the interpretational possibilities and limitations of Pedersen's model" *Electrical Engineering,* 80,pp 105-110 Springer-Verlag, 1997.

[33] G. E. Georghiou, A. P. Papadakis, R. Morrow, and A. C. Metaxas, "Numerical modeling of atmospheric pressure gas discharges leading to plasma production," *Journal of physics D: Appl.Physics.38) R303-R328,* Aug. 2005.

[34] KEMA Transmission & Distribution, *Power cables*, E.F Steennis, Oct. 2001

[35] G. Magula, R Eriksson, U. Gafvert and P. Petterson "Measurement technique for high frequency characterization of semi-conducting materials in extruded cables," *IEEE Transactions on Dielectrics and Electrical Insulation*, vol. 11 no. 3, pp. 471-480, June 2004.

[36] G. Magula, R Eriksson, and P. Petterson "Dependence of XLPE insulated power cable propagation characteristics on design parameters," *IEEE Transactions on Dielectrics and Electrical Insulation*, vol. 14, no. 2, pp. 393-399, Apr. 2007.

[37] N. H. Ahmed and N. N. Srinivas, "On- line partial discharge detection in cables," *IEEE Transactions on Dielectrics and Electrical Insulation*, vol. 5, no. 2, pp. 181-188, Apr. 1998.

[38] T. Broche, W. Hiller, E. Fauser, and W. Pfeiffer, "Novel characterization of PD signals by real-time measurement of pulse parameters," *IEEE Transactions on Dielectrics and Electrical Insulation,* vol. 6, no. 1, pp. 51-59, Feb. 1999.

[39] Y. Tian, P. L. Lewin, D. Pommerenke, J. S. Wilkinsonand, and S. J. Sutton "Partial discharge on-line monitoring for HV cable systems using electrooptic modulators," *IEEE Transactions on Dielectrics and Electrical Insulation*, vol. 11, no. 5, pp. 861-869, Oct. 2004.

[40] C. Nyamupangedengu and I. R. Jandrell, "Influence of supply voltage frequency and magnitude on PD pulse parameter," *IEEE Transactions on Dielectrics and Electrical Insulation*, vol. 15, no. 6, pp. 1590-1600, Dec. 2008.

[41] M. Hikita, S. Okabe, H. Murase, and H. Okubo, "Cross-equipment evaluation of partial discharge measurement and diagnosis techniques in electric power apparatus

for transmission and distribution," *IEEE Transactions on Dielectrics and Electrical Insulation*, vol. 15, no. 2, pp. 505-518, Apr. 2008.

[42] M. Vakilian, T. R. Blackburn, B. T. Phung, and H. Zhang, "Investigation of PD signal propagation characteristics in XLPE cables," *International Conference on Power System Technology - POWERCON 2004*, Singapore, Nov. 2004.

[43] T. Moda and S. Yokoyama "Accurate modeling of core-type distribution transformers for electromagnetic transients studies," *IEEE Transactions on Power Delivery* , vol. 17, no. 4, pp. 969-976, Oct. 2002.

[44] H. Buchalla Teilentladungsmeβverfahren, mit, Storsignalerkennung durch Spektralvergleich, PhD Thesis, TH Darmstadt Germany, 1996.

[45] H. Buchalla, T. Flohr, and W. Pfeiffer, "Digital signal processing methods for inter-reference recognition in partial-discharge measurement-a comparison," *IEEE International Symposium on Electrical Insulation*, pp. 393-396, Montreal, Quebec, 1996.

[46] M. Kurrat, Modelierung und Messung von Teilentlandungen in Hohlramen Zur Bestim-mung schadigungsrelevanter Energien, PhD thesis, University of Dormund, Germany, 1993.

[47] P. H. F Morshuis, Partial Discharge Mechanism Leading to Breakdown, Analyzed by Fast Electrical and Optical Measurements, PhD thesis, Delft University of Technology, 1993.

[48] J.P Reynders, "*Partial discharge pulse shape analysis – A diagnostic tool"* Third International Symposium on HV Engineering, pp 1-4, Milan, Italy, Aug. 1979.

APPENDIX

```
'Calculation of Components for the three models of VOID'

'Section 1: Constants'

Eo = 8.854e-12; Er = 2.26; Za = 0.0005; Rs = 18.27e-3; Rv = 0.0005
Rx = 11.572e-3;
Rc = 9.772e-3; Rcscr =10.37e-3; Rins= 15.87e-3; Rinscr= 16.27e-3;
Rbedscr = 18.28e-3;  Thetamax = 0; sxl= 1e-12; sair = 0.5e-13; vm
=3.9e9*760; ec =  1.602e-19; em = 9.109e-31;
P = 101e3; Rgas= 8.314; mole=6.022e23; sdiss = 2.82e-4; Neaver =
2.0e14;
Vincep = 2e3;

'Eo = permitivity of free space (F/m)'
'Er = Relative permitivity'
'Za = length of the cylidrical void (m)'
'Rs =   radius of sheath of the cable (m)'
'Rv = Radius of void (m)'
'Rx =loacation of the void(m)'
'Rc= radius of the core of the cable (m)'
'Rcscr= radius of the conductor screed (m)'
'Rins = radius of theinsulation(m)'
'Rinsscr= radius of the insulation screed (m)'
'Rbedscr= radius of the bed screed (m)'
'sx1 = conductivity of XLPE (1/ohm.m)'
'sair = conductivity of air (1/ohm.m)'
'vm = effective collision frequency for momentum transfer (Torr/(V.s)-
Raizer)'
'ec=  electrone charge (Q)'
'em = electrone mass(kg)'
'P = pressure (Pa)'
'Rgas universal gas constant (J(K.mole))'
'mole = mole'
'sdiss = conductivity coefficient (Ne/Vm)1/(ohm.cm) - Raizer p-13 '
'Neaver = electrone density (1/cm3)'
'Vincep = inception voltage as per diameter of void'
```

```
'Section 2: The classical capacitive model of void:'

    Phimax = atan(Rv/Rx)
    Ra = Rx - Rv
    Rb= Rx+Rv;
    Phi =   inline ('atan(0.0005*cos(Theta)/(11.572e-3-
0.0005*sin(Theta)))')

    x= Phi(pi/4)
    x1=Phi(Thetamax)



'2.1 Capacitances'

'2.1.1 Healthy of healthy insulation Upper part'

       C1= (2*Eo*Er*Za*x1)/(log(Ra/Rc))



'2.1.2 Healthy insulation Lower part'

       C2= 2*Eo*Er*Za*x1/(log(Rs/Rb))



          '2.1.3 Capacitance of void'

    k = Rx*sin(Phimax) - (Phimax*Ra)

K1 = inline('cos(Theta).*cos(atan(0.0005*cos(Theta)/(11.572e-   3-
0.0005*sin(Theta))))')
       Char(K1)
        Q1 = quad( K1, 0, pi/2)

        Cvoid= (Eo*Er*Za*Ra*k)/(Q1*Rv^2)
```

```
'2.2: Resistances'

'2.2.1 Healthy insulation Upper part'

            R1= log(Ra/Rc)/(2*sxl*Za*Phimax)

'2.2.2 Healthy insulation Lower part'

             R2= log(Rs/Rb)/(2*sxl*Za*Phimax)

 '2.2.3 Void Resistance'

          K2 = inline('sin(Theta).*cos(atan(0.0005*cos(Theta)/(11.572e-
3-0.0005*sin(Theta))))')
       Char(K2)
        Q2 = quad( K2, 0, pi/2)

        Rvoid = Q1/(Za*sair*Q2)


'Section 3: Capacitive model based on the induced charge concept '

'3.1 Cinduced calculations'

       DE = 0.86*2.42/(sqrt(2*Rv))

       Cinduced = (3*pi*Rv^2*Za*Eo*Er*DE*sqrt(3))/(11000*(Rx))


'Section 4: The Advance capacitive model of Void'

'4.1 Resistance of cylindrical void'

'4.1.1 Rstreamer/Rdiss as per L.Niemeyer'


             A=(pi/4)*Eo*(2*Er+1)*25*100e3*(2*Rv)^2

             B = (sqrt(9/4.15e-4))/25
```

```
            G = 1 - 0.16 + B/(sqrt(100e3*2*Rv))

            Qmin = A*G
            Qmind=Qmin/(Za*pi*Rv^2)
            Nemin=1e-6*Qmind/ec
            CondA = (sdiss*Nemin/vm)*1e2

              RstreamerA = Q1/(Q2*CondA*Za)


 '4.1.2 Rstreamer/Rdiss as per Georghiou'

             Qaver =  Neaver*ec*1e6*(Za*pi*Rv^2)
              CondB = (sdiss*Neaver/vm)*1e2

              RstreamerB = Q1/(Q2*CondB*Za)

'4.2 capacitance of cylindrical void'

'4.2.1 geometrical as per Zenonas'

     Cvoidadv1 = Eo*Za

'4.2.1 based on induced charges-L.Numiyer '

     Cvoidadv2 = Qmin/Vincep

'4.2.2 based on induced charges- Georghiou '

        Cvoidadv3 = Qaver/Vincep

'Section 5: HF Model of Cable at 1 Mhz'

 '5.1 Series impedance/meter'
'Data from: DEI Meas Tecnigue for HF Character of semicon mat Vol. 11,
No 3; June 2004'

'constants'
```

```
'mo permeability of free space'
        mo =4*pi*1e-7

'S1: conductivity of Al core  '

    S1 = 3.82e7

's6: conductivity of metalic screen Cu'

    S6= 5.8e7
    'circular frequency omeg at 1 Mhz'
     omeg =  2*pi*1e6

'5.1.1    Core impedance Z1'

    A1 = 1/Rc*sqrt(mo*S1))
    Z1 = (mo/2*pi)*sqrt(i*omeg)*A1

'5.1.2 Metalic screen impedance'

      A2 = 1(Rs*sqrt(mo*S6))
      Z6 = (mo/2*pi)*sqrt(i*omeg)*A2

'5.1.3 External impedance'

      Xe = (i*omeg*mo*log(Rs/Rc))/(2*pi)


'5.1.4   Zt total HF series impedance'

   Zt = Z1 +Z6 + Xe

 '5.2 shunt impedance per/m'
    'Data from: DEI Meas Tecnigue for HF Character of semicon mat Vol.
11, No 3; June 2004'

'5.2.1 Conductor screen'

     aa = 0.5; Ta =300*exp(-9); Aa = 105; ab =0.3; Tb= 0.68*exp(-9); Ab
= 50; Ec = 4; sdc= 0.15*exp(-3);
```

```
        EC= Aa/(1+(i*omeg*Ta)^(1-aa))+Ab/(1+(i*omeg*Tb)^(1-ab))+
sdc/(i*omeg*Eo)+Ec

        Yscr= i*omeg*2*pi*Eo*EC/(log(Rscr/Rc))

'5.2.2 Insulation screen'
     'Data from: DEI Meas Tecnigue for HF Character of semicon mat Vol.
11, No 3; June 2004'
     aa = 0.3; Ta =100*exp(-9); Aa = 95; ab =0.5; Tb= 4*exp(-9); Ab =
90; Ec = 2; sdc= 2.7*exp(-3);

        EC= Aa/(1+(i*omeg*Ta)^(1-aa))+Ab/(1+(i*omeg*Tb)^(1-ab))+
sdc/(i*omeg*Eo)+Ec

        Yinscr= i*omeg*2*pi*Eo*EC/(log(Rinscr/Rins))

 '5.2.3 screen bed '
     'Data from: DEI Meas Tecnigue for HF Character of semicon mat Vol.
11, No 3; June 2004'
     aa = 0.5; Ta =800*exp(-9); Aa = 160; ab =0.7; Tb= 15*exp(-9); Ab =
48; Ec = 1; sdc= 32*exp(-3);

        EC= Aa/(1+(i*omeg*Ta)^(1-aa))+Ab/(1+(i*omeg*Tb)^(1-ab))+
sdc/(i*omeg*Eo)+Ec

        Ybedscr = i*omeg*2*pi*Eo*EC/log(Rbedscr/Rinscr))

 '5.2.4 Shunt impedance of XLPE'

        Yins = i*omeg*2*pi*Eo*EC(log(Rins/Rcscr))

        YST = 1( (1/Ycscr) + (1/Yinscr)+ (1/Ybedscr)+ (1/Yins))

'Section 6: HF Model of Cable at 2MHz and per Km'

'6.1 Series impedance/meter'
    'Data from: DEI Meas Tecnigue for HF Character of semicon mat Vol.
11, No 3; June 2004'

'constants'
```

```
'mo permeability of free space'
    mo =4*pi*1e-7

'S1: conductivity of Al core'
 S1 = 3.82e7

 's6: conductivity of metalic screen Cu'
 S6= 5.8e7
 'Nw: number of wires in metallic screed'

 Nw = 44

 'Nr radius of wires of metallic screed'

 Nr = 0.4e-3

 'circular frequency omeg at 10 Mz'
  omeg =  10*pi*2e6

'6.1.1    Core impedance Z1'

 A11= sqrt((i*omeg*mo/S1))
 A1 = 1/(Rc*sqrt(mo*S1))
 Z1 = (mo/2*pi)*sqrt(i*omeg)*A1
 Z11= A11*1/(2*pi*Rc)

6.1.2 Metalic screen impedance'

 A22= sqrt((i*omeg*mo/S6))
 A2 = 1/(Rs*sqrt(mo*S6))
 Z6 = (mo/2*pi)*sqrt(i*omeg)*A2
 Z66= A22*1/(2*pi*Nw*Nr)

'6.1.3 External impedance'

   Xe = (i*omeg*mo*log(Rs/Rc))/(2*pi)

 '6.1.4   Zt total HF series  impedance per Km'

Zt = (Z11 +Z66 + Xe)* 1000
```

```
'6.2 shunt impedance per/m'
    'Data from: DEI Meas Technique for HF Character of semicon mat Vol. 11, No 3; June 2004'

'6.2.1 Conductor screen'

     aa = 0.5; Ta =300e-9; Aa = 105; ab =0.3; Tb= 0.68e-9; Ab = 50; Ec = 4; sdc= 0.15e-3;

        EC1= Aa/(1+(i*omeg*Ta)^(1-aa))+Ab/(1+(i*omeg*Tb)^(1-ab))+ sdc/(i*omeg*Eo)+Ec

        Yscr= i*omeg*2*pi*Eo*EC1/(log(Rcscr/Rc))

'6.2.2 Insulation screen'

     'Data from: DEI Meas Tecnigue for HF Character of semicon mat Vol. 11, No 3; June 2004'

     Baa = 0.3; BTa =100e-9; BAa = 95; Bab =0.5; BTb= 4e-9; BAb = 90; BEc = 2; Bsdc= 2.7e-3;

        EC2= BAa/(1+(i*omeg*BTa)^(1-Baa))+BAb/(1+(i*omeg*BTb)^(1-Bab))+ Bsdc/(i*omeg*Eo)+BEc

        Yinscr= i*omeg*2*pi*Eo*EC2/(log(Rinscr/Rins))

'6.2.3 screen bed '
     'Data from: DEI Meas Tecnigue for HF Character of semicon mat Vol. 11, No 3; June 2004'

     Caa = 0.5; CTa =800e-9; CAa = 160; Cab =0.7; CTb= 15e-9; CAb = 48; CEc = 1; Csdc= 32e-3;

        EC3= CAa/(1+(i*omeg*CTa)^(1-Caa))+CAb/(1+(i*omeg*CTb)^(1-Cab))+ Csdc/(i*omeg*Eo)+CEc

        Ybedscr = i*omeg*2*pi*Eo*EC3/(log(Rbedscr/Rinscr))

'6.2.4 Shunt impedance of XLPE'
```

```
        Yins = i*omeg*2*pi*Eo*EC/(log(Rins/Rcscr))

        YST = (1( (1/Ycscr) + (1/Yinscr)+ (1/Ybedscr)+ (1/Yins)))*1000

'6.3 R, L ,C  G components of Cable per Km at 10 MHz'

        R = real(Zt)
        L =imag(Zt)/omeg
        G = real(YST)/omeg
        C = imag(YST)/omeg

'6.4 cable attenuation-aaa and phase-bbb2 coefficients at 10 MHz
per/km'

        aaa = 0.5*(R*sqrt(C/L)+G*sqrt(L/C))
        bbb = omeg*sqrt(L*C)
        bbb1= (G/(omeg*C)-R/(omeg*L))^2
        bbb2=bbb*(1+bbb1/8)

'6.5 cable attenuation-aaaa and phase-bbbb3 coefficients of 50 Hz
elements per/km at 10 MHz'

        R1c= 0.1295
        L1c= 0.0331e-3
        C1c= 0.54e-6

        aaaa = 0.5*(R1c*sqrt(C1c/L1c)+G*sqrt(L1c/C1c))
        bbbb = 2*omeg*sqrt(L1c*C1c)
        bbbb1= (G/(omeg*C1c)-R1/(omeg*L1c))^2
        bbbb2=bbb*(1+bbb1/8)

'6.6 Attenuation factor'
        AF= aaa/aaaa
```